# Electrode Life and Weldability Improvement in Resistance Spot Welding of DP600

by

Dongwoon Huh

A thesis
presented to the University of Waterloo
in fulfillment of the
thesis requirement for the degree of
Master of Applied Science
in
Mechanical Engineering

Waterloo, Ontario, Canada, 2017

# AUTHOR'S DECLARATION

I hereby declare that I am the sole author of this thesis. This is a true copy of the thesis, including any required final revisions, as accepted by my examiners.

I understand that my thesis may be made electronically available to the public.

# Abstract

This thesis demonstrates effective methods to improve weldability and electrode life in resistance spot welding (RSW) of zinc coated advanced high strength steel. Six kinds of electrodes were investigated to determine the effect of electrode design/material on electrode life and welding performance. The variables were material (Class 2 and Class 3), electrode shape (Dome and Parabolic), and coating on the electrode surface (Ni/TiC coating). Weld qualities were evaluated with mechanical tests, such as tensile shear and peel test, and analyzed using electrical weld signals. Since electrode life and weldability is strongly related to electrode surface degradation, the electrode surface was printed using carbon paper to clearly record the progression of the electrode life cycle. After finishing the electrode life test, the metallurgy of the electrodes was analyzed using standard cross sectioning techniques, optical microscopy, hardness and scanning electron microscopy (SEM) techniques.

A new type of electrode, with core inserts, is examined for improvements to weldability and increase electrode life when welding zinc coated advanced high strength steel. By using a refractory material insert, the electrode exhibited a local high resistance which promoted weld nugget growth. This type of electrode made a thicker and larger weld nugget, and it improved weldability and mechanical properties, especially with regards to cross tension (CT) strength. The effect and mechanism of inserted electrode were verified with commercial FEA software. The results of different weld current flow, nugget formation, and heat distribution were explored. Additionally, welding signal analysis was performed to verify the performance of the electrode. This type of electrode was also life tested with various diameters and insert materials to measure the effects of these changes.

# Acknowledgements

# Table of Contents

# List of Figures

# List of Tables

# Chapter 1
# Introduction

## 1.1 Overview

Resistance spot welding (RSW) is widely used to join sheet metal in the automotive manufacturing industry [1, 2]. In particular, a short welding time and complete automation make RSW very attractive in mass production applications. Compared to other welding methods RSW lowers manufacturing cost making it highly suitable for mass production. Due to these advantages, RSW continues to be used for joining of advanced high strength steel or lightweight materials used for weight reduction of vehicles.

In recent decades, the weight reduction requirement is driven by environmental concerns. Many countries have signed the Kyoto protocol, which are regulations to reduce greenhouse gas emissions, and took effect on February, 2005. Compared with the 1990s, countries are required to reduce emission of $CO_2$ gas over 5%. Countries are also adopting more stringent global standards or regulations such as the corporate average fuel efficiency (CAFE) standard [3]. For these reasons, many car manufacturers need innovative methods to reduce automotive fleet carbon emissions and improve fuel efficiency.

There are various ways to improve fuel efficiency. The three most common are: increasing engine efficiency, minimizing the drag coefficient, and reducing car weight [4, 5].

The first method requires long-term investment and high expenses, coupled with practical limits. Decreasing the drag coefficient also has limitations related to driver and passenger safety. For this reason, many car manufacturers are adopting car body weight reduction to improve fuel efficiency.

In order to reduce car body weight, the use of light materials, such as aluminum or magnesium, is a consideration. However, due to the cost, these materials are only used for specific parts. More commonly, car weight reduction is performed by decreasing the steel thickness and using high strength steel.

In terms of spot welding, use of these high strength steels makes for more difficult welding conditions. To use this steel in a production line, it is beneficial to find ways to make better welds. To increase productivity and reduce maintenance effort, electrodes should have longer life, reduced welding time, and produce stronger welds.

The aim of this thesis is to show improvement in RSW of zinc coated advanced high strength steel. This is done by examining a new type of electrode which can maximize electrode life, decrease

production time, reduce maintenance time, and reduce material cost. The performance of this electrode was analyzed by using mechanical tests, metallurgical tests, weld lobe diagrams, and welding data analysis. Finally, diameter and material parameters were effectively optimized for electrode life and weldability.

## 1.2 Problems

The main problems in RSW can be divided into two major sections: increase of use of AHSS, and coatings on the steel surface. These problems can lead to the fast electrode degradation or wear out.

### 1.2.1 Increase of Use of Advanced High Strength Steel (AHSS)

To meet the environmental requirements, many car makers and steel companies are trying to make an effort to reduce the car weight and to develop light, high strength steel. For the purpose of a light weight vehicle and reinforcement of crashworthiness, steel companies are developed, and developing many kinds of advanced high strength steel (AHSS) such as Dual Phase (DP), Complex Phase (CP), Transformation Induced Plasticity (TRIP), Martensitic (MART), and Twinning Induced Plasticity (TWIP) as shown in Figure 1.1 [6]. Generally, these steels have a higher strength than conventional steels. Therefore, they can be used with reduced thicknesses while maintaining strength, which helps to reduce car weight.
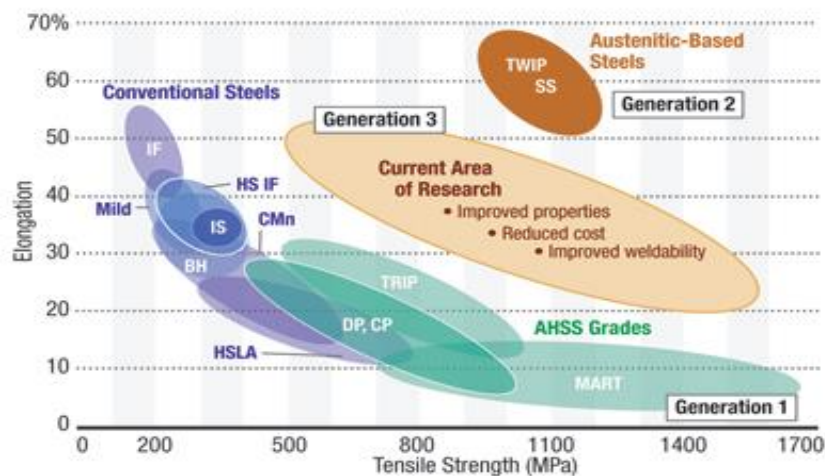


**Figure 1.1** Steel Application Trend in Automotive Industry [6]

2

According to a survey in North American light vehicles, the use of AHSS increased from 9.5 percent in 2007 to 34.8% in 2015 as shown in Figure 1.2. On the other hand, the use of mild steel and medium high strength steel has been dramatically reduced [6].
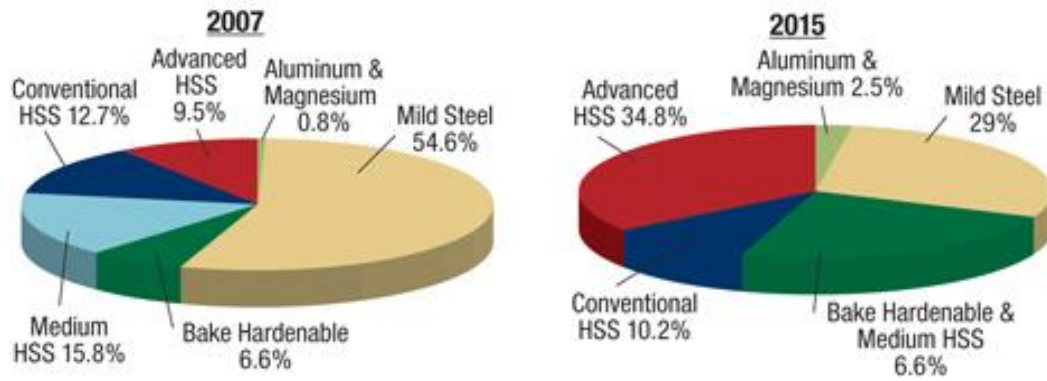


**Figure 1.2** Metallic Content in North America Light Vehicles [6]

The spot welding characteristics of AHSS are different in comparison to the mild steels. Due to the high percentage of carbon equivalent, AHSS has a high bulk resistivity [7]. As shown in Figure 1.3, the electrical resistivity increased steeply above 0.3 wt% of carbon. Therefore, AHSS steels require a lower weld current than mild steel. This result was confirmed via weld lobe diagram, the same as the Figure 1.4 [8]. In this figure, the welding possible current range of DP steel was formed narrower and moved to lower welding current area than HSLA and mild steel.
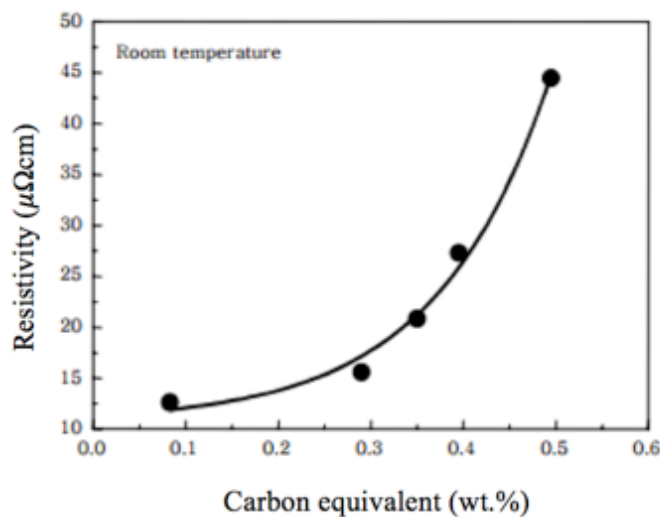


**Figure 1.3** Effect of carbon equivalent on bulk resistivity at room temperature [7]
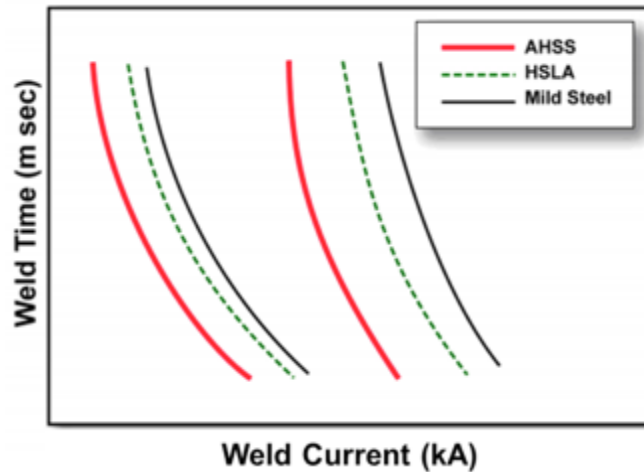
**Figure 1.4** Weld lobe curves for the AHSS, HSLA, and mild steel [8]

For these above reasons, as the next generation of high strength steels are created, making high quality welds will become a greater challenge.

### 1.2.2 Application of Coatings on the Steel Surface

Presently, many zinc coating methods are used on the steel surfaces in order to enhance corrosion resistance. Some examples are: hot-dip galvanized (GI), electrolytic galvanized (EGI), and galvannealed (GA). Two basic mechanisms used to protect steel surfaces are: barrier protection and cathodic protection [9]. Barrier protection occurs when the steel surface is protected by a zinc layer which fully covers the steel surface from the corrosive agents. Cathodic protection occurs when the zinc layer preferentially reacts to the corrosive agents. Due to improvements of steel durability, reducing maintenance costs, zinc coatings are applied by default in automotive industries.



**Anodic reactions**

$$Zn + H_2O \rightarrow Zn(OH)_2 + 2H^+ + 2e^-$$
$$Zn(OH)_2 \rightarrow H_2O$$
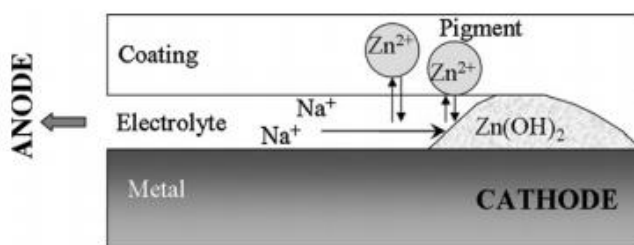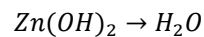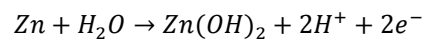
**Cathodic reactions**

$$O_2 + 2H_2O + 4e^- \rightarrow 4OH^-$$
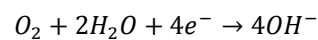
**Figure 1.5** The Corrosion Reactions of Zinc [10]

4

When spot welding is performed, however, the zinc layer is not beneficial in improving weld quality. Zinc is soft and has low electrical resistance, causing it to form a more conductive contact condition between electrodes and steel sheets. The lower resistance makes for more difficult welding conditions, detrimental to form a weld nugget. This means that zinc coated steel requires higher weld current or longer weld time to make the same diameter of weld nugget. Furthermore, these excessive welding conditions increase the possibility of creating an expulsion. As shown in Figure 1.6 below, the minimum weld nugget diameter for GI sheet steel requires a higher weld current, a longer weld time, or a combination of both [11].
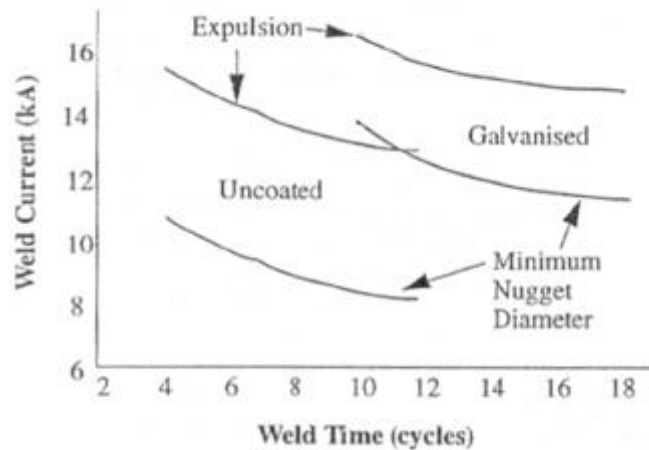


**Figure 1.6** Welding possible range of uncoated and GI coated steel [11]

## 1.3 Objectives

The objectives of this thesis are as follows:

1. To investigate RSW performance for different electrode materials, geometries, and surface coatings and to analyze the effect of these variables on welding performance, particularly on electrode life.

2. To develop and propose a new type of electrode which significantly improves weld quality and increase electrode life when used with zinc coated advanced high strength steel.

5

## 1.4 Thesis Outline

This thesis is comprised of six chapters as follow:

Chapter 1: Introduction - This chapter includes the thesis overview, explanation of current problems, and the objectives and constraints of the supporting research.

Chapter 2: Literature Review - This chapter summarizes findings of prior publications relevant to the research.

Chapter 3: Experimental Methods - This chapter gives details of the material, equipment, electrodes, experimental procedure, and mechanical and metallurgical testing methods used in the research.

Chapter 4: Effects of TiC/Ni Coating on Electrode Life - This chapter shows the results of electrode weld performance for different electrode materials, geometries, and coating.

Chapter 5: Effect of Electrode Inserts on Electrode Life and Weldability - This chapter introduces the concept of an inserted electrode and reports on weld performances including the result of electrode life tests and weldability tests.

Chapter 6: Conclusions and Recommendations - This chapter summarizes the main findings and conclusions of the research. In addition, future research work is proposed.

# Chapter 2
# Literature Review

## 2.1 Resistance Spot Welding (RSW)

The resistance spot welding (RSW) is the most commonly used method to join steel sheets because it can be performed at low cost, fast speed, and does not required additional materials, such as filler metal, or shielding gas [12]. The three most important components for joining steel (using RSW) are: electrical current, clamping pressure on the steel sheet, and time period for steel melting.

## 2.1.1 Fundamentals

A basic principle of RSW can be expressed by the Joule's law equation as below because joining is created by use of resistance heating [13].

$$Q = I^2 Rt$$

A high clamping force is applied to the overlapped steel sheets and a high electrical current (I [Amps]) flows through electrodes and the steel sheets. In this process, resistance (R [Ω]) is present between the electrodes and the steel sheets during the welding period (t [sec]). The flow of current through this resistance generates heat (Q [J]), and the steel starts melting when the heat generated in the weld area is sufficiently high. When welding is complete, a weld nugget is created between the faying surface of steel sheets as shown in Figure 2.1. The resistive heating causes the melting and joining of the steel sheets during the welding period. Figure 2.2 shows a schematic of weld area and temperature distribution which is created by the resistive heating.
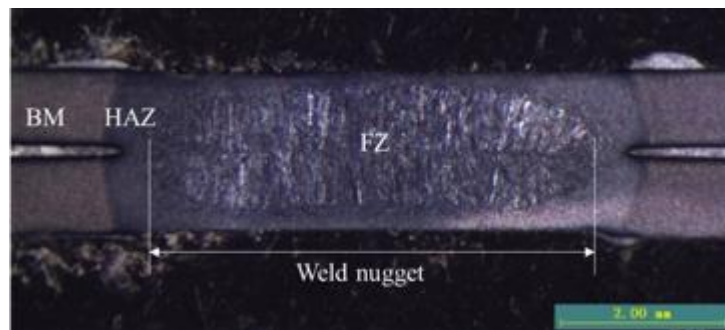


**Figure 2.1** Cross sectional shape of RSW weld
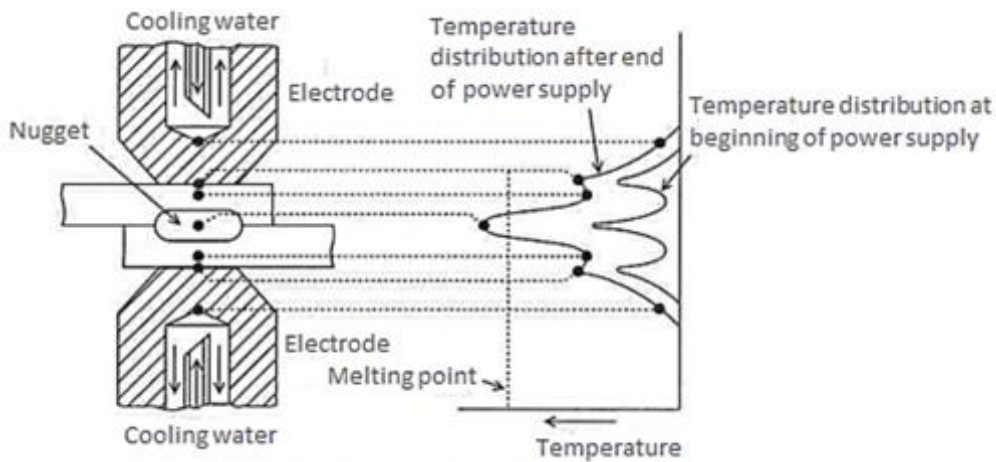
**Figure 2.2** Schematic of RSW weld and temperature distribution [14]

## 2.1.2 Welding Parameters

Based on the previous equation, the total heat input is greatly influenced by the weld current, weld time, and weld force. Weld current has the largest effect on the resistive heat because the generated heat is directly proportional to the square of the weld current [15]. Weld current density also has an impact on the weld performance [16]. If the weld current density is low, melting starts with difficulty, and the weld nugget is small or non-existent. Conversely, if the weld current density is too high, melting starts quickly but the possibility of expulsion and excessive deformation increase. Therefore, the weld current needs to be controlled carefully. Weld time is also an important factor in the RSW process [17]. Given the same total heat input, the maximum weld temperature changes depending on the weld time because the heat flux is different. A shorter weld time leads to a smaller melt area, and the weld may not form sufficiently. Conversely, if the weld time is too long, heat loss increases and the heat affected zone (HAZ) is larger. It is important to control the size of heated area around weld because it can change the mechanical or metallurgical properties. The weld force is also important parameters in the RSW process [18]. Contact resistance changes based on the amount of weld force. Low weld force results in defects such as porosity in the weld nugget, and cracks in the steel. High weld force results in a low contact resistance which then reduces the heat created. Figure 2.3 shows a weld nugget created using unsuitable welding parameters. High weld current, low weld force, and long weld time generated a void and excessive indentation depth in the nugget.

8

**Figure 2.3** Weld defects of RSW weld

Other factors also affect RSW weld quality. There are many such parameters, e.g.: base materials, coatings on the steel surface, electrodes, electrode condition, and so on. Accordingly, all these parameters should be carefully considered and properly selected.

### 2.1.3 Welding Process

The RSW process can be divided into five separate steps as shown in Figure 2.4 [19]:

    1. The upper and lower electrodes clamp the steel sheet during the squeeze time.

    2. Weld force is applied to steel sheet.

    3. Weld current is generated.

    4. The steel sheet cool down.

    5. The electrodes release from the steel sheet.
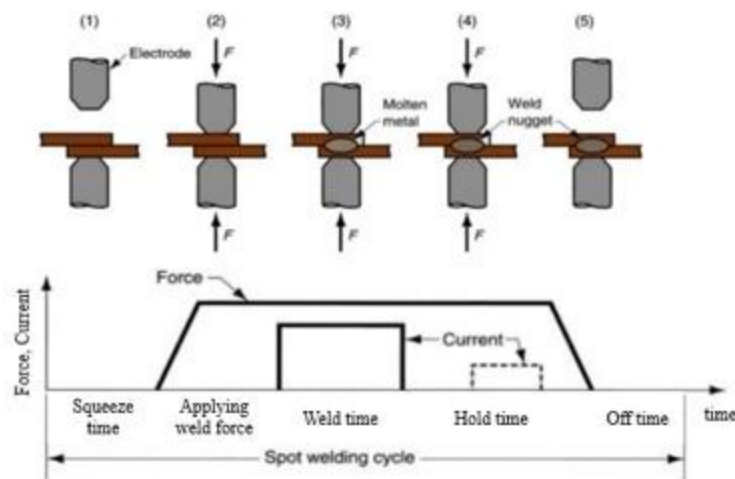


**Figure 2.4** The sequence of RSW process [19]

9

### 2.1.4 Weld nugget formation

The weld nugget formation is closely related to contact resistance and the bulk resistance of steel itself [20]. Shortly after the weld time starts the steel surfaces make better contact, and the contact resistance rapidly decreases. During the weld time the bulk resistance of the steel increases. Particularly, it rises sharply when the steel is changing phase from solid state to liquid state [13]. Weld current, weld time, and weld force all have an effect on the shape of the dynamic resistance curve. This is because they affect the rate of temperature change within the nugget.

One can evaluate and estimate weld nugget growth through weld data analysis. For example, Cho et al. studied the secondary dynamic resistance to analyze the weld nugget growth [21, 22]. In the case of AC RSW, the dynamic resistance can be calculated using the equation below. The resistance can be calculated with the selected currents and voltage which is measured every half weld cycle from the secondary circuit of the welding machine and a monitoring system. The currents and voltages selected the inflection points, the peak values when the current and voltage become di/dt =0 and dv/dt =0.

$$\mathrm{R}_{dynamic} = \frac{V_{dv/dt=0}}{I_{di/dt=0}}$$

Figure 2.5 shows an example of a dynamic resistance curve obtained from uncoated steel [21]. The dynamic resistance curve can be divided into five parts. First, the electrodes clamp the steel sheets, and the electrical weld currrent flows first through the micro-contacted points. At this point, the resistance is same as the sum total of bulk resistance including electrode to steel sheet and steel sheet to steel sheet. The initial resistance can change depending on the steel surface condition, coatings, and other factors. If the surface, both of the electrodes and the steel, is clean, the slope will be sharp and decreases quickly. In the second stage, the bulk resistance of steel is still high, but better contact condition is made due to the increased welding temperature. The minimum resistance, called α-peak, is observed at this point. After this peak, as the temperature rapidly increase, dynamic resistance also increases. The resistance then reaches the maximum point, called β-peak. The resistance of the steel increases with the elevated temperature and a small weld nugget is created. In the fourth stage, the bulk resistance of steel keeps increasing due to the increasing temperature. However, the indentation allowed by the softening of the steel forms a shorter weld current path. Consequently, the resistance starts to decrease according to the electrical resistance formula below.

10

$$R = \rho \, \frac{l}{A}$$ $l$: the length of the material
$A$: the cross sectional area of the material

In the fifth stage, the weld nugget continues to grow until the weld process is complete. If the heat generated in the weld nugget is allowed to become excessive, an expulsion occurs, where molten material exits the weld.
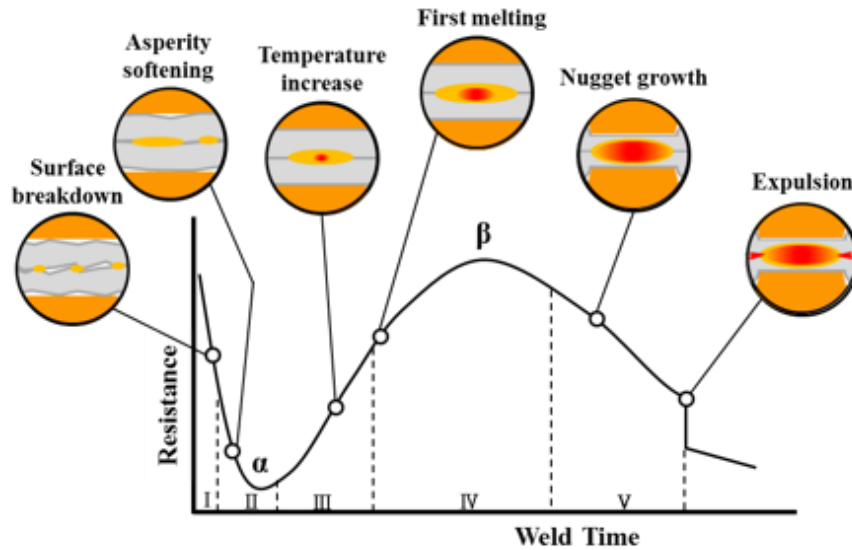


**Figure 2.5** Changing of D-resistance curve during the weld nugget formation [21]

## 2.2 Mechanical and Metallurgical analysis of RSW

As mentioned in chapter 1, the AHSS steels have a high bulk resistivity and hence these have a high sensitivity to welding parameters to produce a good weld that meets requirements such as strength or geometric criterions. In this section, RSW weldability is investigated from a mechanical perspective.

### 2.2.1 RSW weldability of AHSS

Basically, weld lobe curves have been used to characterize RSW weldability for different materials, steel sheet combinations and weld joints [1]. Normally, the lobe curves are shown in a 2-dimensional representation, plotting two main welding parameters, weld current and weld time, as seen in the Figure 2.6 below. The lower boundary is determined when the weld nugget diameter does not meet the

11

minimum requirement, $4\sqrt{t}$ ($t = thickness\ of\ steel\ sheet$), and the upper boundary is defined by the existence of expulsion [23]. As a result, weldability can be visually judged based on the relative size of the weld lobe curve.
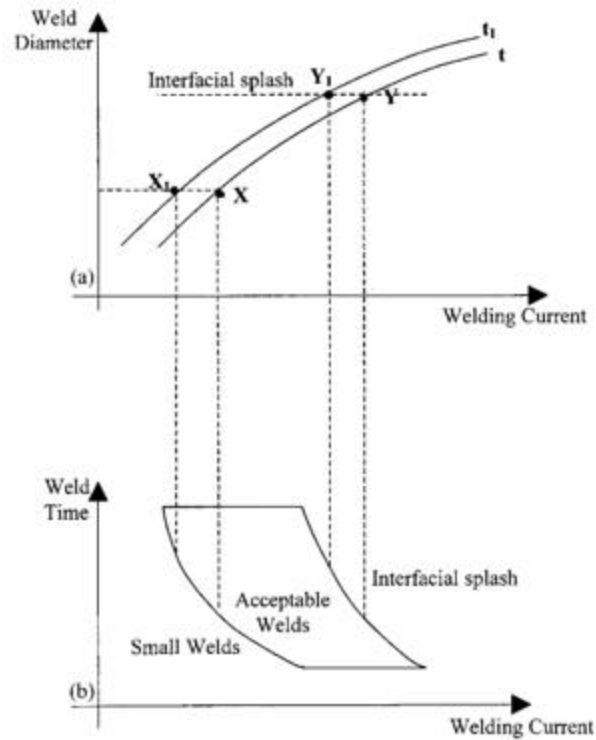


**Figure 2.6** Weld lobe curve [1]

Generally, low strength steels having a low carbon equivalent result in a wide acceptable welding range, but AHSS steels that have high resistivity result in a relatively narrow range. Yu et al. reported on the weld lobe curve for TWIP980 [24]. TWIP 980 steel displayed a possible welding current range of only 0.5kA, and expulsions were likely in most of welding range. In the case of TWIP steel, a high manganese (Mn) content of 18% was present. Although this alloying material increases the strength, the bulk resistivity also increased and the weldability suffers [25]. Another factor that results in a narrower weld lobe curve is the rigidity of the material. Higher rigidity leads to a spring back effect, and makes it more difficult to get sufficient contact area for spot welding [26]. The result is more resistance heat being generates at the electrode to steel interface and this encourages expulsion. In view of this, applying a higher weld force is recommended for the high-Mn steel joining. Saha et al. investigated welding defects of high-Mn steel [27]. The cracks are usually formed with higher welding current conditions due to the combination of increased nugget growing force, high rigidity of material,

and tensile stress in HAZ. As a result, the defects are made in the weld as the form of (a) liquation cracking in HAZ, (b) intergranular crack, and (c) shrinkage cavity as seen in Figure 2.7.
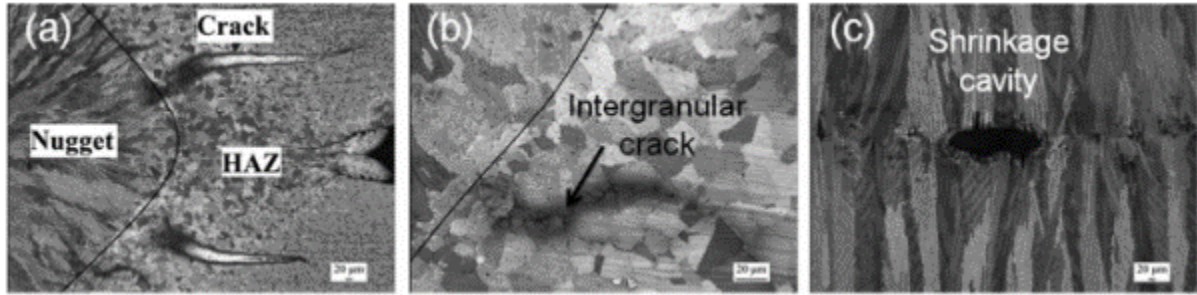


**Figure 2.7** Welding defects of high-Mn steel [26]

## 2.2.2 The effect of coating in AHSS

Zinc coating layers, such as galvanized (GI), galvanealed (GA), and Al-Si, are widely used to prevent corrosion [28]. However, these coating layers make a good surface contact condition and decrease contact resistance [13]. As a result, the weld lobe curve moves to high current range. In the case of GI coated steel, once a spot weld starts, the zinc starts to melt when the temperature reaches approximately to 460°C and moves around the edge of the weld due to the mechanical welding force. Then the extruded zinc forms a better contact and lowers the contact resistance. Figure 2.8 shows the differing contact resistance distribution between uncoated and coated steels. When starting to form a weld nugget, the zinc layer should be removed as soon as possible. However, part of the energy will necessarily be spent on melting and removing the zinc layer, which can result in an unacceptable weld nugget.
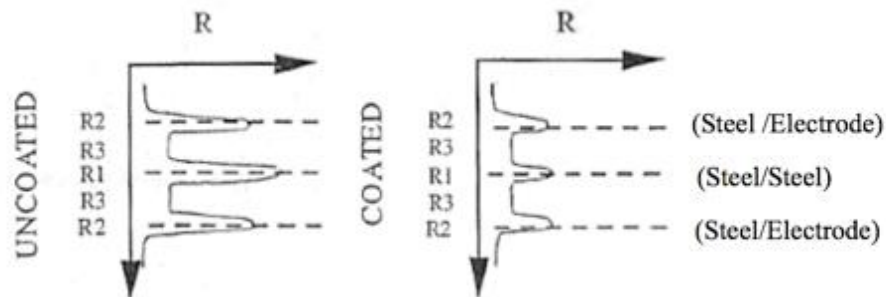


**Figure 2.8** Contact resistance distribution between uncoated and GI coated steels [29]

13

Gedeon et al. investigated changing lobe curves and dynamic resistance curves by varying the thickness of coating and kinds of coating [30, 31]. Figure 2.9 shows dynamic resistance curve for uncoated and GI coated steel. Uncoated steel displays an α-peak at an early stage in the welding and a clear β-peak. On the other hand, the GI coated steel did not display distinct peaks, and the resistance was lower than for uncoated steel. The zinc coating layer resulted in a better mechanical contact (formation of low resistance) and delayed the formation of weld nugget. Figure 2.10 illustrates changes to the weld lobe curve depending on the thickness of the coating. As the thickness of the coating increases, the weld current needed to melt the steel also increases [32].



| (a) Uncoated steel | (b) GI coated steel |
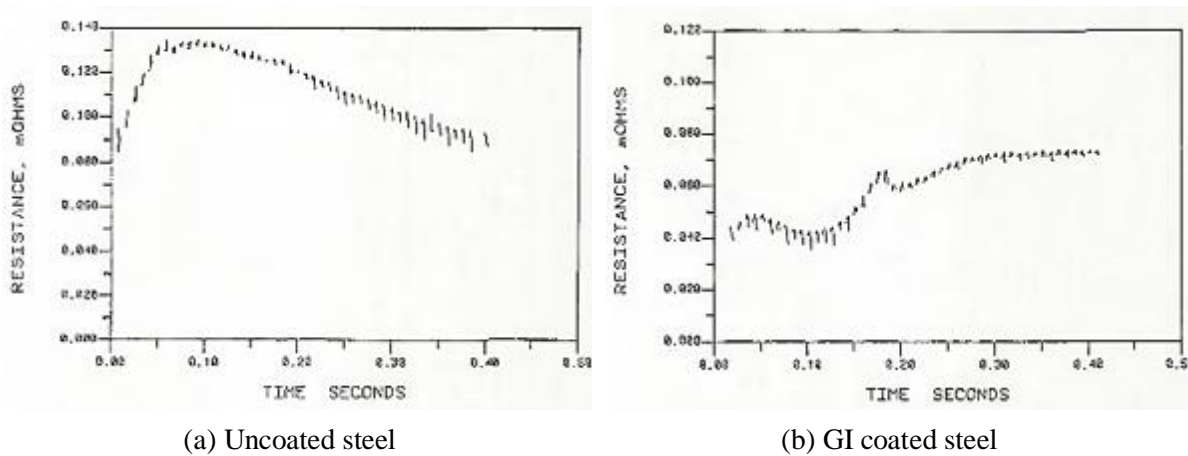
**Figure 2.9** Dynamic resistance curves [31]
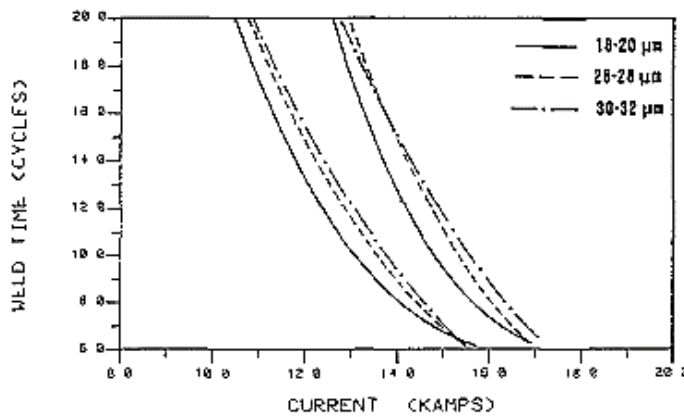


**Figure 2.10** Changing of weld lobe curve depends on the thickness of coating [30]

## 2.2.3 Factors affecting the mechanical properties

Lee et al. and Ma et al. investigated the stress distribution in the weld nugget using a static equilibrium to explain the crack initiation [35, 36]. The forces can be divided into three types: normal force (F), shear force (Q), and moment (M) which is generated by inertia as seen in Figure 2.11. If it is assumed that the weld nugget is symmetric and welded perfectly under optimal welding conditions, interfacial fracture does not happen, and the stresses can be calculated with equation (2-1) and (2-2) below. The nominal stress is expressed by equation (2-1), and it is strongly related to the nugget diameter, 2r. The moment can be expressed by equation (2-2), and the modulus of section was applied to an elliptical shape that is similar to real weld nugget shape. As seen in these equations, the stresses are dependent to the nugget dimensions, such as nugget diameter, 'a', and thickness, 'b'. Therefore, a larger and thicker nugget experiences a higher tensile shear strength.
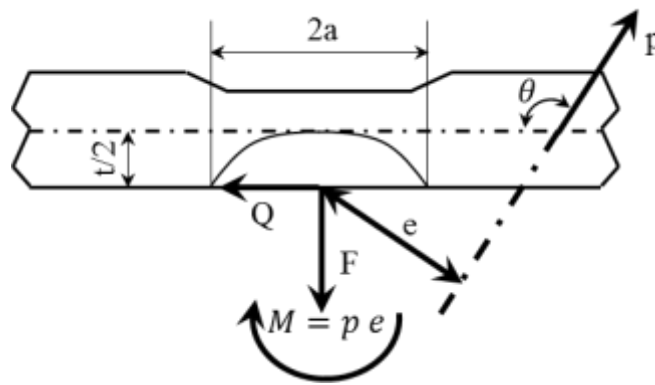


**Figure 2.11** Diagram of applied forces in a weld [35]

$$\sigma_n = \frac{F}{\pi r^2}$$

(2-1)

$$\sigma_m = \frac{My}{I} = \frac{Pe}{z} , \qquad z = \frac{\pi a b}{8}(a^2 + b^2)$$

(2-2)

Chao studied the failure mechanism and strength relationship of the weld with tensile shear and cross tension tests [37]. Figure 2.12 shows the stress distribution of weld nugget in lap shear and cross tension specimens. Tensile shear specimens show maximum stress at the edge of the weld nugget that is parallel

15

to the loading direction and maximum shear stress was also observed around the edge of the weld nugget. Therefore, in the case of representative weld nuggets, cracks form and propagate from the edge of the weld nugget. The equations (2.3) to (2.6) describe the failure stresses and strengths.



(a) Tensile shear speciemen          (b) Cross tension specimen
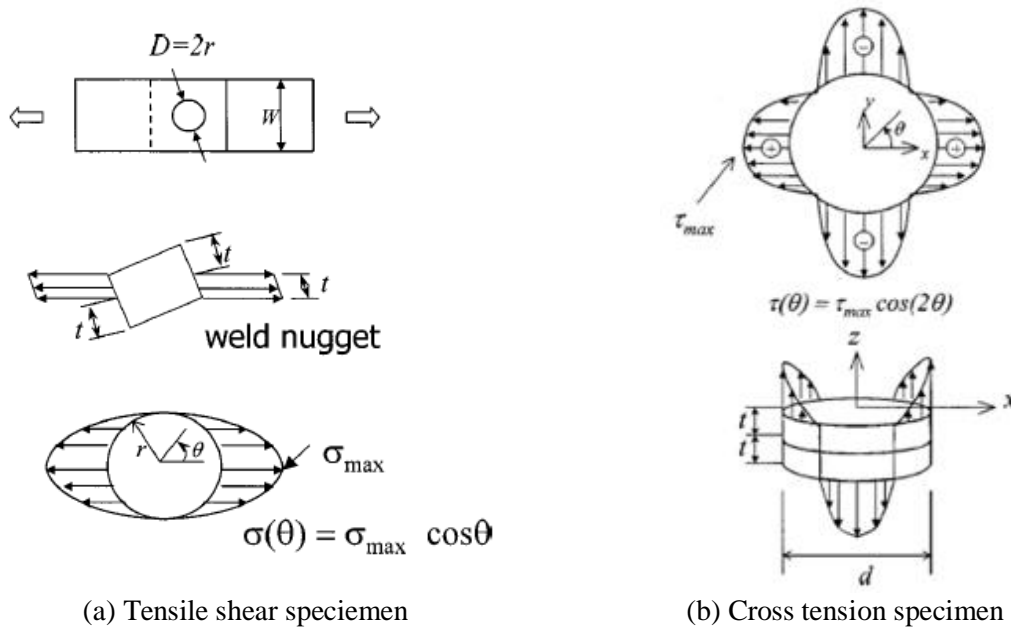
**Figure 2.12** Diagram of applied forces in a weld [35]

$$P = \int_{-\pi/2}^{\pi/2} \sigma(\theta) \cdot \frac{d}{2} t \cdot \cos\theta \, d\theta = \frac{\pi}{4} \, t \, d \, \sigma_{max} = 0.785 \, t \, d \, \sigma_{max}$$

(2-3)

$$P_{failure} = 0.785 \, t \, d \, \sigma_{failure}$$

(2-4)

$$P = \int_{-\pi/4}^{\pi/4} \tau(\theta) \cdot rt \, d\theta = t \, d \, \tau_{max}$$

(2-5)

$$P_{failure} = t \, d \, \tau_{failure}$$

(2-6)

16

Based on these equations, the correlation between tensile shear and cross tension strengths is expressed in equation (2-7) with the Von Mises criterion criteria.

$$P_{failure}{}^{CT} = 0.735 \, P_{failure}{}^{TS}$$

(2-7)

From a metallurgical perspective, the weld area shows a number of separate zones. Hernandez et al. studied about HAZ softening in DP steel. As shown in Figure 2. 13, a HAZ is formed around the weld nugget after the weld completes and it can be classified in detail as UC HAZ and SC HAZ depending on the thermal effect. Generally, HAZ softening is formed by tempering of martensitic between UC HAZ and SC HAZ and demonstrates lower hardness than the base metal (BM) [38, 39]. In terms of the mechanical properties, Ghosh et al. investigated HAZ softening and its role in decreasing strength [40].
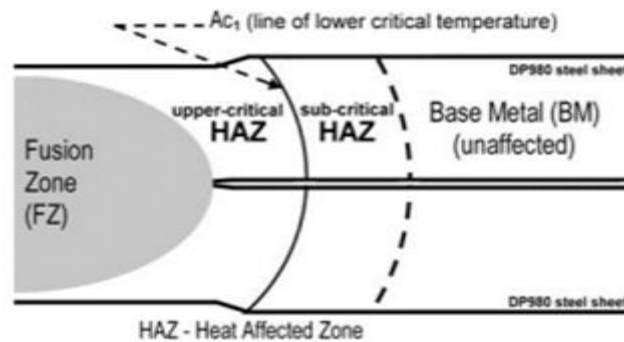


**Figure 2.13** Cross section of a spot weld [41]

Xia et al. reported that HAZ softening was caused by an increased martensitic volume fraction as demonstrated in Figure 2.14, and tensile strength had a linear correlation with HAZ softening. This suggests that the total heat input and the welding process have an effect on the creation of HAZ softening. In general, maximum HAZ softening is occurs on the $Ac_1$ (refer to Figure 2.13) which does not cause an austenitic transformation. When spot welding uses a longer welding time and higher heat input, it will cool down more slowly and results in a large $Ac_1$ width and increased HAZ softening. Figure 2.15 shows the HAZ softening resulting from different heat sources and heat input conditions. Softening is related to the chemical composition of the material, but shows a steep increase with increased heat input.

17
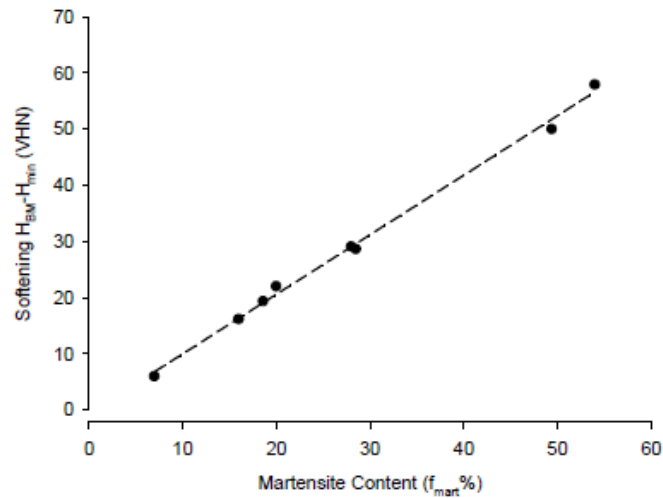
**Figure 2.14** Relationship between DP martensitic volume fraction and HAZ softening [42]
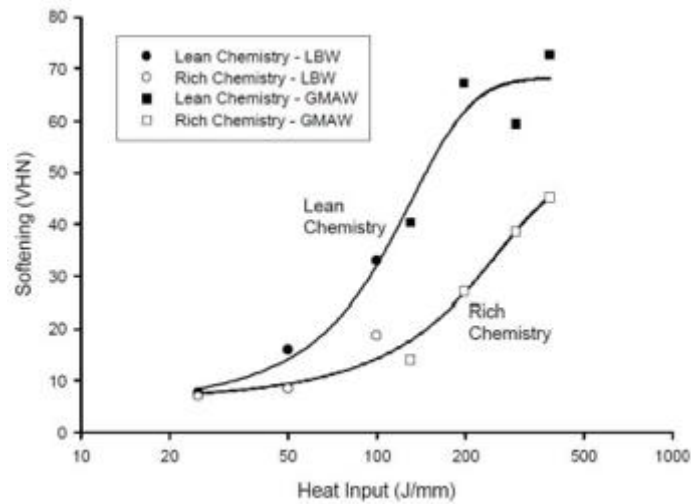


**Figure 2.15** HAZ softening in DP600 steels with different heat sources and total heat input [43]

## 2.3 The influence of the electrode

The electrode is a very important factor in determining the weld qualities in RSW because the weld current last flows through the electrodes. However, as welding is progressed, the electrode surface progressively deforms and wear out, causing the weld current density to decrease rapidly and weld qualities to also deteriorate rapidly.

## 2.3.1 Electrode wear mechanism

Electrode wear is mostly caused by the repetitive high temperature and pressure over multiple welds. Well known mechanisms of electrode wear are alloying, pitting, and deformation [44].

The main cause of alloying is the zinc on the surface of the steel that diffuses to the electrode surface. This alloying between the electrode material and the coating layer contributes significantly to the overall damage process, particularly through enlargement of the electrode surface area. This enlargement depends on the welding conditions, electrode material, composition, zinc coating thickness, and others.
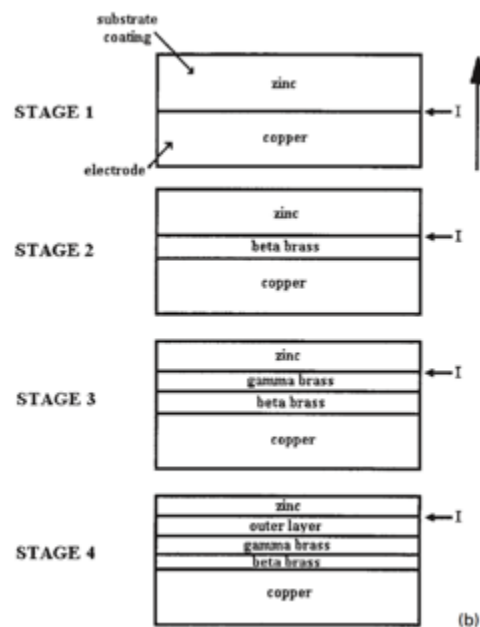


**Figure 2.16** Alloy formation on the electrode when welding hot-dip zinc coated steel [44]

Williams et al. reported that the metallurgical changes occurred during the alloying process are composed of four stages as seen in Figure 2.16 [44]. As welding starts, zinc concentration increases as seen in Figure 2.17 ⓐ, and the FCC α phase with zinc in solid solution changes to BCC β brass (CuZn) at 33.6 wt% Zn as a phase diagram for copper-zinc as shown in Figure 2.17 ⓑ. Next, a β brass layer starts to form at the melting temperature, around 900°C, depending on the amount of zinc. In the stage 3, γ brass (Cu5Zn8) begins to form when the zinc content reaches 50.6 wt% shown in Figure 2.17 ⓒ. These layers form unevenly and continuously on the electrode surface during the welds. Electrode wear is correlated to the amount of gamma phase brass formed.
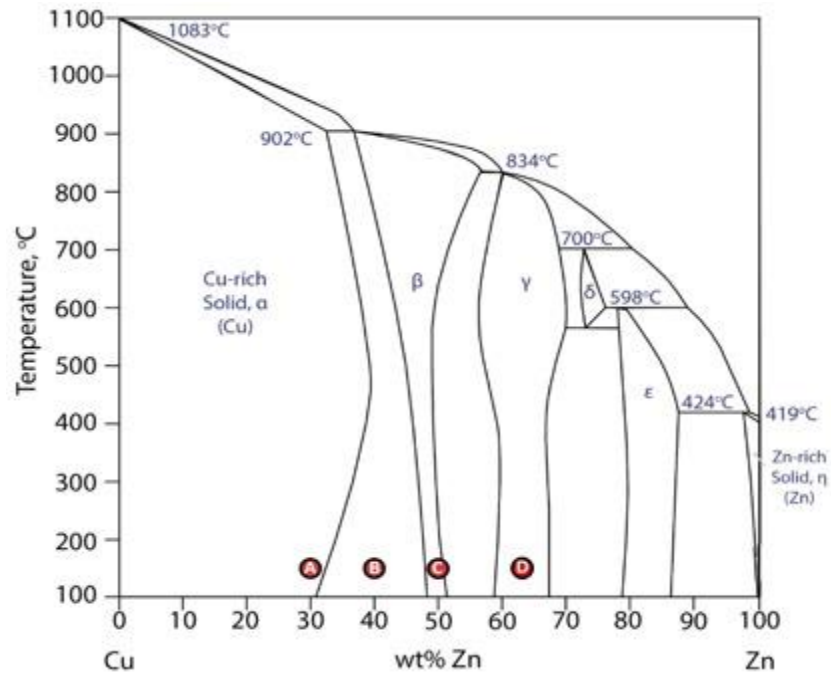
**Figure 2.17** Cu-Zn phase diagram [45]

The second wear mechanism is pitting which is caused by melting and alloying of the contact area. Maroie et al. have studied pitting and surface oxidation in connection with copper and brass formation [46]. In many alloys, an oxide layer plays an important role in interface bonding, which, when broken, creates pitting. During oxygen exposure at room temperature, ZnO and $Cu_2O$ are formed. ZnO starts to form first, and then $Cu_2O$ formed later. If these oxides are then exposed to higher oxygen atmosphere, $Cu_2O$ is transformed into CuO which creates an outer layer, preventing any further $Cu_2O$ oxidation. Following the oxidation, if the temperature increases sufficiently, CuO is reduced to $Cu_2O$. These reactions are expressed in the two sets of chemical reactions below. One set describes brass and the other copper.

For copper,

$$CuO \rightarrow 1/2\ O2 + Cu \quad \text{(decomposition)}$$

or

$$Cu + CuO \rightarrow Cu_2O \quad \text{(solid state reaction)}$$

20
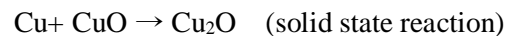
For brass, two other solid state reactions can be made thermodynamically.

$$2CuO + Zn \rightarrow Cu_2O + ZnO$$

and

$$CuO + Zn \rightarrow Cu + ZnO$$
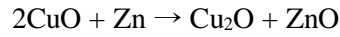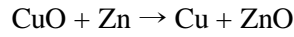
Figure 2.18 shows the evolution of a Cu surface during oxygen exposure to α and β brass. As shown in the graph, β brass forms easily in higher temperatures and longer oxygen exposure times, but the formation of α brass decreases after a certain amount of exposure time. We expect therefore, that electrodes which have reached the end of their useful life will have higher amounts of β brass as opposed to α brass.



(a) α brass        (b) β brass
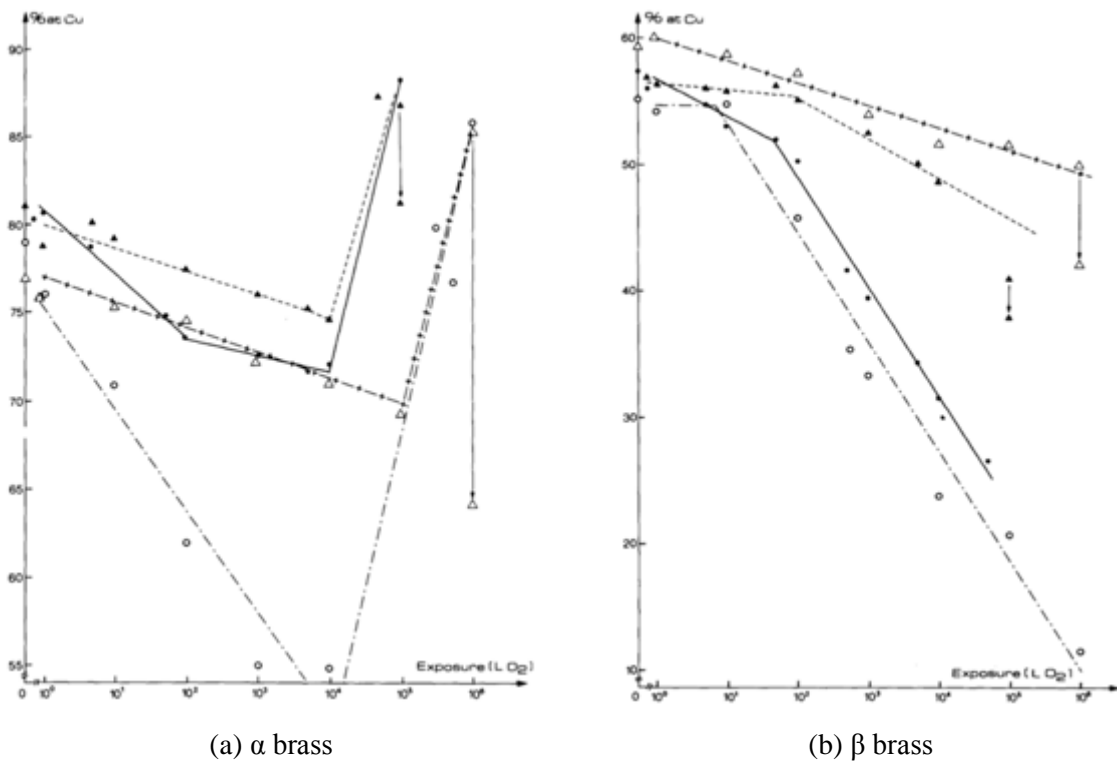
**Figure 2.18** Cu surface concentration during oxygen exposure with different annealing and temperature conditions [46]

Kimchi et al. analyzed the process of pitting using finite element analysis [47]. The electrode faces alloyed and adhered to the zinc with high welding temperature and high weld force. Subsequently, when the electrode was separated from the steel, electrode pitting occurs as base material was removed from the electrode surface. After repeated welds, the pitting area increased, and many small pitting areas joined together to form a large cavity. The large cavity influenced current distribution (unbalanced weld current) on the electrode surface. Higher temperatures and pressures were generated at the edge of the cavity, and this cavity area can detach. Figure 2.19 shows the carbon imprint tests for dual phase steel (DP600) [48]. As a consequence, the weld nugget shape can become ring shaped because weld current flows only through the contact area. This can lead to a weld nugget with low weld strength and shortens useful electrode life.
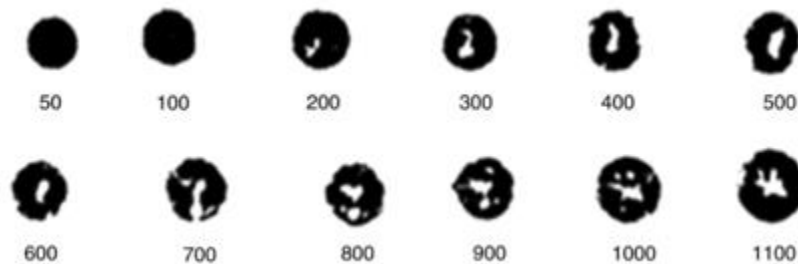


**Figure 2.19** Electrode face of carbon imprint method at different weld numbers [48]

Another factor is that electrode surface deformation accelerates electrode degradation. Electrode deformation results from the high pressure and temperature conditions present in spot welding. On a microscopic level, recrystallization of the electrode leads to deformation since electrodes soften – and therefore deform – in the process of recrystallization. Re-crystallization as a process depends on both time and temperature. The force producing new grain structure is the difference in internal energy between the strained and unstrained material caused the re-crystallization temperature as shown in Table 2.1 [49]. The new grains form as very small nuclei and grow until they completely replace the base material. During recrystallization, the mechanical properties of ductility and strength are changed to high and low, respectively. Recrystallization proceeds faster in pure metals than in alloys. Therefore, electrodes are made of various materials such as Cu, Cr, Zn, and etc., to increase the recrystallization temperature and hinder electrodes recrystallizing [50]. However, high weld temperatures which cause recrystallization and pressure on the electrode surface creates large grains (coarse grains). At the same

22

time, these grains tend to allow dislocations to move with less force (low strength, hardness). Due to the repeated rising and falling temperatures during the welding process, grain growth and plastic deformation increase until they reach an unacceptable level.

**Table 2.1** Recrystallization and melting temperatures for various metals and alloys [49]

| Materials | Recrystallization temp. | Melting temp. |
|---|---|---|
| | °C | °C |
| Zinc | 7~75 | 420 |
| Cu (99.999 wt%) | 200~250 | 1085 |
| Cr | 636~954 | 1907 |
| Zr | 618~928 | 1855 |
| Brass (60Cu-40Zn) | 475 | 900 |
| Be | 725 (429~644) | 1287 |
| Ni (99.99 wt%) | 600 (485~728) | 1455 |
| Fe | 450 | 1538 |
| Tungsten | 1200 | 3410 |

Generally, the Hall-Petch relationship theory explains the strength vs grain size relationship of electrodes [51, 52]. This theory describes the dependency of a material's characteristics based on its grain size; the bigger the grain size, the lower the yield strength and hardness. This is shown in equations (2-8) and (2-9). When electrodes experience higher temperatures during welding, electrodes soften and recrystallize on the surface. As shown in Figure 2.21, Cu and Brass which can form on the surface of electrodes decrease yield strength as grain sizes increase.

$$\sigma = \sigma_0 + kd^{-1/2}$$

(2-8)

$$H = H_0 + k_H d^{-1/2}$$

(2-9)

σ: Yield stress

$σ_0$: A materials constant for the starting stress for dislocation movement
   (or the resistance of the lattice to dislocation motion)

k: Strengthening coefficient (a constant specific to each material)

d: Average grain diameter

H: Hardness
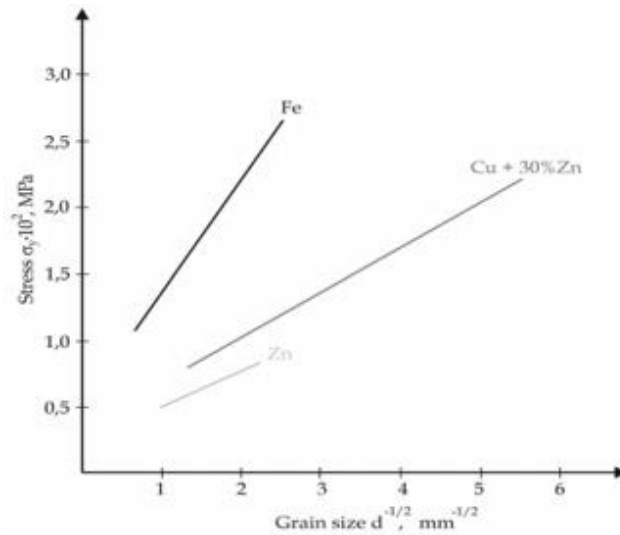


**Figure 2.20** Linear relationship between yield strength and grain size [53]

Parker et al. measured the micro-hardness in cross sections of the electrode at 0.05, 1.0, and 5.0 mm depth from the top surface [53]. As the number of welds increased, hardness decreased steadily as shown in Table 2.2. The hardness reduction for the first 10 welds was very rapid and the hardness reduction from 10 to 100 welds was far less. There was very slight change between 100 and 1000 welds. This indicates that recrystallization and grain growth are essentially complete. The largest amount of softening particularly occurs near the surface. This is attributed to the effect of the cooling water on all but the surface material. Dong et al. studied electrode surface extrusion using a finite element analysis [47]. As shown in Figure. 2. 21, maximum plastic deformation starts and accumulates at the edge of the electrodes. Eventually, weld current density decreases due to the increased total surface area. From the FEA results, they also found that long holding times and higher weld forces can accelerate this deformation. Based on these results, it appears that welding parameters and the process should be controlled to minimize or delay the electrode degradation.

**Table 2.2** Microhardness results of electrodes welded with different coated steel [53]

| Depth below alloy product, mm | Hardness reduction, HV/100 welds | | | | | |
|---|---|---|---|---|---|---|
| | Hot dip Zn coated steel | | | Zn–Al coated steel | | |
| | 0–10 welds | 10–100 welds | 100–2000 welds | 0–10 welds | 10—100 welds | 100–2000 welds |
| 0·05 | 330 | 26 | 0·5 | 360 | 25 | 1 |
| 1 | 50 | 4 | 0 | 40 | 5 | 0 |
| 5 | 0 | 1 | 0 | 10 | 0 | 0 |

\* Based on average values for locations specified in Fig. 2 (Cu–Cr–Zr electrodes).
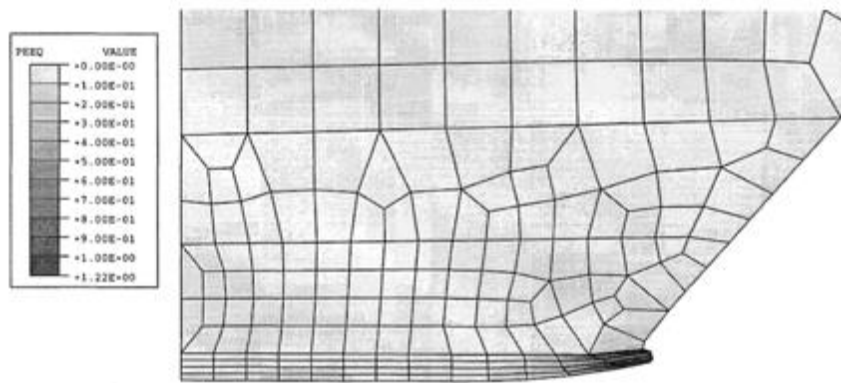


**Figure 2.21** Plastic strain distribution of electrode [47]

## 2.3.2 Attempts for improving electrode life and weldability

Improving electrode life is one of the challenges in the automotive industry because it is correlated with productivity and stabilized weld qualities. However, it is clear that electrodes cannot be used permanently, and weld quality decreases as welding occurs. To address these problems, some methods were suggested for maximizing electrode life.

Kevin, Zou et al., and Chen et al. studied about TiC/Ni coated electrode as a solution for reducing a formation of alloying, sticking, and deformation on the electrode surface [54, 55, 56]. Titanium carbide (TiC) is a hard-ceramic material and is generally used in harsh conditions that require a high corrosion,

thermal, and mechanical resistance. Most of all, because the TiC does not react with zinc, the TiC/Ni coated electrode was expected to block the interaction between copper electrode and zinc. TiC/Ni coated electrode is manufactured by an electrode spark deposition (ESD) technique using a TiC/Ni sintered composite rod. Figure 2.22 (a) shows the cross section of TiC/Ni coated electrode having a 30 to 50 µm of coating thickness. This coating layer acts as a barrier to prevent electrodes from alloying with the zinc and helps to operate at a lower weld current.
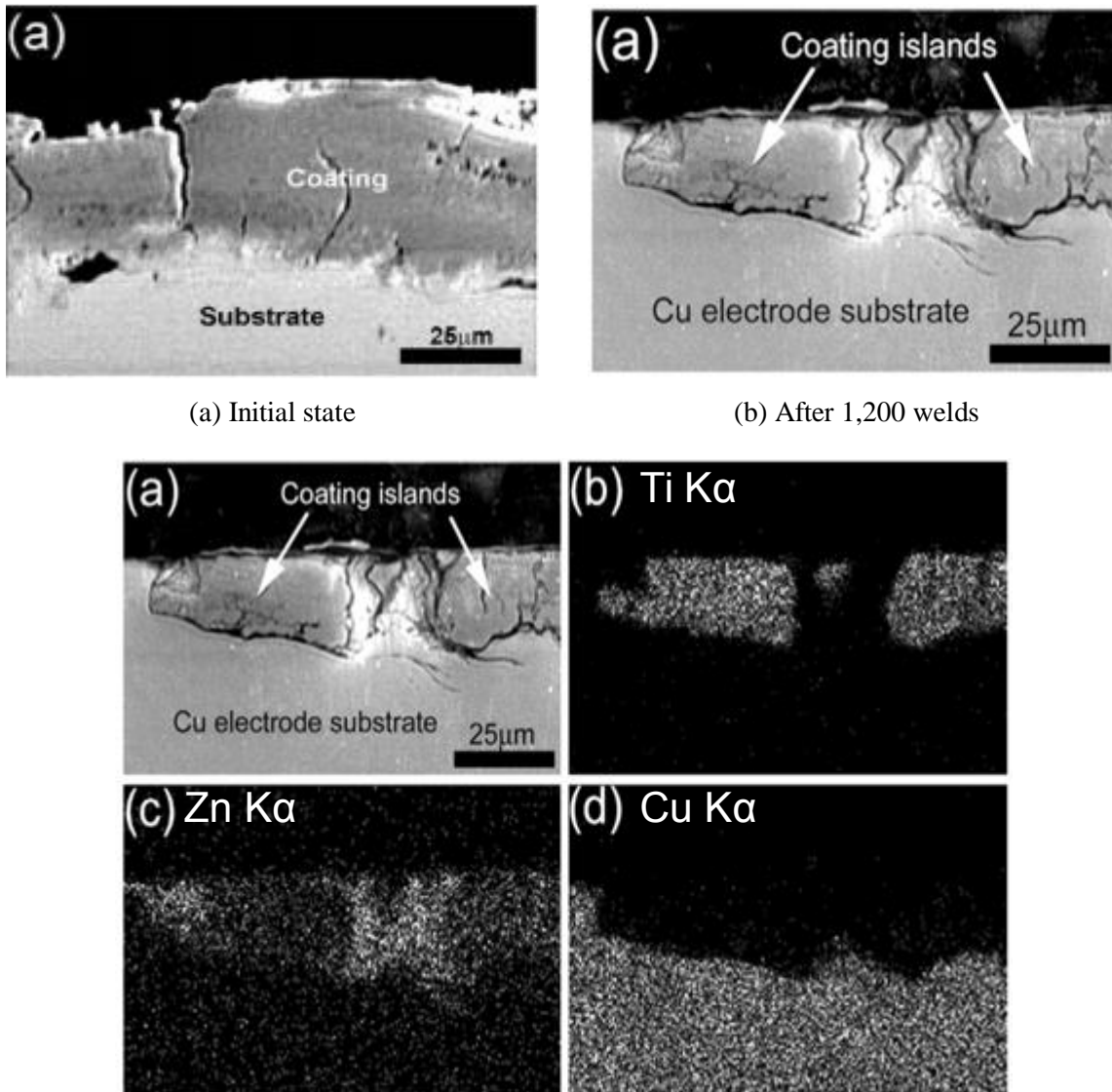


(a) Initial state

(b) After 1,200 welds

(c) Element maps after 1,200 welds

**Figure 2.22** TiC/Ni Coated electrode [55, 56]

26

As the welding progressed, the TiC/Ni coating layer break, and the zinc penetrates through the copper as shown in Figure 2.22 (b). There is still remained some of TiC/Ni coating, but Zn penetrated into Cu electrode substrate through the area which is removed TiC/Ni. Therefore, weld current density becomes low and finally form unacceptable weld. TiC/Ni coating layer was effective to delay the formation of the zinc alloying on the electrode surface. However, TiC/Ni coating layer is not permanent and will eventually wear out under the repeated high temperature and pressure welding conditions.

Key et al. studied an inserted electrode using a sintered composite insert to improve electrode life as seen in Figure 2.23 [57]. The basic concept of this electrode was reducing an electrode deformation by using refractory materials having a high hardness. The composite insert materials, such as W and Mo, were able to withstand a high welding temperature and were worn out instead of Cu electrode. As a result, with a specific volume fraction and manufacturing process, 32 vol. % W in a Cu matrix sintered for an hour, electrode degradation was reduced. As shown in Figure 2.24, the changing of electrode surface diameters between composite electrode and normal electrode has shown a different trend. In the initial stage of electrode life test, the normal electrode has shown a steady speed in electrode surface growth, but degradation speed of the composite electrode has decreased gradually. However, the composite insert introduces severe deformation from the elevated temperature which is generated from the refractory materials having a higher resistance than copper, and finally reaches to failure. Consequently, the composite insert electrode has a weakness for the deformation of the composite insert.
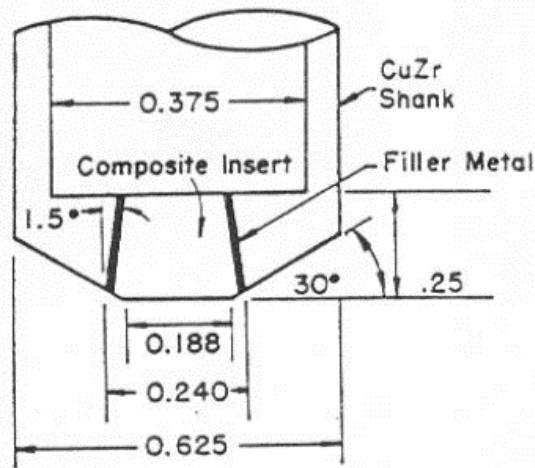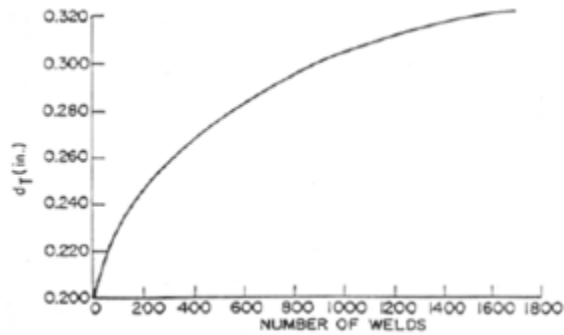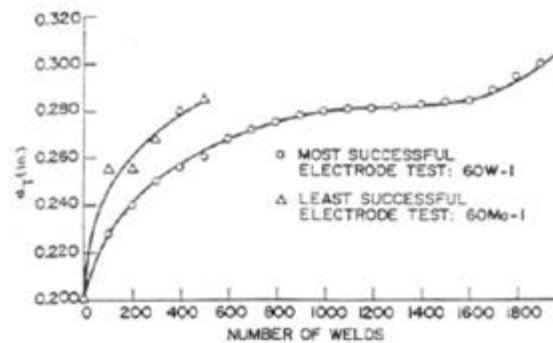


**Figure 2.23** A sintered composite insert electrode [57]

(a) Normal electrode (CuCr)



(b) Composite electrodes

**Figure 2.24** Changings of electrode surface diameter [57]

In a similar way, Shafers et al. and Mukae et al. have developed other types of inserted electrode as seen in Figure 2.25 and 2.26 [58, 59]. Insert materials were assembled to Cu electrode with same diameter of the electrode surface diameter. Many kinds of refractory materials, such as Nb, Rh, Ta, Mo, W and its alloy, were tested to find a suitable material for the insert. These electrodes, in common with composite insert electrode, were invented to solve the electrode degradation. Shafers et al. have used Rhodium (Rh) and Rhenium (Re) for insert material to weld Niobium (Nb) alloys as seen in Figure 2.25. Cu electrode has a lower melting temperature than Nb, and it caused an electrode sticking problem in spot welding of Nb alloys. However, due to a higher melting temperature of Rh and Re insert materials, the sticking problem was reduced, and electrode life was increased. Another type of inserted electrode was an electrode having a double structured insert material as seen in the Fig 2.26. To reduce cracks or deformation of insert material, Mukae et al. have controlled average particle diameters (S, L, and X in Figure 2.26) of insert material by using a heat treatment. Depending on the degree of heat

28

treatment time and temperature, insert materials have different hardness, particle diameters, and different number of cracks. As a result, the heat treated inserted electrodes have formed electrode life from 3,000 to 10,000 welds.
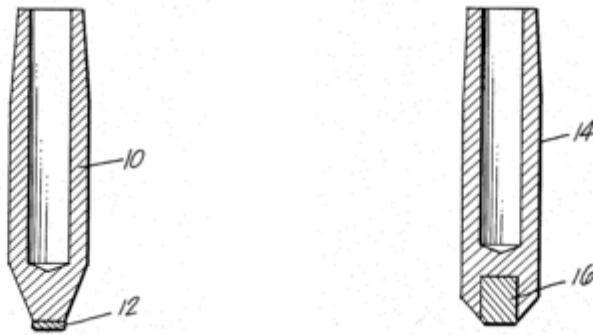


**Figure 2.25** Inserted electrode having a Nb insert [58]
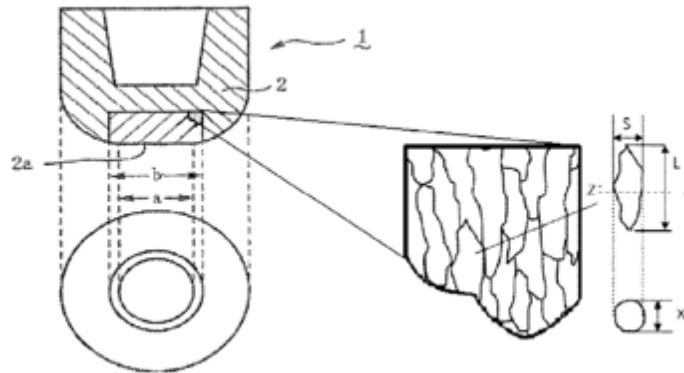


**Figure 2.26** Heat treated inserted electrode [59]

These inserted electrodes mentioned above have advantages for increase electrode life and improve weldability. However, some issues, such as sticking problem, durability, and manufacturing, have been reported. Basically, the inserted electrodes were required additional process of heat treatment and different assembly methods, and filler metal for fabrication. These factors made the manufacturing difficult and increased the manufacturing cost. In addition, due to the high resistance which is formed high between electrodes and base materials, sticking problem is occurring and makes a pitting from the loss of insert material.

Electrode geometry is also an important factor for increase of electrode life and improvement of weldability [32,33,34,67]. Figure 2.27 shows general electrode external shapes, and these electrodes are adopted with consideration for the welding conditions or requirement such as flange/corner weld, high criterion of weld qualities, and so on [50].
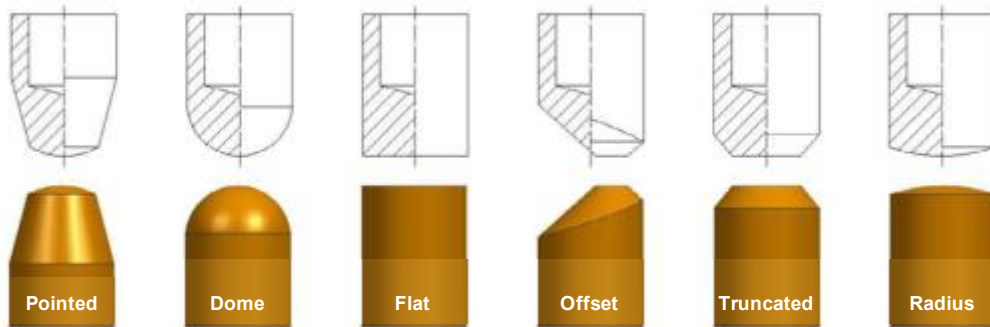


**Figure 2.27** Electrode external shapes [50]

Kim et al. studied about heat conduction of truncated shaped Class 2 electrodes having different face lengths of 2.8, 4.7, 6.6, and 8.5 mm as seen in Figure 2. 28 [32]. As the face thickness increases, the maximum electrode surface temperature increased except 2.8 mm. After 20 welds, 8.5mm electrode shown a constant temperature, but 2.8mm electrode made a steep increase after 10 welds.



**Figure 2.28** Changing of maximum electrode surface temperature [32]

30

Based on this result, shorter face length did not guarantee a better heat conduction, and there existed an optimal face thickness between 4.7 and 8.5mm. Rao et al. investigated the effect of cooling water with a new cone-fin electrode [33]. As seen in Figure 2.29, the new cone-fin electrode has an extruded fin on the 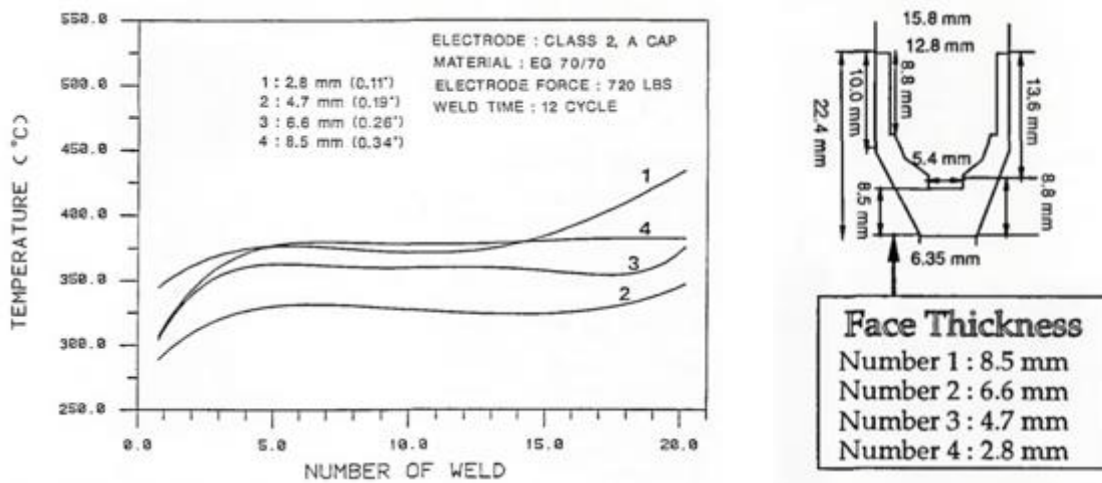inner side of the electrode, and it improved the heat transfer between cooling water and electrode. To evaluate the effect of the fin, fin temperature was calculated using a Bessel type differential equation. In the case of conventional electrode, the temperature increased to 126.85℃. On the other hand, fin electrode decreased the temperature up to 26.85℃.
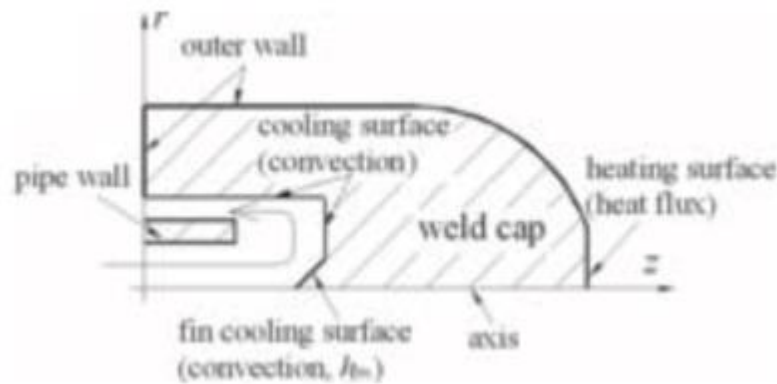


**Figure 2.29** Changing of maximum electrode surface temperature [33]

In terms of external shape of electrode, Li et al. demonstrated the effect of cone angle of truncated electrode on heat transfer and used four kinds of cone angles, 15, 30, 45, and 60° [67]. When weld current flew through steel sheet, current density was formed unequally. Especially, the low cone angle electrode had more ununiformed weld current density (same as stronger electromagnetic stirring in the weld nugget), and it was effective for mixing the weld metal and reduced the temperature gradient. Thus, the lower cone angle electrode allowed the lower maximum temperature and faster cooling rate during the weld. Figure 2.30 (a) shows a temperature distribution for each cone angle electrodes. The highest (60°) angle electrode made a higher temperature on the electrode surface than the others because the smaller volume and mass caused a lower heat dissipation. Figure 2.30 (b) demonstrated the performance of heat dissipation. As the cone angle increases, the temperature gaps between electrode surface and 3mm distance away became smaller, and average temperature was increased. Eventually, a high angle electrode accelerated electrode degradation, and electrode life became short as seen in Figure 2.31.

31
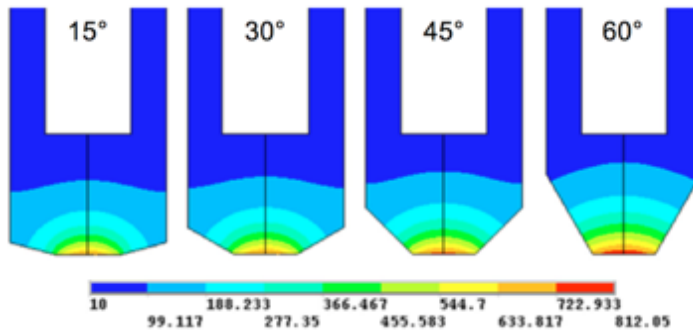
(a) Temperature field of different cone angle electrode
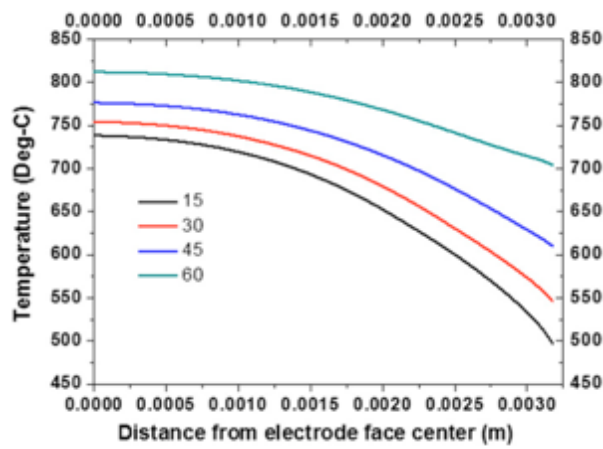


(b) Temperature distribution from the electrode surface

**Figure 2.30** Temperature distribution of different cone angle electrode [67]
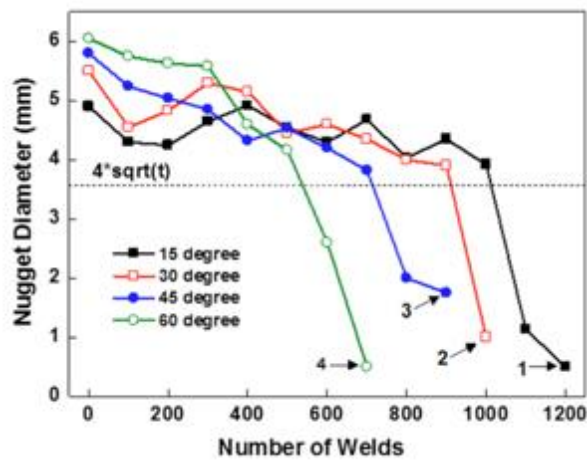


**Figure 2.31** The results of electrode life tests [67]

## 2.4 Summary

In this chapter, the basic principles about the RSW were introduced and investigated the fundamental causes for cracking and decreasing the weld qualities in AHSS from a mechanical and metallurgical perspectives. As a result, the bigger weld nugget geometry helps to further improve the mechanical performance. However, more heat input is required to melt a larger area, and it may also lead to the enlarged HAZ. Therefore, the welding parameters should be adjusted properly to make a bigger weld nugget with the smaller heat input, and in terms of weldability and reliability, expanding the lobe curve is another big challenge in the steel and automotive industry.

Additionally, the electrode plays an important role in determining the weldability and reliability. Even if the optimized welding parameters are selected, it is because the electrode condition continuously changes. Therefore, the weld qualities cannot be guaranteed during a large number of welds. To solve this issue, there has been a lot of effort, and electrode life has accomplished much improvement through these methods.

# Chapter 3
# Experimental Methods

## 3.1 Materials

The steel sheet used in this study was 1.0 mm thick AHSS DP600 with galvanized (GI) coating, supplied by ArcelorMittal Dofasco, Hamilton Canada. The chemical composition and mechanical properties of DP600 steel are listed in Tables 3.1 and 3.2, respectively. The average coating thickness on the top and bottom steel surfaces was 7.11 µm as shown in Figure 3.1.

**Table 3.1** Chemical Composition of DP600

[Unit: wt%]

| C | Mn | P | S | Si | Cu | Ni | Cr | Mo |
|------|------|-------|-------|-------|-------|-------|--------|-------|
| 0.1 | 1.83 | 0.011 | 0.003 | 0.15 | 0.02 | 0.01 | 0.35 | 0.003 |
| Als | Alt | Cb | V | Ti | Ca | N | B | |
| 0.034 | 0.036 | 0.002 | 0.003 | 0.018 | 0.004 | 0.006 | 0.0002 | |

**Table 3.2** Mechanical properties of DP600

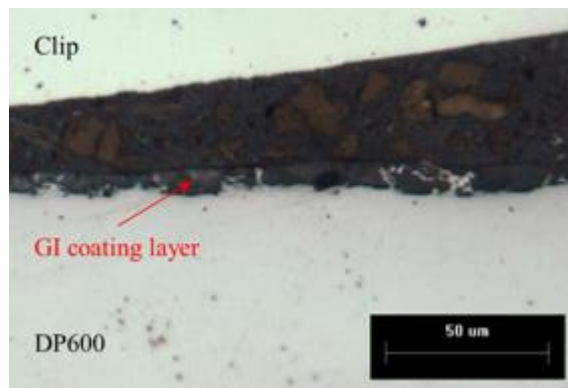| Yield Strength | Ultimate Strength | Elongation | Coating Thickness |
|----------------|-------------------|------------|-------------------|
| 356 MPa | 648 MPa | 25% | Top surface: 6.19 **µm** <br> Bottom surface: 8.02 µm |



**Figure 3.1** GI coating layer of DP 600

34

## 3.2 Equipment

### 3.2.1 Welding Machine

Welding experiments were conducted with a pedestal-type, pneumatically controlled, 250 kVA, 60Hz single phase AC RSW machine with constant current control operating. Welding parameters were controlled by a Robotron[TM] Series 400 system controller. Figure 3.2 shows the setup of the AC RSW machine used in this study. The automatic spot welding system was developed by using an Arduino UNO R3 microcontroller and is used to keep a steady welding speed (20 welds/min.) during the electrode life tests.
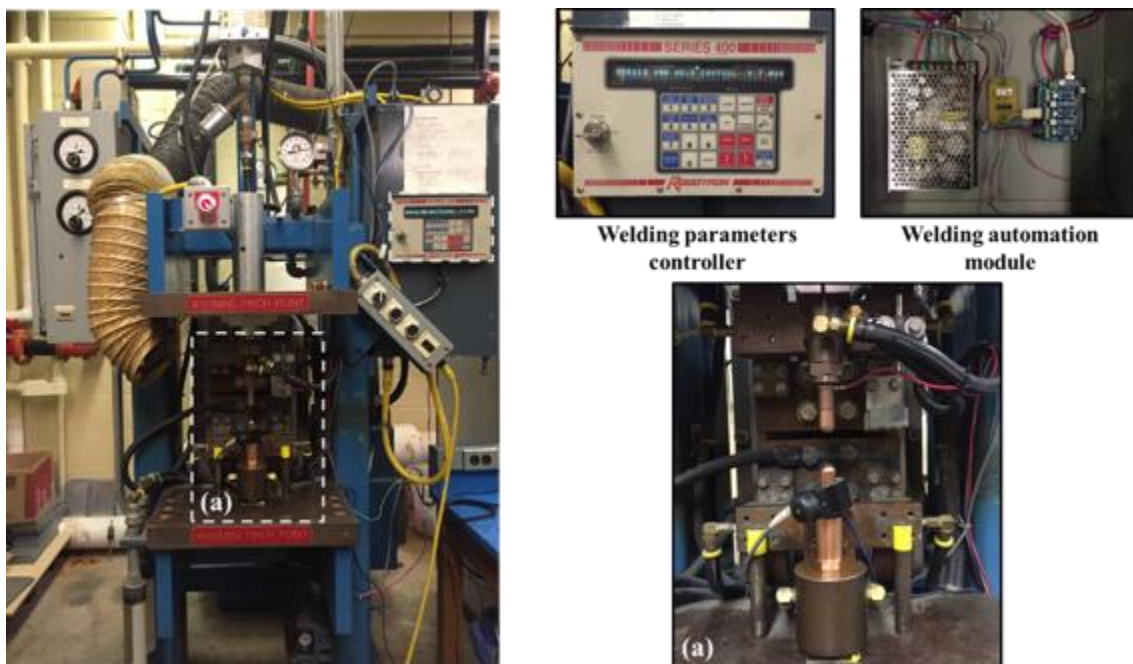


**Figure 3.2** The AC RSW machine

### 3.2.2 Measurement of Welding Signals

A data acquisition system (DAQ) was used for weld quality monitoring and measurement of the welding signals; weld current, weld force, weld voltage, and electrode displacement. Figure 3.3 describes the schematic of the welding signal measurement. A DLD-V SENSOTEC LVDT sensor and modulator were used for the measurement of electrode displacement, and a KISTLER 9041A force sensor was used for measurement of the weld force. For the measurement of weld current, a Miyachi

MB-25E hall sensor was used. The raw welding signals are collected by the DAQ board and displayed using LabVIEW software. At this point, the welding signals are not yet converted to real values, so secondary data processing is required. In this study, the mathematical software MATLAB R2015a was used for conversions. Figure 3.4 indicates the raw welding signals which are seen in the LabVIEW software before secondary data processing.
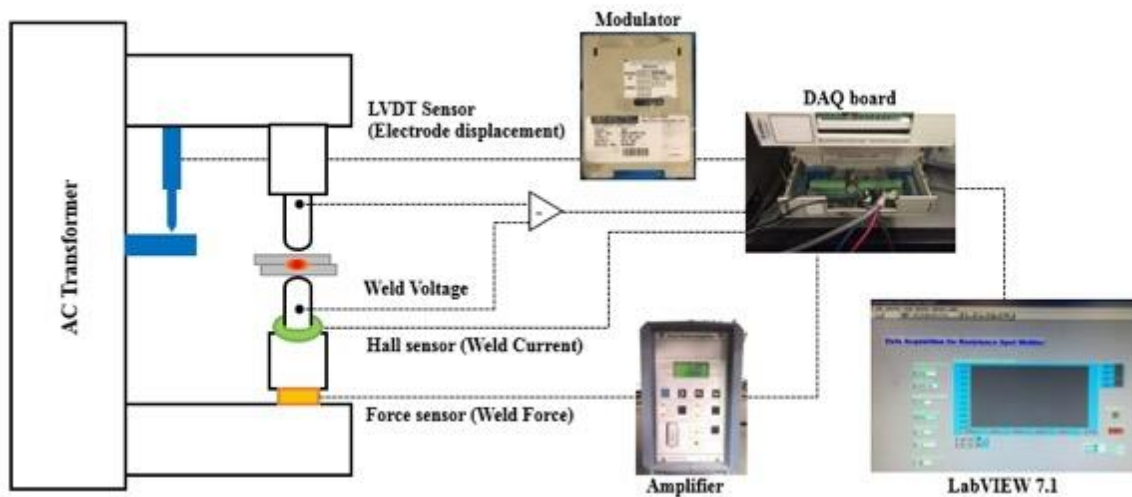


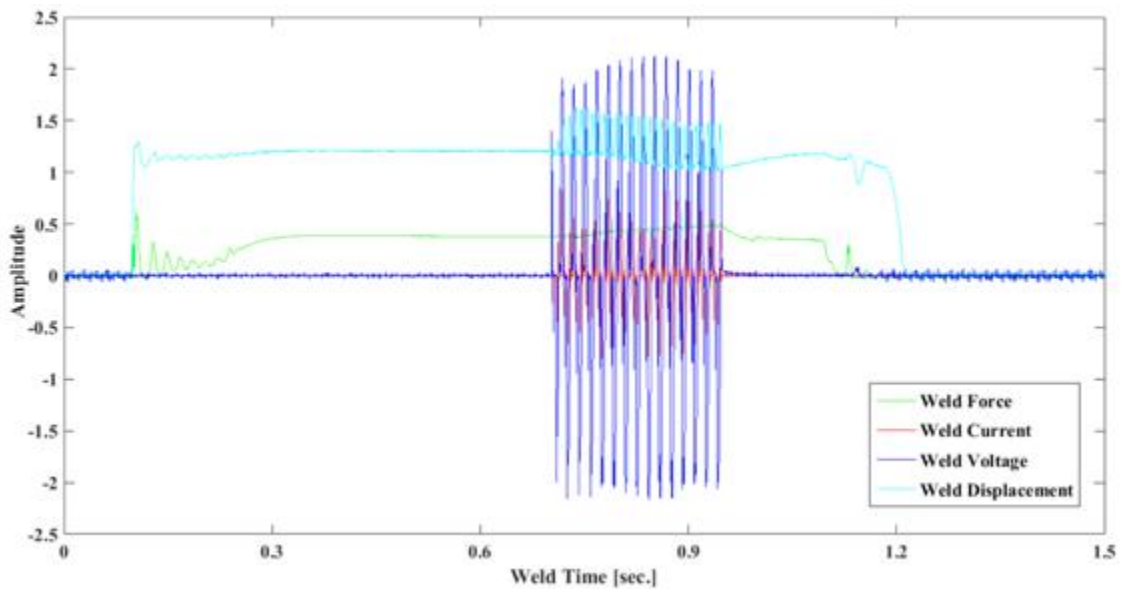**Figure 3.3** Schematic of the welding signal measurement



**Figure 3.4** Measured raw welding signals

36

## 3.3 Electrodes

The electrodes used for this study have a diameter of 16mm and a face diameter of 6mm, as specified by AWS D8.1M for group 3 (tensile strength > 500~800MPa) steels at 1.0mm in thickness [61].

### 3.3.1 Electrode Material

Class 2 (Cl2) and Class 3 (Cl3) copper electrode were compared to investigate the effects of material on electrode life. The material properties of Cl2 and Cl3 Cu are shown in Table 3.3. The difference between these electrodes is that Cl2 electrode has a higher electrical conductivity and a lower micro-hardness than the Cl3 electrode [50].

**Table 3.3** Material properties of Class 2 and Class 3 electrodes [50]

| Electrodes | Hardness [HV] | Electrical conductivity | Chemical compositions | | | | | | |
| --- | --- | --- | --- | --- | --- | --- | --- | --- | --- |
| | | | Cu | Fe | Ni | Cr | Si | Be | Zr |
| Cu | < 105 | 100 %IACS | 100 | - | - | - | - | - | - |
| Class 2 | 170~190 | 75~80 %IACS Min. | Rem. | - | - | 0.5~ 1.5 | - | - | 0.02~ 0.2 |
| Class 3 | 200~210 | 45 %IACS Min. | Rem. | 0.1 max. | 1.4~ 2.2 | - | 0.2 max. | 0.2~ 0.6 | - |

### 3.3.2 Electrode Geometry

Dome shaped and parabolic shaped electrodes were tested to investigate the geometric effects on electrode life. Figure 3.5 demonstrates the geometric differences between these two kinds of electrodes. The face thickness of parabolic shaped electrode is shorter than that of dome shaped electrodes.
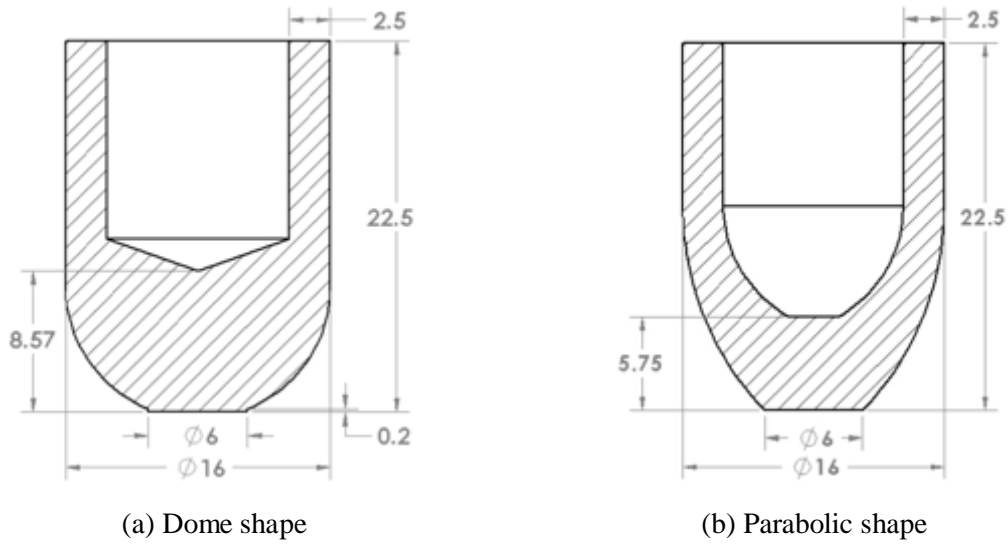
|               |               |
|:-------------:|:-------------:|
| (a) Dome shape | (b) Parabolic shape |

**Figure 3.5** Electrode Geometry

### 3.3.3 Electrode Coated with TiC/Ni

TiC/Ni coated electrodes were investigated to study effects of coating on electrode life. A TiC/Ni coating was applied to the electrode's surface by Electro Spark Deposition (ESD) process. The thickness of the TiC/Ni coating was approximately 30 to 50 µm and a cross-sectional image of a TiC/Ni coated electrode is shown in Figure 3.6.
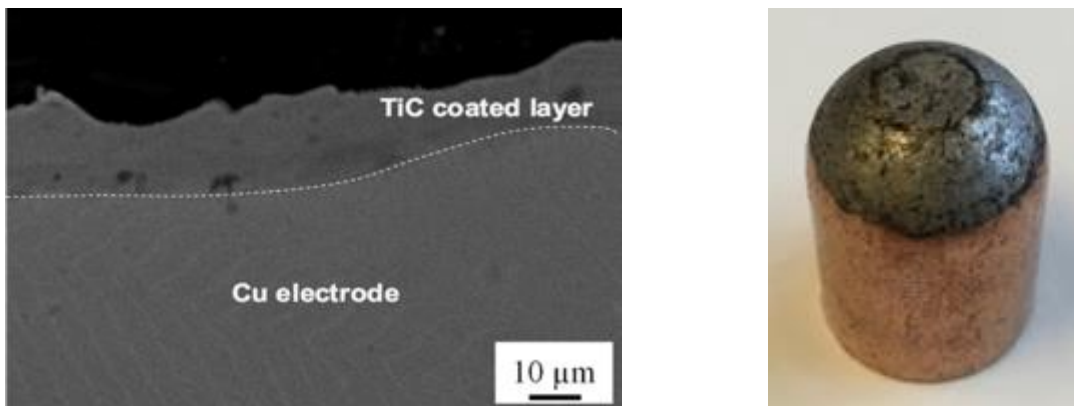


**Figure 3.6** Cross sectional and surface images of the TiC/Ni coated electrode

### 3.3.4 Electrode Static Resistance

To verify how the electrode resistance changes depends on the electrode surface conditions and applied weld forces, four-wire static resistance measurement was performed as shown in Figure 3.7 (a). The resistance was measured by using a four-wire micro ohmmeter (Agilent 34420A 7 ½ digit Nano Volt / Micro Ohm Meter) under different force values. To measure the resistance of the electrodes and avoid a misalignment problem, 1mm thick copper plate was inserted between electrodes. The force was manually applied and measured with force gauge (M5-1000) from 100 to 400kgf. Figure 3.7 (b) shows the measurement system for the electrode static resistance.
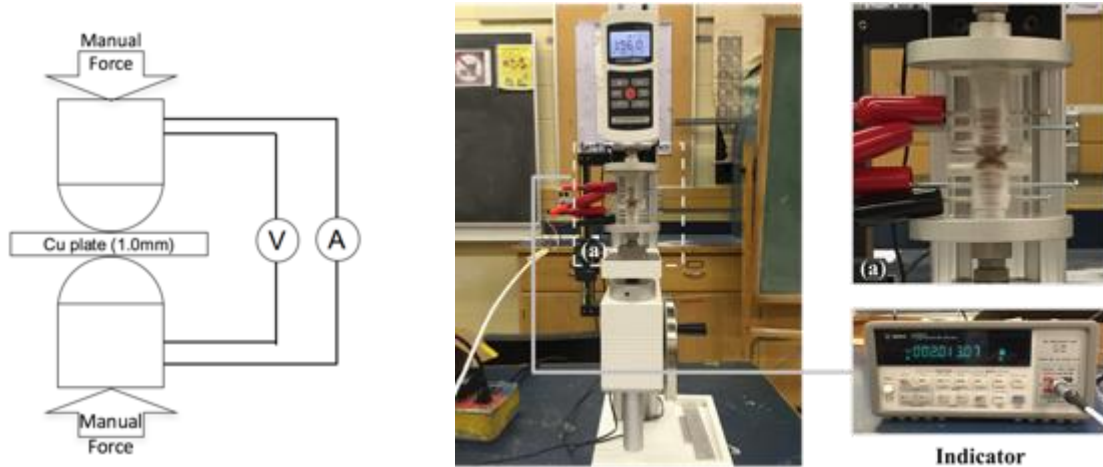


(a) Schematic of measurement device      (b) Experimental setup

**Figure 3.7** Measurement of electrode static resistance

### 3.4 Electrode life test

Electrode life testing was performed following AWS D8.9 standards [61]. Endurance testing was carried out on a panel measuring 126mm x 360mm as shown in Figure 3.8 and conducted with a prescribed welding direction. Table 3.4 shows the fixed welding parameters for electrode life testing. Welding current can change due to electrode conditions. Therefore, the operating weld current was set 200A below the weld current that resulted in expulsion during the preliminary tests. During electrode life testing, one tensile shear test, one peel test, one cross sectional examination, and one imprinted image were made every 100 welds.
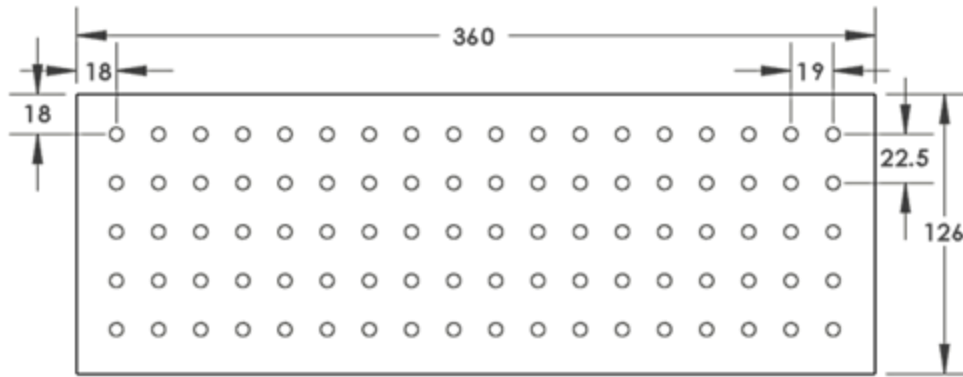
**Figure 3.8** Endurance test panel

**Table 3.4** Welding conditions for electrode life test [61]

| Squeeze time | Weld time | Weld force | Hold time | Cooling water | Welding rate |
|---|---|---|---|---|---|
| 30 cycles | 15 cycles | 326 kgf | 5 cycles | 4 l/min. | 20 welds/min. |

## 3.5 Mechanical tests

### 3.5.1 Strength tests

Strength tests for tensile shear and cross tension specimens were performed using an Instron universal testing machine with 10 mm/min of strain rate. Each specimen was prepared according to the dimensions in AWS D8.9 standard and tested with specific fixtures. Figure 3.9 shows the specimen dimensions and test method.
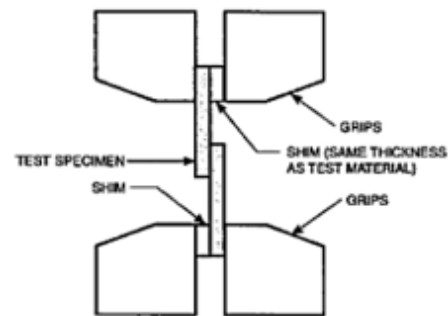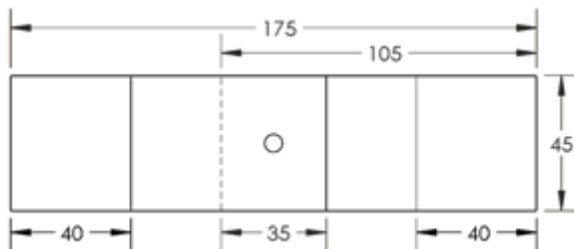


(a) Tensile shear specimen and test set-up

40
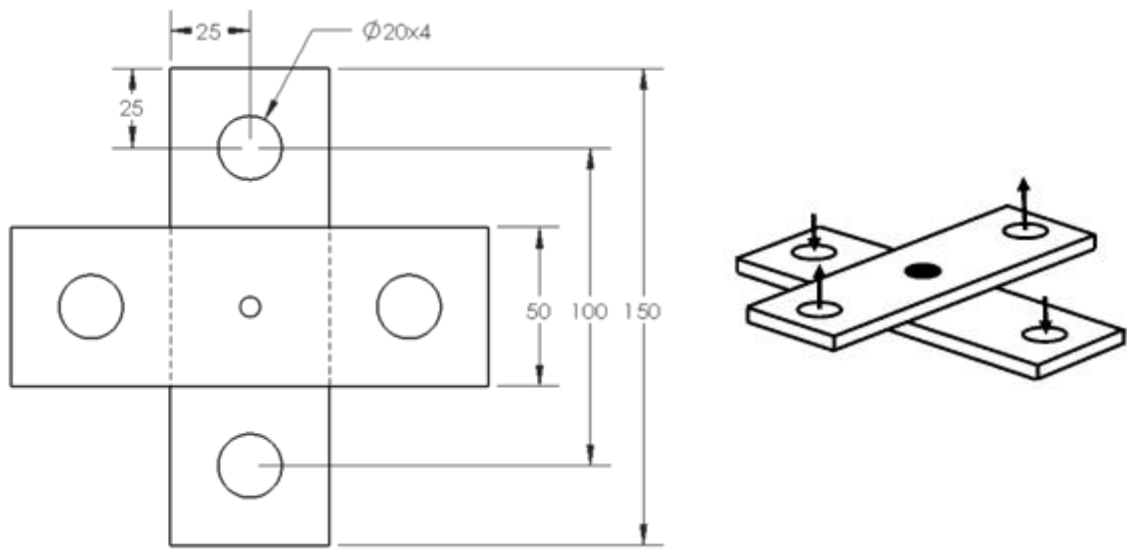
(b) Cross tension specimen and test set-up
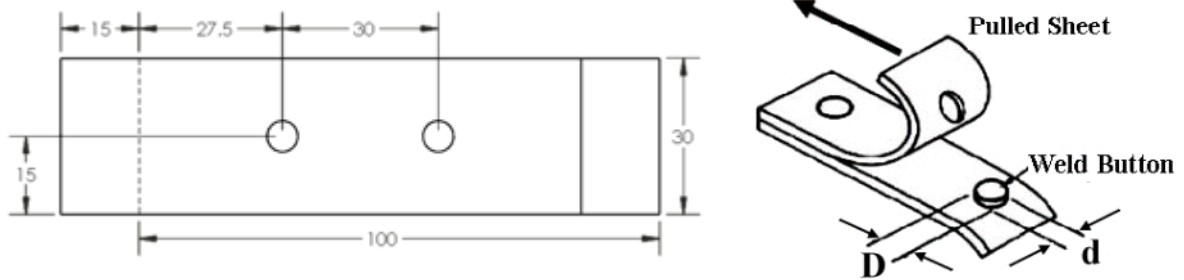


(c) Peel test specimen and test set-up

**Figure 3.9** Strength test methods [61]

## 3.5.2 Imprinting Image

Imprints were made to measure changing electrode surface area during electrode life testing. As the number of welds increase, the electrode surface area increases as well. To analyze the electrode surface degradation, imprinted images were measured every 100 welds by using a carbon paper as shown in Figure 3.10 below while applying weld force. The electrode contact surface areas were calculated with Image J software.
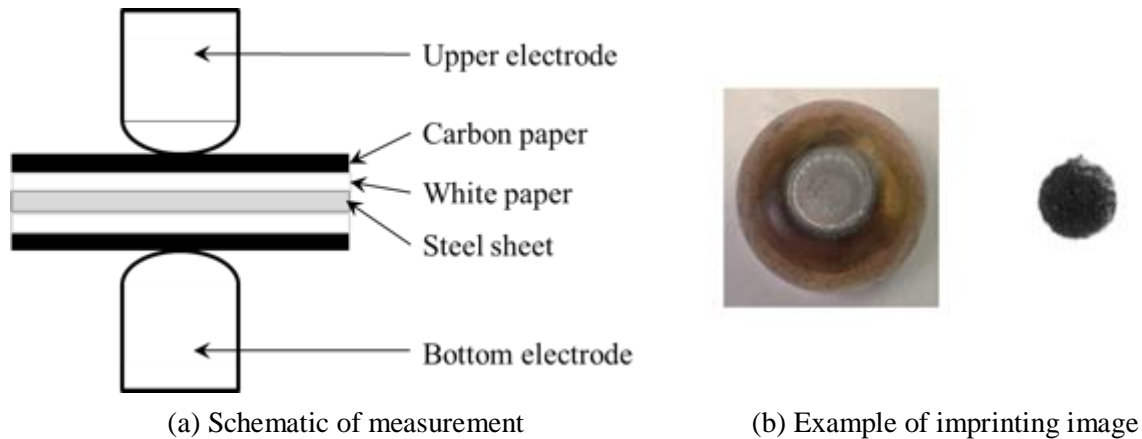
| (a) Schematic of measurement | (b) Example of imprinting image |

**Figure 3.10** Measurement of imprinting test

## 3.6 Metallographic Characterization

Metallographic cross section samples were cut through the center of the weld using an abrasive cut-off saw. The cross sectioned samples were hot mounted in conductive phenolic compound (Struers Polyfast$^{TM}$) or cold mounted in epoxy resin. The mounted samples were mechanically ground using finer silicon carbide papers (180, 600, 1200grit) and polished with diamond suspended lubricants from 6.0µm to 1.0µm particle size. Metallographic etching was conducted with 4% (HNO3OH) Nital etching for a few seconds for optical microscopy and scanning electron microscopy (SEM) test. Copper electrodes were etched using an etching liquid mixed with 50% Acetic acid and 50% Nitric acid. This process was performed very quickly due to the strong acid reaction.

Optical microscopy for observing the spot weld area was performed using an Olympus BX51M microscope with QCapture Pro Ver. 5.1 imaging analysis software. Scanning Electron Microscope (SEM) for analysis of the electrode coating layer and microstructural examination (JEOL JSM-6460) was performed using a Zeiss Leo model 1550. An EDS (Oxford Instrument Microanalyses System) fitted to the electron microscope was used to analyze elemental compositions in the coatings.

## 3.7 Microhardness

Microhardness in the polished cross section weld specimens was measured by using a Clemex-JS 2000 automated hardness test machine with 500g load and 15sec dwelling time. The measurement pattern of hardness profile was followed the AWS D8.9 standard as shown in Figure 3.11 [61]. There were larger

42

changes in the hardness in the HAZ area, as compared to the other regions, therefore, the measurement distance interval in the HAZ was set to half the length of that in the BM and weld nugget regions.
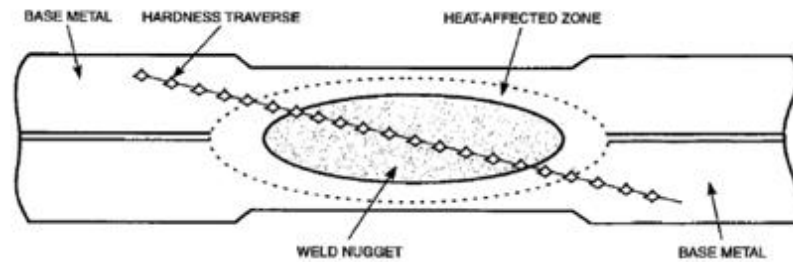


**Figure 3.11** Measurement of Hardness [61]

# Chapter 4
# Effects of TiC/Ni Coating on Electrode Life

In this chapter, electrode life was evaluated for the zinc coated AHSS. From the literature review in Chapter 2, it was revealed that the electrode is one of the most important factors which is deciding the weld qualities in RSW process. Using more specific electrode parameters, such as electrode material, geometry, and coating layer on the electrode surface, electrode life was evaluated through the mechanical and metallurgical methods and analyzed to select the general specification for the electrode.

## 4.1 Evaluation of Electrode Life

Electrode life was evaluated by weld strength from tensile shear test, button size from peel test, and nugget diameter from cross section test. Figure 4.1 shows the changing of these weld qualities through electrode life tests. The criterion of weld strength is the same as the ultimate strength of DP 600 steel, 648MPa, and electrode life is defined as the number of weld when the strength is less than the criterion. The minimum allowable weld button and nugget diameter are 4.0 mm which is derived from the AWS D8.1 standard criterion, $4\sqrt{t}$ (t, being the thickness of the steel). Electrode life was determined as the number of welds at which button diameter is below the corresponding criterion value [61], but the other weld qualities, TS strength and nugget diameter, were used for evaluation of electrode life. Each criterion for TS strength and nugget diameter were 648MPa, same as the ultimate strength of base material and $4\sqrt{t}$, same standard criterion. Based on the results, the Class 2 TiC/Ni coated dome shaped electrode has the most improved electrode life of around 1,900 welds. Parabolic shaped electrodes have shown fluctuated weld qualities on uncoated and TiC/Ni coated electrodes because the contact area has greatly increased during this period, and it made the decrease of weld current density speed up. Especially the button size, which is getting a shunt effect from the first weld, decreases faster than the other weld qualities. The electrode life for uncoated parabolic shaped electrodes was about 500 welds and the TiC/Ni coating did not exhibit significant effects on electrode life. The results indicated that Class 3 electrodes, both of uncoated and TiC/Ni coated, had shorter electrode life than Class 2 electrodes due to higher heat loss between electrode and steel sheet and within the electrode itself. As a result, the Class 3 electrodes had the shortest electrode life around 200 welds. Even if the electrode coated with TiC/Ni, it did not improve the electrode life as much as Class 2 electrode.
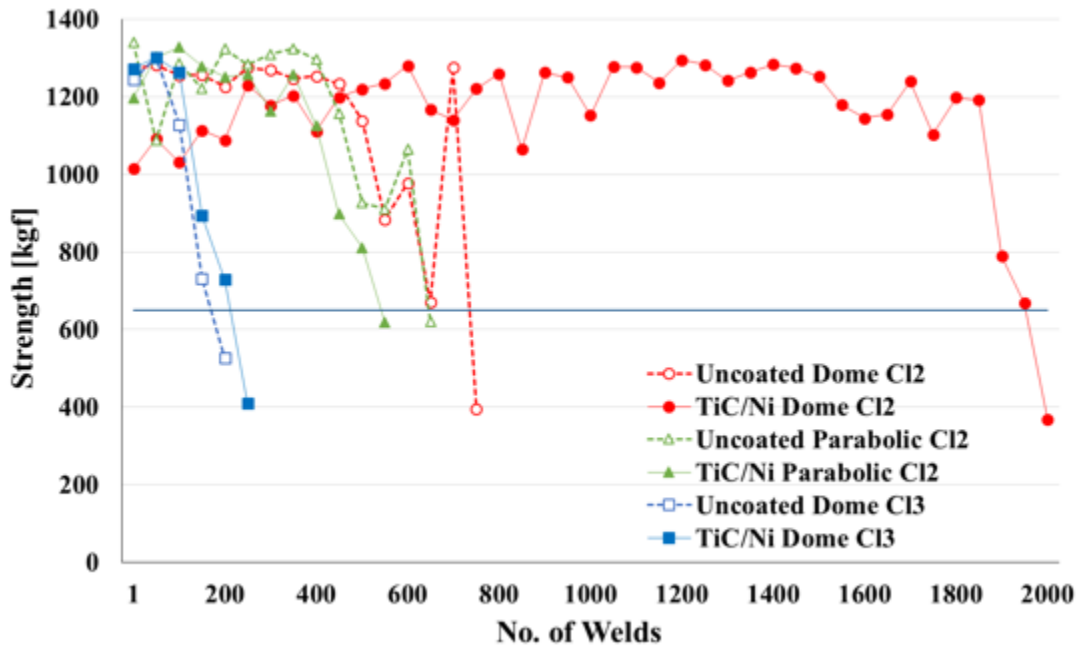
(a) Tensile shear strength
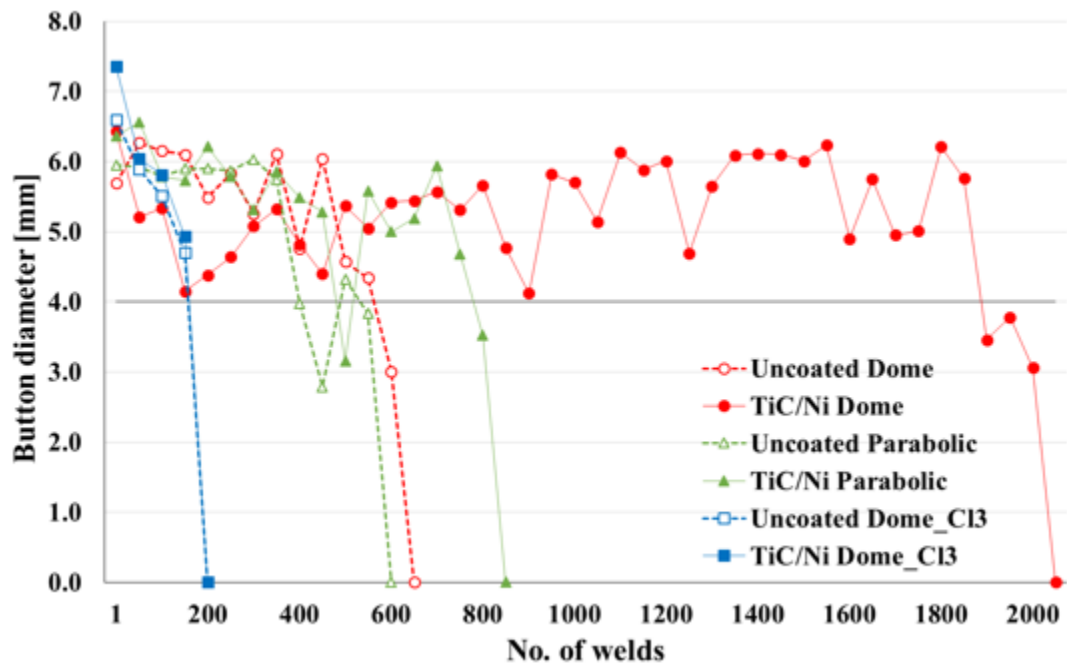


(b) Button diameter from peel test

45
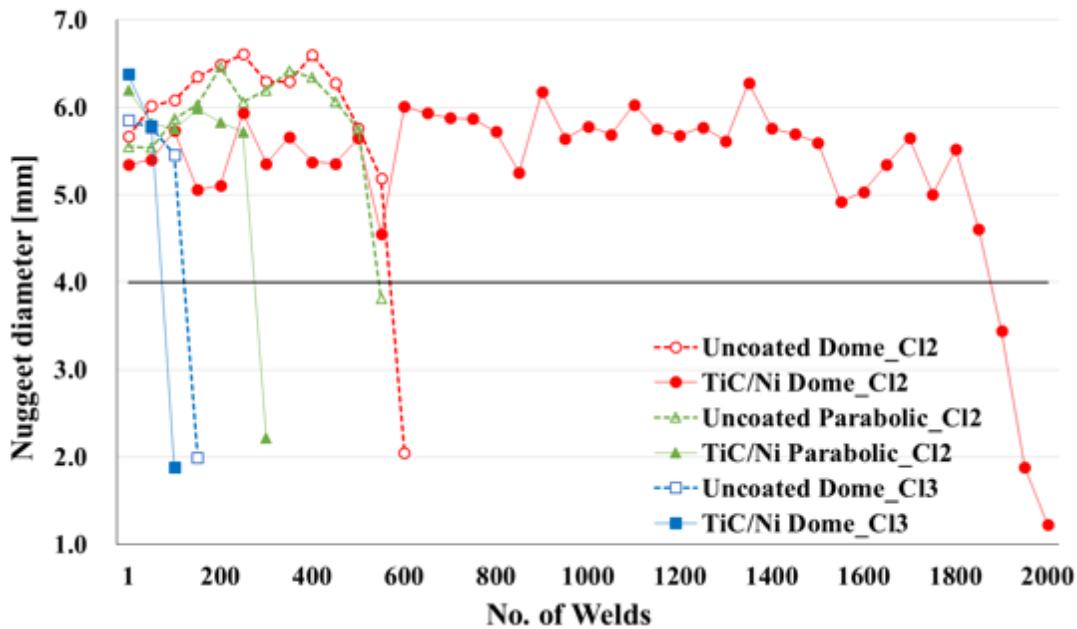
(c) Nugget diameter

**Figure 4.1** The results of electrode life test

## 4.2 Requirements for the Electrode

The electrode serves to deliver the weld current and force to steel, and it has a significant influence on electrode life. Therefore, selecting the appropriate electrode is necessary to meet the weld requirement, such as strength or nugget diameter [50]. Generally, there are some of the requirements for the electrode. First, the material of the electrode should have a high thermal conductivity and a low resistivity. The main component of the electrode is copper, and it is easy to soften from the resistance heat and makes deformation at the temperature about 500℃ above [62, 63]. If the thermal conductivity is high, the cooling effect is better, and the electrode degradation can be slow down. Second, the electrode is subjected to a high pressure repetitively during the weld. Thus, the electrode requires appropriate mechanical properties, such as hardness, compressive strength [13]. Last, the electrode has to have an optimal outer shape which can prevent the electrode from overheating. The electrode having a larger surface area is more effective to conduct the welding temperature to cooling water [64]. However, all these properties cannot be satisfied at the same time. Therefore, it is necessary to investigate and understand the welding characteristics for the different electrodes.

46

### 4.2.1 The Effect of Electrode Material and Coating

To evaluate the effect of electrode material, Class 2 and Class 3 electrodes were tested. The main difference between the two electrodes is having a different electrical resistivity and hardness [50]. Under the condition applying only weld force, the measured contact resistances are the same as the Figure 4.2. The electrical resistance of the Class 3 electrode was formed two times higher than Class 2 electrode at the operating weld force, 326 kgf. In the case of TiC/Ni coated electrodes, the contact resistance was formed higher than uncoated electrodes due to the high resistance of TiC/Ni layer, and also Class 3 electrode had a higher contact resistance as well. For this reason, the operating weld current of TiC/Ni coated electrode was set to lower than uncoated electrodes.
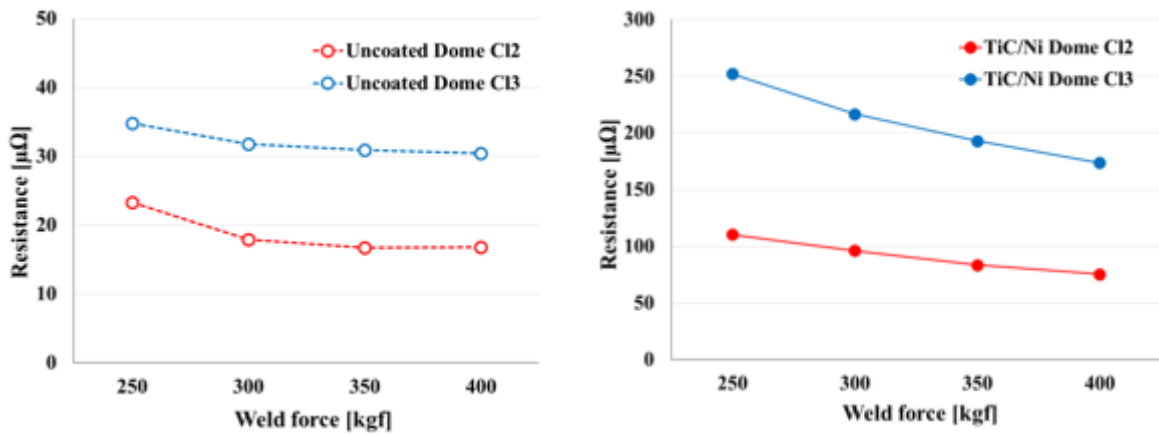


| (a) Uncoated electrodes | (b) TiC/Ni coated electrodes |

**Figure 4.2** Initial static contact resistance of Class 2 and Class 3 electrodes
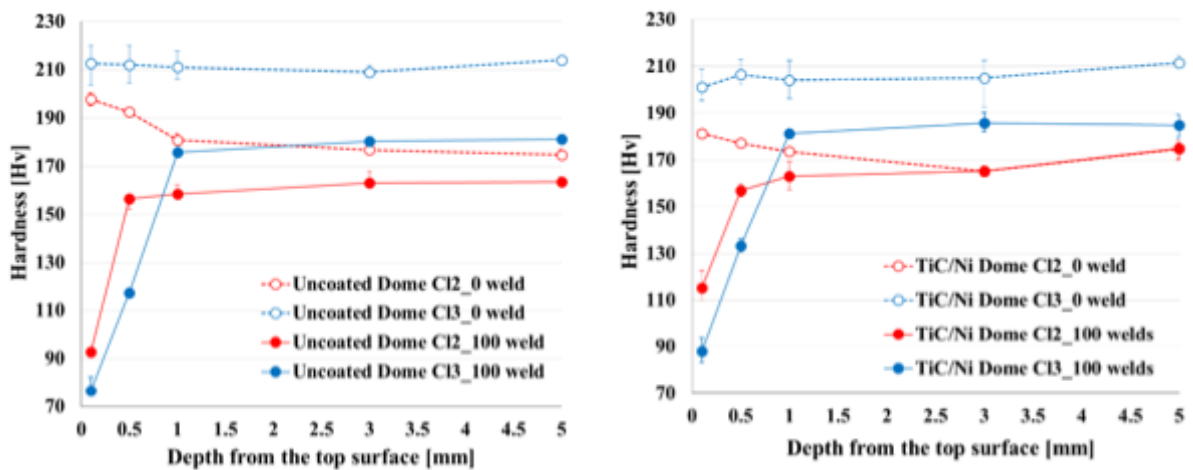


| (a) Uncoated electrodes | (b) TiC/Ni coated electrodes |

**Figure 4.3** Hardness of Class 2 and Class 3 electrodes

From the measurement of static contact resistance, it was revealed that Class 3 has a higher resistance and will generates more resistance heat between electrode and steel sheet. To observe the effect of contact resistance, a hardness test was performed on the cross-sectional samples of each electrodes as shown in Figure 4.3, and repeated three times. Using the electrodes completed 100 welds, the hardness was measured 0.1, 0.5, 1.0, 3.0, and 5.0mm below from the top of the electrode. The hardness of the Class 3 electrode was higher than Class 2 at initial condition of electrode. However, the bigger hardness drop was made on the Class 3 electrode after it finished 100 welds. Especially, the hardness drop was made until 1.0mm below from the top surface of electrode. The more heat, which is generated from the weld nugget, contributed to acceleration of softening on the electrode surface and also led to decrease the hardness. Through these results, it was revealed that the higher hardness property of Class 3 electrode was not effective to maintain the initial surface area for the weld temperature.

**Table 4.1** The melting temperature of the alloying elements of the electrodes

| Electrode | Alloying | Fe | Ni | Cr | Si | Be | Zr |
|---|---|---|---|---|---|---|---|
| Class 2 | Elements (wt %) | - | - | 0.5~1.5 | - | - | 0.02~0.2 |
| | Melting temp. [℃] | | | 1,860 | | | 1,854 |
| Class 3 | Elements (wt %) | 0.1 max. | 1.4~2.2 | - | 0.2 max. | 0.2~0.6 | - |
| | Melting temp. [℃] | 1,538 | 1,453 | | 1,411 | 1,285 | |

The recrystallized area is another way to evaluate the degree of softening [63]. If the recrystallization occurs, the fine or elongated grain structures are detected near on the electrode surface, and these regions are accompanied by a low hardness. Generally, the recrystallization is defined as the nucleation and grain growth of the stress-free grains in the material, and there are some critical variables which are influencing the recrystallization; temperature, strain, initial grain size, and purity of the material [65]. Most of all, the temperature is the most important factor to decide the degree of recrystallization in RSW. For the copper material, the recrystallization temperature is formed in the range of 30% (350℃) to 50% (550℃) of the melting temperature. The electrode is made with some of the elements, therefore, the recrystallization temperature increases more than the pure copper. Considering the melting temperature of alloying elements in the Table 4.1, Class 3 electrode has a lower

recrystallization temperature than Class 2 electrode. Even though the Class 3 electrode has a higher hardness, it is not suitable for delaying the electrode deformation as much as Class 2 electrode.



(a) Recrystallized depth of Class 2 electrodes
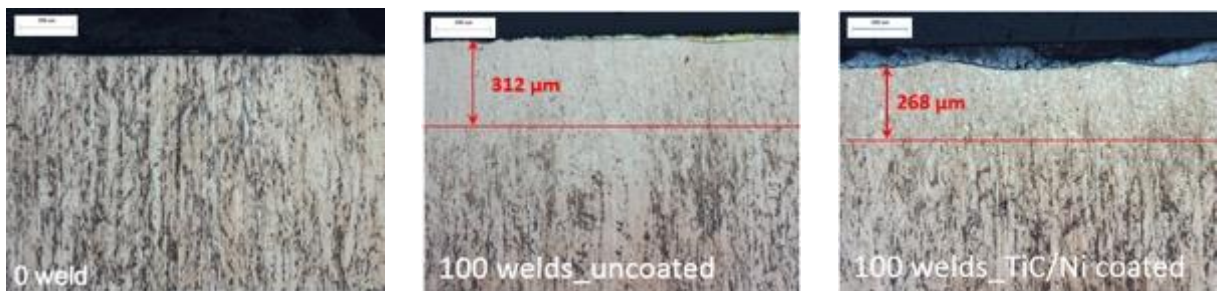


(b) Recrystallized depth of Class 3 electrodes

**Figure 4.4** Recrystallization of the electrodes

Figure 4.4 shows the recrystallized area that is formed at 100 welds and final welds. To compare the changing of recrystallization, initial state electrode was observed. In the case of uncoated and TiC/Ni coated Class 3 electrode have shown a thicker recrystallized depth, 312µm and 268µm. On the other hand, the Class 2 electrodes have a relatively thinner recrystallized area. The formation of recrystallized depths has shown a similar trend to the hardness result in Figure 4.3. The TiC/Ni coated electrodes have a slightly higher hardness than uncoated electrodes.

Based on the above results, imprinting results were analyzed for the evaluation of electrode life as Table 4.2 below. Using these results, weld current density was derived as Figure 4.5 (a). The initial weld current density was almost same, but the decreasing speed (slope of each curves) was different. Most of all, all electrodes, except TiC/Ni coated Class 2, have reached to 6.6 mm of electrode diameter at 300 welds as shown in Figure 4.5 (b). Thus, TiC/Ni coated Class 3 electrode requires a lower operating weld current of 9.5kA, resulting in a smaller nugget diameter by the lower weld current density.

**Table 4.2** Degradation of Class 2 and Class 3 electrodes

| | Normal Dome Class 2 | | TiC/Ni Dome Class 2 | | Normal Dome Class 3 | | TiC/Ni Dome Class 3 | |
|---|---|---|---|---|---|---|---|---|
| | Contact Area [mm$^2$] (Diam.) | Imprint image | Contact Area [mm$^2$] (Diam.) | Imprint image | Contact Area [mm$^2$] (Diam.) | Imprint image | Contact Area [mm$^2$] (Diam.) | Imprint image |
| 1 weld | 27.99 (5.97) | | 28.37 (6.01) | | 28.27 (6.00) | | 27.06 (5.87) | |
| 100 welds | 29.32 (6.11) | | 28.94 (6.07) | | 30.88 (6.27) | | 28.75 (6.05) | |
| 200 welds | 32.47 (6.43) | | 29.32 (6.11) | | 32.67 (6.45) | | 32.57 (6.44) | |
| 300 welds | 35.15 (6.69) | | 31.37 (6.32) | | 34.32 (6.61) | | 34.52 (6.63) | |
| 500 welds | 37.07 (6.87) | | 32.88 (6.47) | | | | | |
| 700 welds | 39.15 (7.06) | | 33.49 (6.53) | | | | | |
| 2,000 welds | | | 46.48 (7.69) | | | | | |

Incidentally, the operating weld current of Class 3 electrode was 300A higher than the Class 2 electrode, and the degree of the contamination of electrode surface was not severe as much as far beyond unusable as shown in Table 4.2. However, a smaller button size and intermittent interfacial fracture were made from the peel test within 200 welds on Class 3 electrode. Even if the shunt effect is considered, Class 2 uncoated electrode has made an acceptable button diameter until the numbers of 600 welds. As mentioned in Table 3.3, Class 3 electrode has a low electrical conductivity, and hence it is difficult to deliver the weld current to faying surface of steel sheets effectively. Instead, the contact resistance between the electrode and the steel sheet was increased significantly from the formation of alloying, and the electrical energy was spent for the reaction of zinc layer and electrode more, not for the melting of steel sheets. Figure 4.6 to 4.9 are the SEM images and EDX results to analyze how deep the zinc diffuses to each electrode when electrode life tests were finished 100 and final welds. As shown in SEM figures, line scan method was used and measured every 10 or 20µm for a precise measurement.
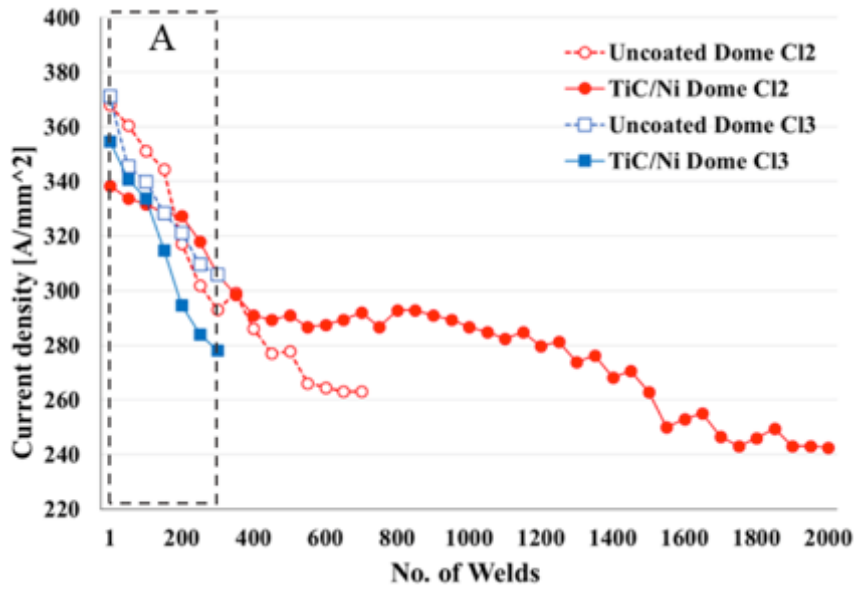
(a) Changing of weld current density
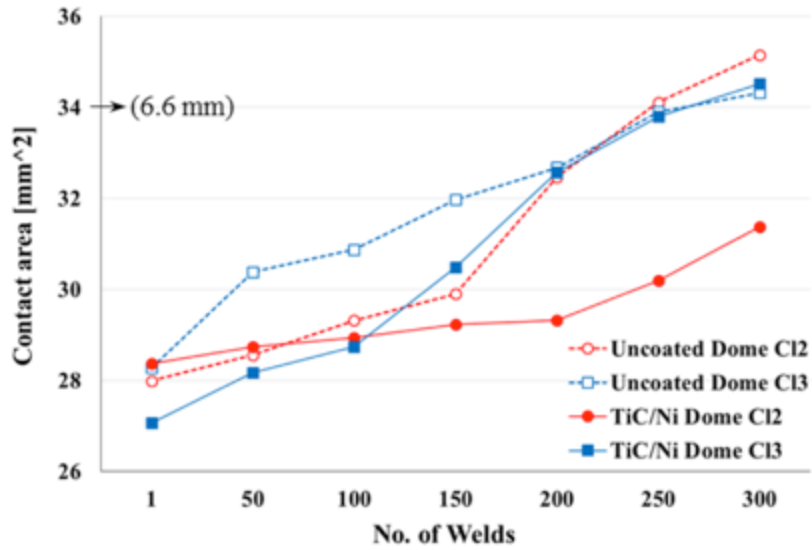


(b) Changing of contact area in region 'A'

**Figure 4.5** Weld current density and contact area for Class 2 and Class 3 electrode

In Figure 4.6, zinc diffusion on Class 2 electrode was made until the depth of 10 to 20μm from the top surface of electrode at 100 welds. After finishing electrode life test (refer to Figure 4.7), the electrode has a deeper zinc diffusion depth of 40 to 50μm because the repeated resistance heat and weld force accelerate the alloying formation on the electrode surface.
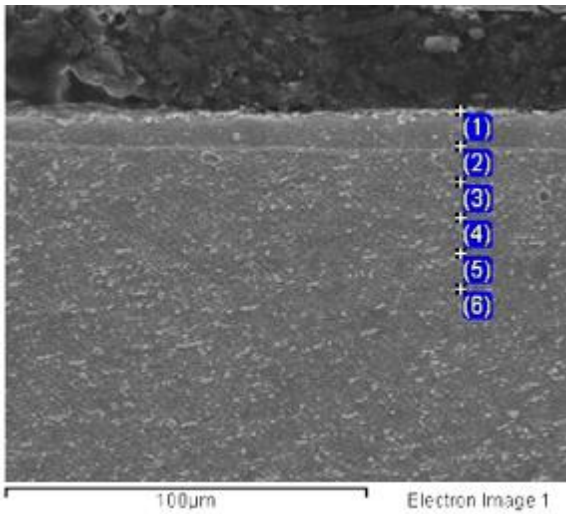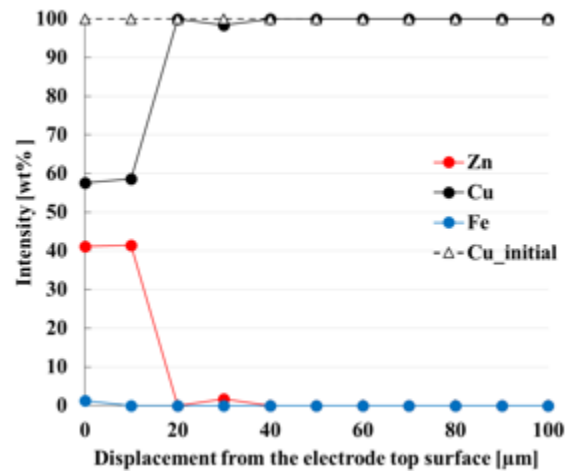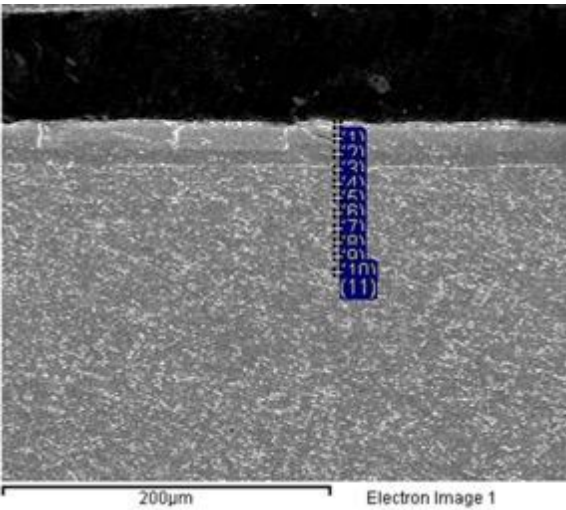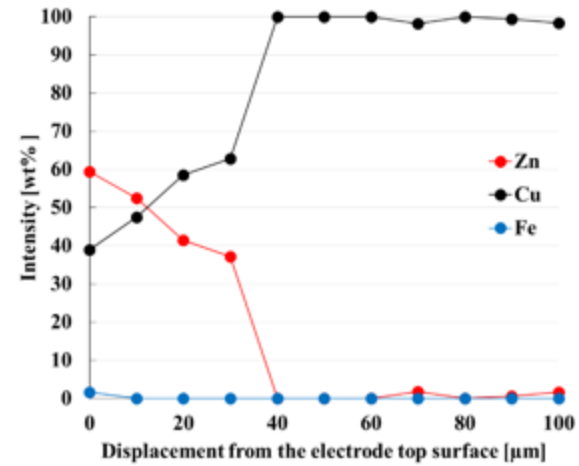
(a) SEM images at the center of the electrode        (b) EDX results

**Figure 4.6** SEM test result of the Class 2 uncoated electrodes at 100 welds



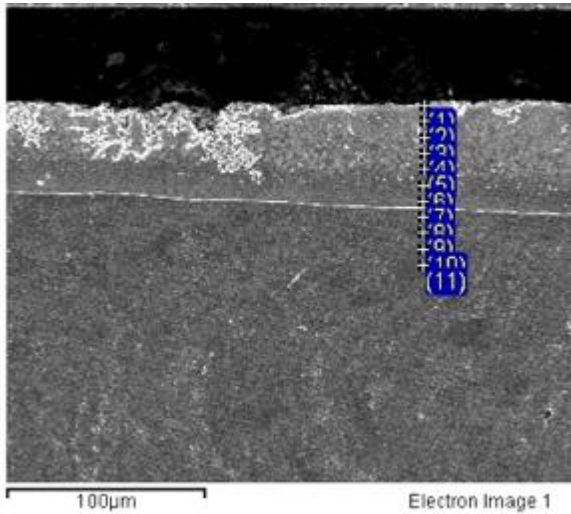(a) SEM images at the center of the electrode        (b) EDX results
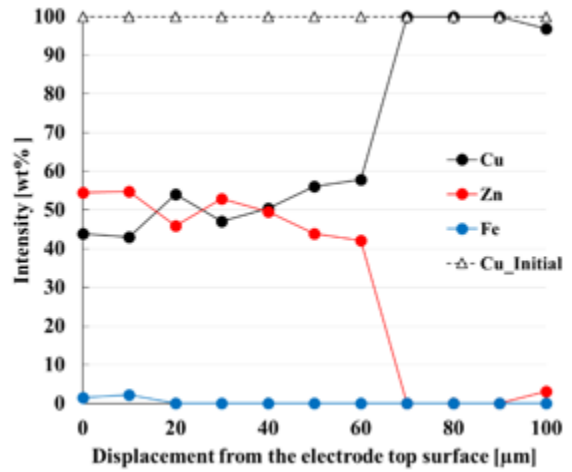
**Figure 4.7** SEM test result of the Class 2 uncoated electrodes at final welds

In the case of the Class 3 electrode, a thicker zinc diffusion depth was found same as seen in Figure 4.8 and 4.9. About 60μm thickness of alloying layer formed within 100 welds. At the final welds, a pitting area, which is formed from the localized removing of copper material during the weld, was detected at

52

the center of the electrode. For this reason, the zinc is able to accumulate in this area easily, and the total diffused depth has also increased to 100µm.
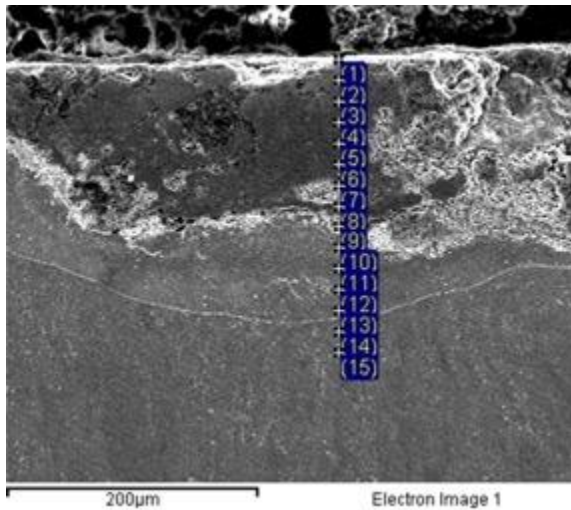


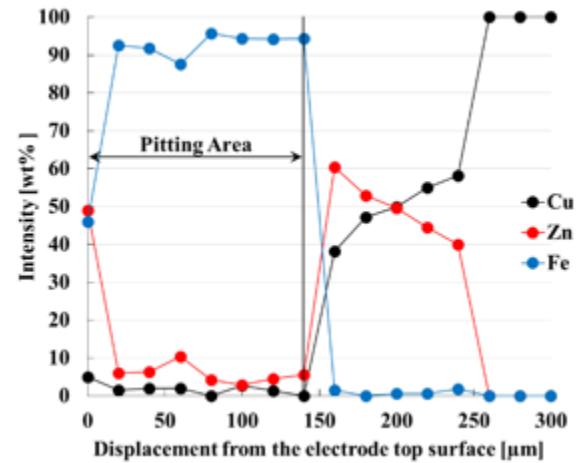(a) SEM images at the center of the electrode          (b) EDX results

**Figure 4.8** SEM test result of the Class 3 uncoated electrodes at 100 welds



(a) SEM images at the center of the electrode          (b) EDX results

**Figure 4.9** SEM test result of the Class 3 uncoated electrodes at final welds

### 4.2.2 The Effect of Electrode Shape and Coating

Dome and parabolic shaped electrode were selected for the second parameter to analyze the effect of improving electrode life. The heat conduction equation (4.1) for one-dimensional indicates the heat transfer rate ($\dot{Q}_{cond}$) is closely associated with the area (A) and temperature gradient ($\partial T/ \partial x$) during the process [64, 66]. The heat transfer is normal to an isothermal surface, and hence the total volume is a very important parameter for electrode.

$$\dot{Q}_{cond} = -kA\frac{\partial T}{\partial x}$$

(4.1)

$$\overrightarrow{\dot{Q}_n} = \dot{Q}_x\vec{\imath} + \dot{Q}_y\vec{\jmath} + \dot{Q}_z\vec{k}$$

(4.2)

$$\dot{Q}_x = -kA\frac{\partial T}{\partial x} \quad \dot{Q}_y = -kA\frac{\partial T}{\partial x} \quad \dot{Q}_z = -kA\frac{\partial T}{\partial x}$$

(4.3)

Li et al. also investigated that the effect of electrode shape has a negative effect on thermal conductivity and electrode life [67]. It was revealed that the less mass and volume cannot deliver the resistance heat effectively toward the cooling water side. Finally, the weldability is getting lower, and also electrode life becomes shorter.

In this study, the parabolic shaped electrode having a shorter face length, the length between the outer electrode surface and inner electrode surface, was selected to evaluate the cooling effect of face length (refer to Figure 3.4 in Chapter 3). As mentioned above, the parabolic shaped electrode has a 26% smaller volume and 33% less weight (16.90 g, 2,185 mm$^3$) than dome shaped electrode (25.08 g, 2,961 mm$^3$). With regard to the heat transfer, the total volume is dominant in deciding the electrode performance. The cooling water reaches close to the electrode surface, the resistance heat can be cooled down effectively. Thus, the shorter face thickness was assumed that it will help to improve the cooling effect.

Table 4.3 shows the imprinting images at different number of welds, and the contact area and electrode diameter was calculated. The electrode surface deformation was severe on the parabolic shaped electrode, and the weld current density also started to decrease steeply after the 300 welds as shown in Figure 4.10 (a). However, the weld current density did not decrease continuously because the pitting makes the weld current density increases temporarily. At the numbers of 300 and 350 welds, the slope of weld current density has changed because the total contact surface area decreased due to the expansion of pitting. In the case of TiC/Ni coated dome shaped electrode, this phenomenon was found at 600, 900, 1200, and 1400 welds, respectively. In the case of TiC/Ni coated parabolic shaped electrode, there was no positive effect on the increase of the electrode life. The surface area was not expanded over $34mm^2$ (same as diameter of 6.6mm) until 300 welds as shown in Figure 4.10 (b), but it was steeply increased between 300 to 500 welds. Thus, the TiC/Ni parabolic shaped electrode has a similar weld current density to uncoated dome shaped electrode from 600 welds.

**Table 4.3** Degradation of dome and parabolic shaped electrodes

| | Uncoated Dome Cl2 | | TiC/Ni Dome Cl2 | | Uncoated Parabolic Cl2 | | TiC/Ni Parabolic Cl2 | |
|---|---|---|---|---|---|---|---|---|
| | Contact Area [mm2] (Diam.) | Imprint image | Contact Area [mm2] (Diam.) | Imprint image | Contact Area [mm2] (Diam.) | Imprint image | Contact Area [mm2] (Diam.) | Imprint image |
| 1 weld | 27.99 (5.97) | | 28.37 (6.01) | | 26.97 (5.86) | | 24.54 (5.59) | |
| 100 welds | 29.32 (6.11) | | 28.94 (6.07) | | 27.62 (5.93) | | 26.24 (5.78) | |
| 200 welds | 32.47 (6.43) | | 29.32 (6.11) | | 29.71 (6.16) | | 30.00 (6.18) | |
| 300 welds | 35.15 (6.69) | | 31.37 (6.32) | | 36.00 (6.77) | | 31.47 (6.33) | |
| 500 welds | 37.07 (6.87) | | 32.88 (6.47) | | 40.72 (7.07) | | 36.00 (6.77) | |
| 700 welds | 39.15 (7.06) | | 33.49 (6.53) | | 44.89 (7.56) | | 39.82 (7.12) | |
| 2,000 welds | | | 46.48 (7.69) | | | | | |
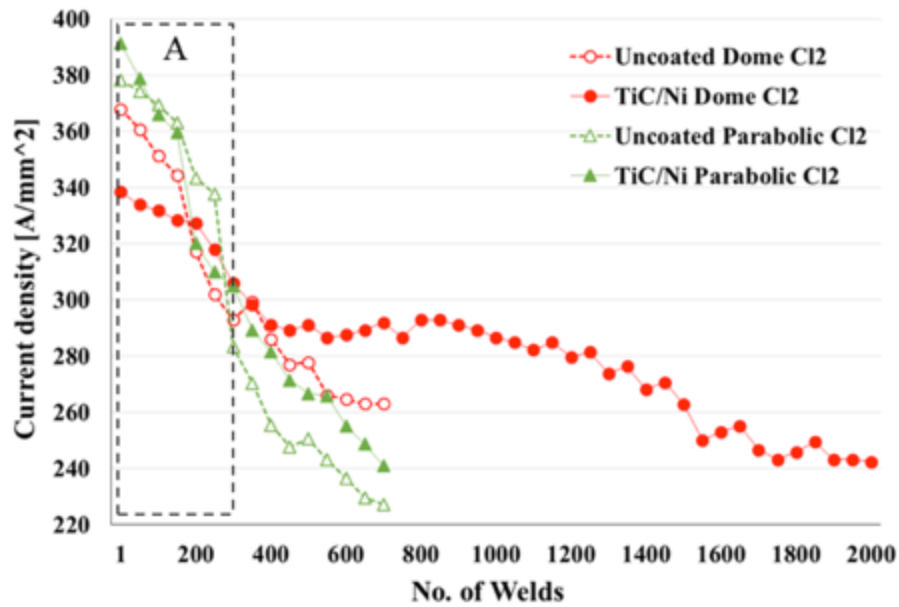
(a) Changing of weld current density
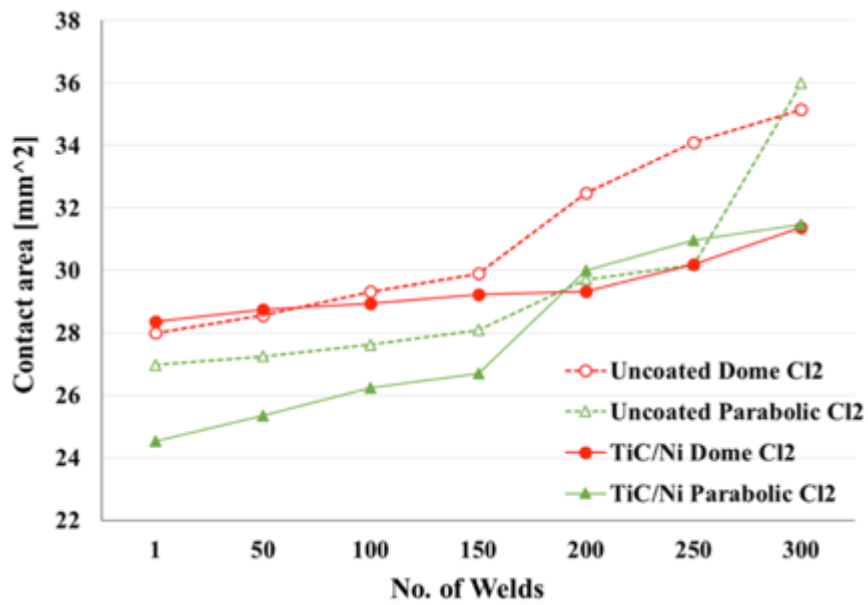


(b) Changing of contact area in region 'A'

**Figure 4.10** Weld current density of dome and parabolic shaped electrodes

The geometry effect was verified from the hardness result of Figure 4.11. As explained in equation (4.1) to (4.3), the parabolic shaped electrode, having a small volume, will soften earlier at the same

56

number of weld. Since the contact area increased significantly after 300 welds, hardness was measured using the electrodes which is finished 700 welds. A more significant drop in hardness was observed in both uncoated and TiC/Ni coated parabolic shaped electrodes. Therefore, the sharp geometry can accelerate the softening on the electrode surface.
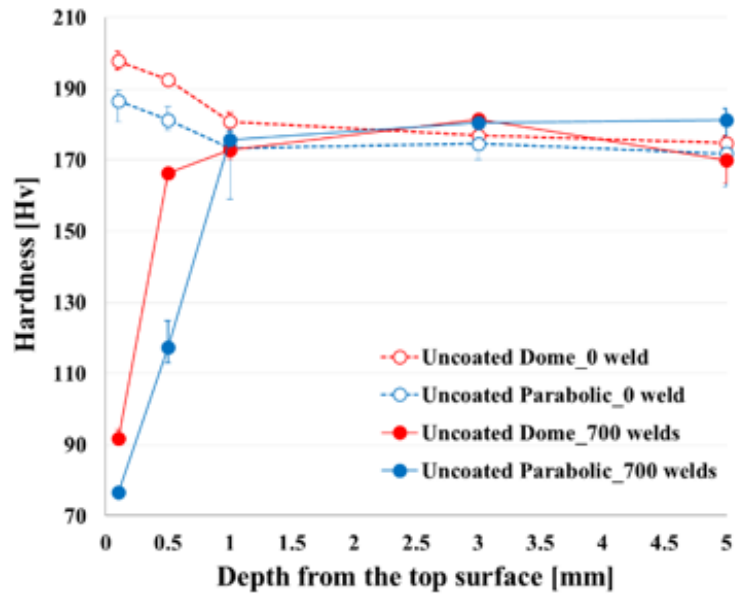


(a) Uncoated electrodes
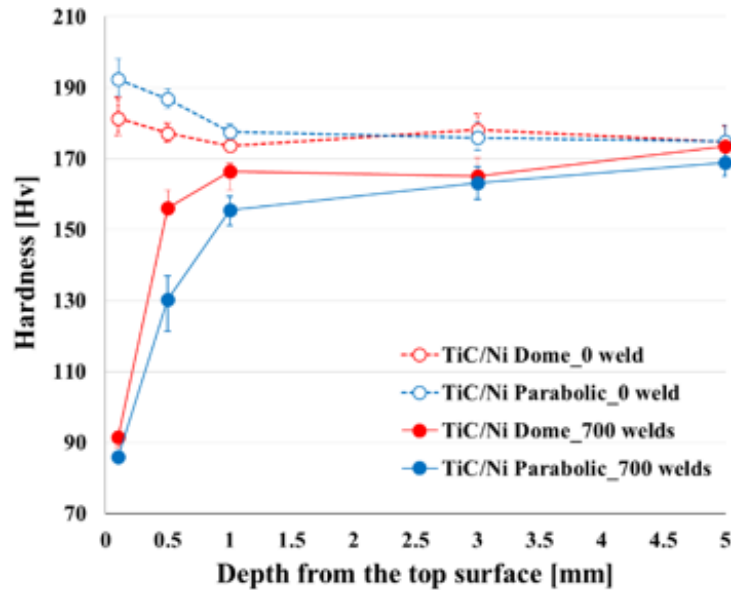


(b) TiC/Ni coated electrodes

**Figure 4.11** Hardness of dome and parabolic shaped electrodes

In terms of electrode geometry, when it assumed that all electrodes have a same reduced face length, the dome shaped electrode is vulnerable to expand the electrode surface due to the large curvature. Thus, the deformation speed of parabolic shaped electrode can be explained clearly by tracing of reduced face length. Figure 4.12 shows the reduced face length after finishing electrode life test of 100, 300, and final welds, respectively. Until 100 welds, the reduced face lengths for uncoated electrodes were almost same because the dome shaped electrode has an extruded length of 0.2 mm on the surface (refer to a Figure 3.4 in Chapter 3), and this geometric condition works the same as the parabolic shaped electrode. For this reason, the uncoated dome and parabolic shaped electrodes have shown a similar trend on reducing face length until 300 welds. However, the real contact surface area was uncoated parabolic shaped electrode has larger than uncoated dome shaped electrode. It means that parabolic electrode has been made an additional expansion on the electrode surface.
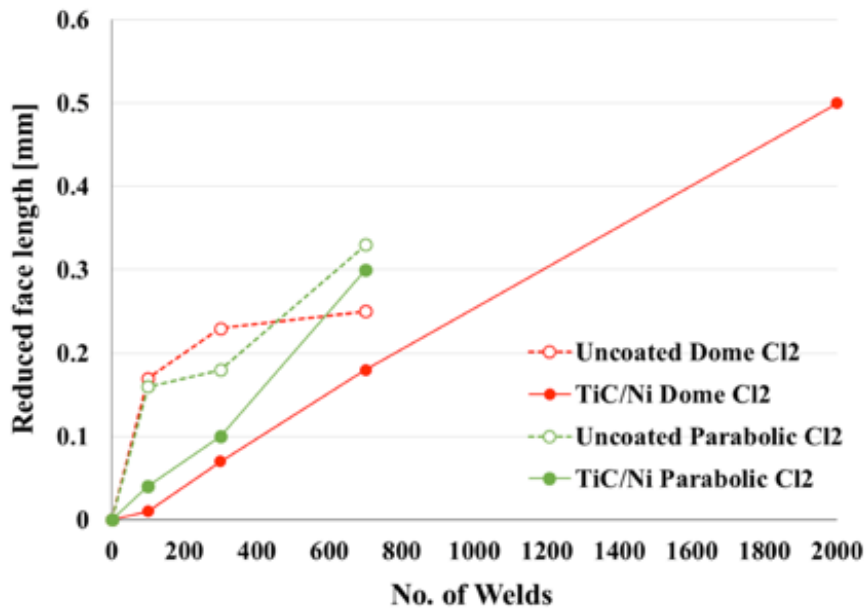


**Figure 4.12** Changing of the electrode face length

Figure 4.13 shows the electrode deformation at final welds, and the dotted lines indicate the initial geometry of each electrodes. From the Figure 4.13 (b) and (d), the deformed material of parabolic shaped electrodes (region A) was rolled up and accumulated around the top surface of the electrode, and the total contact area was increased. As a result, the button diameter of uncoated parabolic shaped

58

electrode was made intermittently below the criterion at 400 welds (refer to the Figure 4.1 (b)). On the other hand, dome shaped electrodes made a sharp and thin alloying material on the edge of electrode as shown in Figure 4.13 (a) and (c), and some of alloying were naturally removed when the zinc coating removes during the weld or electrodes are released after finish the weld. Generally, the TiC/Ni coating layer is well known as a barrier reducing or delaying a formation of local bonding and alloying between the electrodes and steel sheet surface [68], but this layer did not work normally on parabolic shaped electrode. Uncoated and TiC/Ni coated parabolic shaped electrodes have started to overtake the reduced face length of uncoated dome shaped electrode after 300 welds. Finally, parabolic shaped electrodes had a larger contact area than uncoated dome shaped electrode. When the contact area reaches 40 $mm^2$ (same as the diameter of 7.0 mm), electrode life test was over. Therefore, the TiC/Ni coated dome shaped electrode exhibits a slow deformation speed, which offers an improved long electrode life.



(a) Uncoated Dome shaped

(b) Uncoated Parabolic shaped

(c) TiC/Ni Dome shaped

(d) TiC/Ni Parabolic shaped
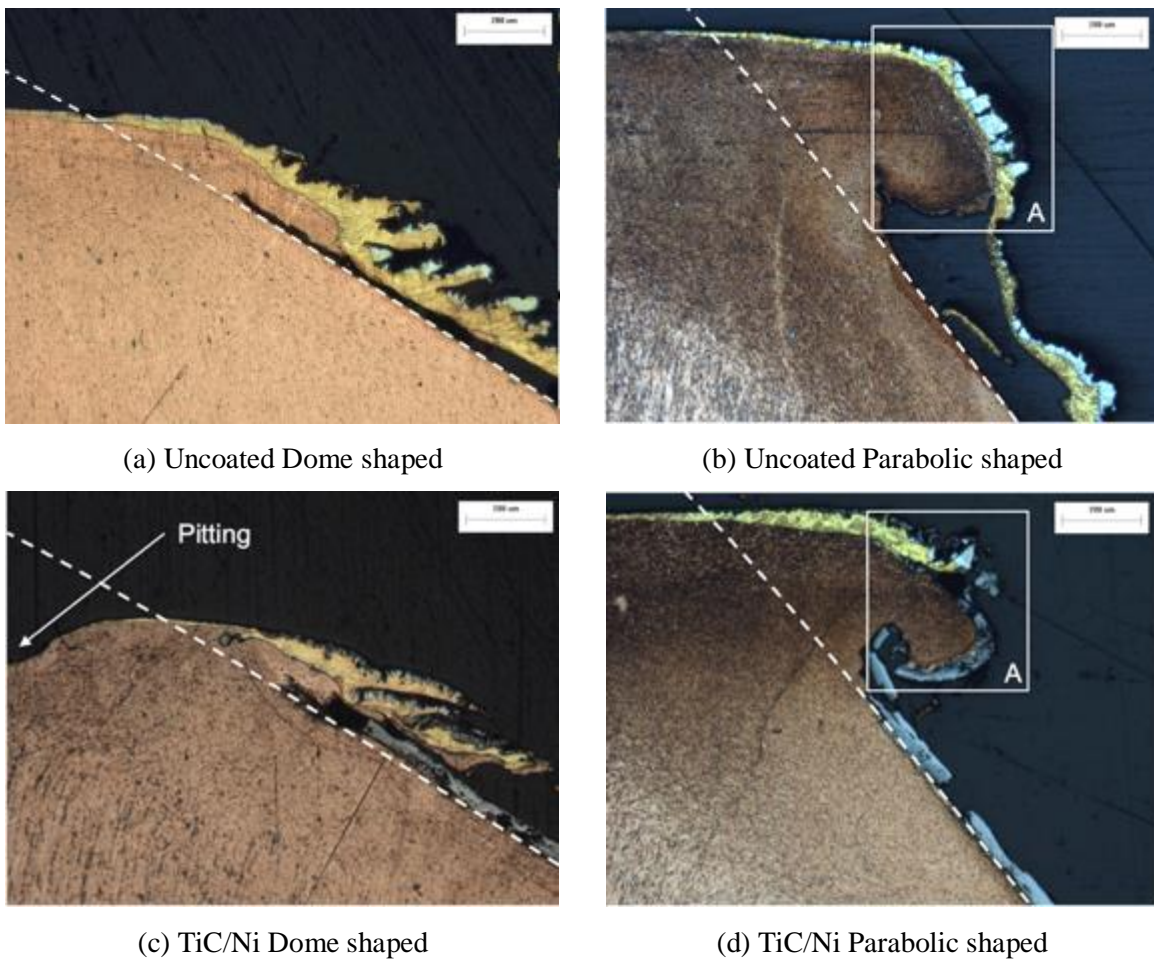
**Figure 4.13** Electrode deformation at final welds

## 4.3 Summary

The study reported here evaluates electrode life for RSW of Zn coated AHSS. The effects of electrode material, geometry and TiC/Ni coating on electrode life are discussed. Some key conclusions include:

Class 3 electrode exhibited shorter electrode life than Class 2 electrode. The larger recrystallized area (heat affected area) in class 3 electrode was made, and it led to accelerate the electrode softening. In addition, Class 3 electrode has a thicker alloying on the surface, and it caused more heat loss during the weld. From a view of material, since Class 3 electrode has a high resistance (lower electrical conductivity), the electrical energy loss in electrode itself is more than Class 2. As a result, Class 3 electrodes had a shorted electrode life. Thus, Class 3 electrode is not suitable for zinc coated AHSS RSW.

Parabolic shaped electrode showed shorter electrode life than dome shaped electrode on the basis of the result of button diameter. The main reason for the short electrode life is electrode deformation. Due to the short face length and small volume, parabolic shaped electrode provided a negative effect from the aspect of heat transfer. The contact surface area of parabolic shaped electrode increased quickly after 300 welds, and it induced the fast decreasing of weld current density. In addition, the accumulation of the deformed material on the top surface of electrode is contributed to increase the total contact area. Therefore, the parabolic shaped electrode is not as effective as the dome shaped electrode.

TiC/Ni coated, dome shaped, and Class 2 electrode showed the best electrode life of 1,900 welds. The TiC/Ni coated electrode have shown a less reduction of hardness and formed a thinner recrystallized area. Thus, it is effective to delay the growing of electrode contact area, and maintained the weld current density relatively constant. The TiC/Ni coated Class 3 electrode exhibited a short electrode life around 200 welds. The more heat loss within the electrode and the low operating weld current led to insufficient weld current density. The TiC/Ni coating on parabolic shaped electrode did not show significant effect to improve electrode life. Rapid increase of contact area 600 welds accelerated the decrease in weld current density and results in limited electrode life.

# Chapter 5

# Effect of Electrode Inserts on Electrode Life and Weldability

The electrode, which is made with TiC/Ni coating, dome shaped, and Class 2 material, was verified as the most effective electrode to improve electrode life in Chapter 4. However, the coating layer is not permanent and finally disappeared from the repeated force and high resistance temperature. Another problem is that it is hard to make a uniform thickness of coating layer. However, that does not mean that making an excessive coating is not appropriate because it is not economical and can generate very high contact resistance. For these reasons, the electrode life of TiC/Ni coated electrode is likely to be influenced and fluctuated by these external factors except main welding parameters. In Chapter 5, it was proposed another type of electrode which is able to increase electrode life and improve the spot weldability for zinc coated AHSS. To evaluate the weldability performance of the electrode, mechanical strength tests, and welding signal analysis were performed, and electrode life tests were also conducted for the promising electrodes.

## 5.1 Principle of the Modified Inserted Electrode

In previous studies, an inserted type of electrode was developed and evaluated to improve the weldability and increase electrode life. Key et al. [57], Nealon et al. [69] and Shingo et al. [70] tried to improve electrode life with inserted electrode that the electrode surface area is only contacted with refractory materials. The refractory materials increase the resistance between electrode and steel sheet, and help to form a weld nugget easier than the normal electrode. However, this type of electrode was reported that the inserted materials are broken from the repeated force and high temperature. Therefore, the inserted materials needed to be protected properly. Based on these concepts, a modified inserted electrode was suggested having a different design which is divided into two parts, copper part and inserted material part, to improve thermal conductivity and prevent too much resistance increase. At the center of the electrode, refractory materials, such as W and Mo were inserted and assembled to the copper electrode. Figure 5.1 shows the schematic of inserted electrode. Part number ① is a Class 2 normal copper electrode, and part number ② is an inserted material. These two parts were assembled only by using a mechanical tolerance to minimize the manufacturing process. Depending on the diameter of inserted material or welding conditions, the specific dimensions of two parts can be flexibly changed. Another characteristic is that a penetrated hole was drilled to be able to contact the inserted

material and cooling water directly same as the number ③, and ④. This is because the larger contact area can help to maximize the cooling effect [4-1, 2, 5]. In addition, there is a space which the inserted material can move up by the weld force. From the results of electrode life tests in Chapter 4, the maximum reduced face length was less than 1.0mm. Therefore, this space was expected that it can help to push up the inserted material automatically by the weld force toward the top surface of the copper electrode.
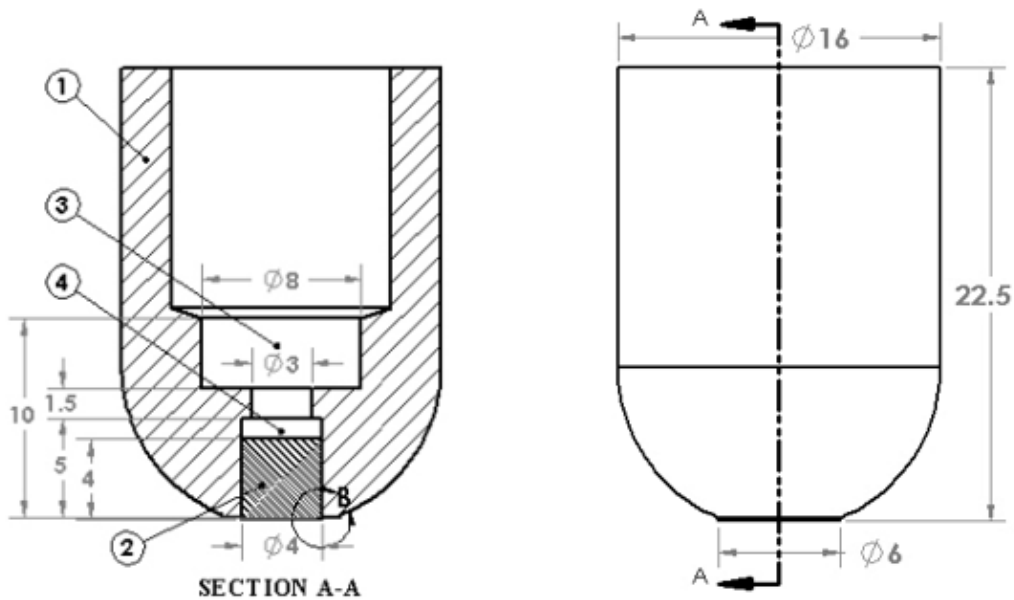


(a) Detailed dimensions
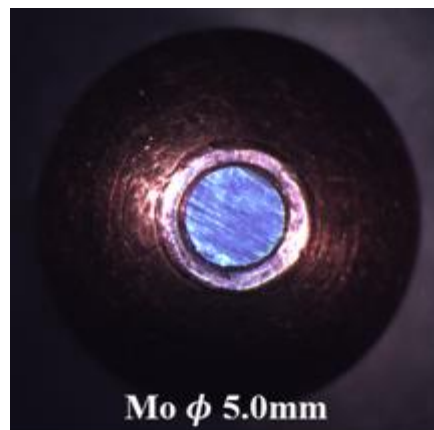


(b) Examples of inserted electrodes

**Figure 5.1** Schematic of modified inserted electrode

### 5.1.1 Material properties for the insert materials

Table 5.1 shows the material properties for the various insert materials. Most of all, under the harsh welding conditions, the insert material is required to have high thermal and mechanical properties, such as a compressive strength, fracture toughness, appropriate hardness, and high thermal resistance, to prevent an excessive deformation or degradation. In terms of electrical properties, the insert material should also have an acceptable high resistivity, but not too extremely high. Theoretically, a weld nugget starts to be made by the resistance which is formed between electrodes and steel sheets. Thus, in order to make the weld nugget in early stage of the weld, the selection of the insert material is very important. Through the above prerequisites for the selection of insert material, the refractory metals, W and Mo, were finally selected. To evaluate the effect of diameter of insert material, ∅3 and ∅4 mm rods were used for W inserted electrode, and ∅3 and ∅5 mm rods were used for Mo.

**Table 5.1** Material properties for the inserted materials [49]

| Material | Cu | W | Mo | WC | TiB2 | TiC |
|---|---|---|---|---|---|---|
| Yield Strength [MPa] | 248 | 1725 | 1900 | 530 | 374 | 295 |
| Compressive Strength [MPa] | 248 | 3975 | 1900 | 3347 | 3735 | 3020 |
| Fracture Toughness [MPa$\sqrt{m}$] | 47.8 | 135 | 27.5 | 3.8 | 6.2 | 2.55 |
| Vickers Hardness [GPa] | 1.23 | 7.36 | 5.64 | 36 | 25 | 27.95 |
| Thermal Expansion Coefficient | 16.9 | 4.5 | 5.2 | 7.1 | 8.1 | 7 |
| Melting Temp. [°C] | 1080 | 3415 | 2615 | 2870 | 3045 | 3205 |
| Max. Service Temp. [°C] | 325 | 1018 | 1089 | 777 | 1259 | 862 |
| Thermal Conductivity [W/m°C] | 394 | 172.5 | 138 | 88 | 96 | 21.5 |
| Electrical Resistivity [mΩ·m] | 0.021 | 0.057 | 0.056 | 1 | 0.15 | 2.145 |

## 5.2 Mechanism of Inserted Electrode

Electric current only flows through the conductor in an electrical circuit. Therefore, copper having a low electrical resistivity, is the most commonly used material as a good conductor of heat and electricity. However, as shown in Table 5.1, W and Mo are worse conductors than copper, and the weld current is not easy to flow through these materials because of the relatively high resistivity. In the previous research, the only way the weld current can flow was through the insert material. However, the high resistivity of insert material can creates an excessive resistance heat, and the melting of steel sheet and electrode was made. In severe cases, melting can lead to electrode sticking or damage to insert material such as the loss of material.

To prevent these problems, a new type of inserted electrode was designed so that the weld current can flow through the both parts. Figure 5.2 (a) describes a section view of Ø4mm inserted electrode which was applied different mechanical dimension on the electrode surface, and Figure 5.2 (b) illustrates a detail view of electrode surface area, B. The mechanical tolerance of 20µm in detail view inevitably occurs in the process of the assembly of insert material and copper electrode. However, this gap plays a role in changing the passage of weld current during the weld.
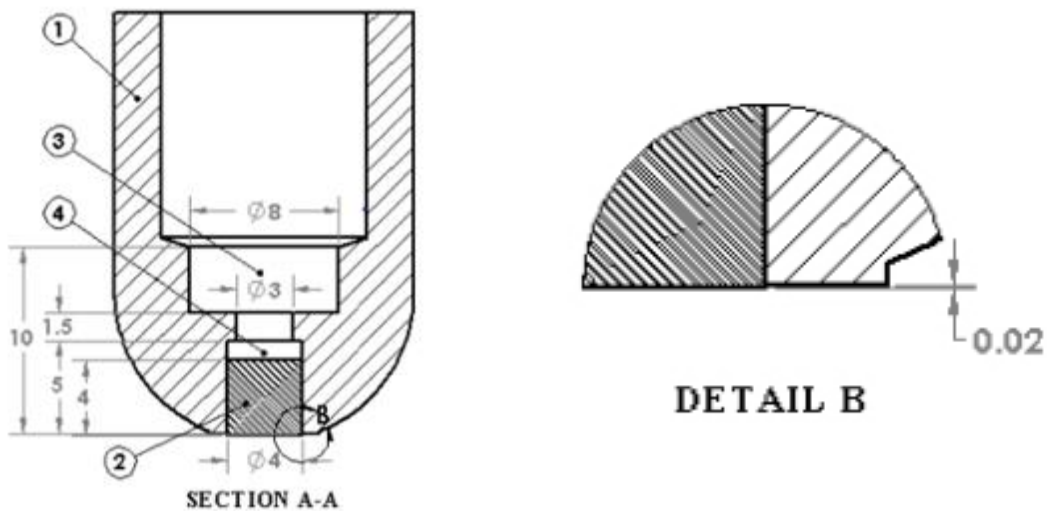


(a) Section view of the inserted electrode          (b) Detail view of the inserted electrode

**Figure 5.2** Dimensions of modified inserted electrode (unit: mm)

As explained above, the weld current flows through the good conductor, therefore, it is necessary to use the gap in order that the weld current flows through the inserted material first. If there is no gap, for example, when the inserted material and copper electrode assembled perfectly flat or the inserted material pushed up more, the weld current only flows through the copper part. In these cases, it is hard to get the effect of insert material. Therefore, the inserted electrode is required to be carefully controlled to maintain an appropriate tolerance when inserted electrode is assembled.

### 5.2.1 Characteristic of modified inserted electrode in weld nugget

Figure 5.3 is the results of microstructure for normal electrode and WØ3mm inserted electrode. Normal electrode and W inserted electrode welded with 10.5kA and 9.5kA of weld current, respectively. The other welding conditions were used the same as the welding condition of electrode life test. When spot welding was performed with the inserted electrode, nugget diameter and nugget thickness were increased 16 % and 7% more than normal electrode. In spite of the lower weld current, inserted electrode has melted thicker and larger. Therefore, this result shows that the insert material helps the melting of steel sheet. This type of weld nugget was commonly observed in the other inserted electrodes, WØ4.0, MoØ3.0, and MoØ5.0 mm. (Refer to Appendix A)
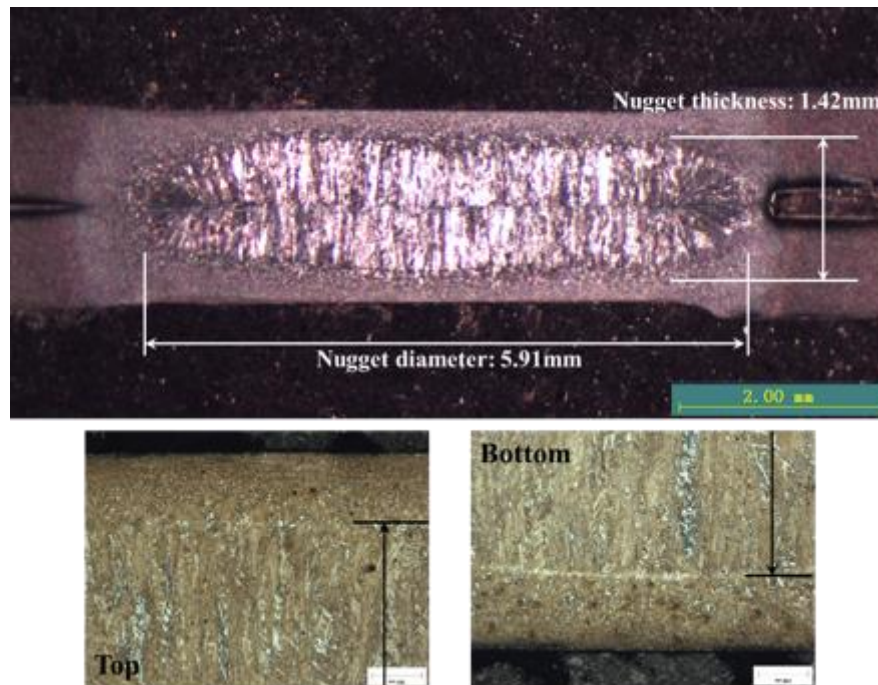


(a) Normal electrode
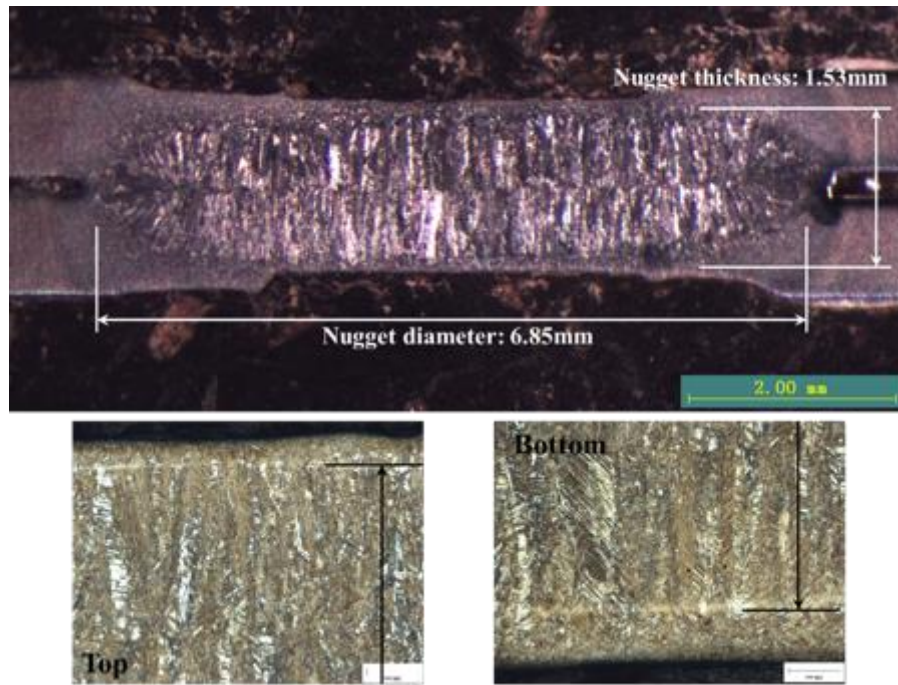
(b) W ∅3mm inserted electrode

**Figure 5.3** Macrostructure and microstructure of weld

## 5.2.2 Electrode temperature

In terms of the increase of the thickness of the weld nugget, it was expected that there was a difference on the distribution of weld temperature between electrodes and steel sheets. However, it is hard to prove experimentally because RSW welding condition is coupled with mechanical, electrical, and thermal, and hence is limited to measure the temperature on the contact area by using a thermocouple. Instead, Gould et al. identified an analytical model for estimating a temperature and cooling rate of resistance spot welds by using a one dimensional thermal model [60, 71]. This analytical model has following assumption to make the model simple. First, thermal losses around the steel were ignored, and second, resistance heat flows from steel sheet to electrode surface. Last, the temperature distribution in weld was described by a sine wave half period having a peak at the faying surface of steel sheets. With these assumptions, the boundary condition can be expressed as the equation (5-1). Additionally, it is assumed that the thermal gradient in the electrode is linear, extending from electrode temperature to the temperature of the cooling water. Equation (5-2) shows the boundary condition expression for the temperature variation in RSW.

$$\theta = (\theta_P - \theta_E) \cos\left(\frac{\pi}{2\Delta x} x\right) e^{-\frac{\alpha\pi^2}{4\Delta x^2}t} + \theta_E$$

<div align="right">(5-1)</div>

$$\frac{d\theta}{dx}_{x=\Delta x} = -\frac{k_E}{k_S}\frac{\theta_E}{\Delta x_E}$$

<div align="right">(5-2)</div>

$\theta_P$: the peak temperature in the spot weld

$\theta_E$: the temperature between electrode and steel

$x$: the distance from the faying surface toward electrode face

$\Delta x_E$: the thickness of the electrode face, $\Delta x$: the thickness of the electrode face

$t$: the time after termination of the weld current

$k_E$ and $k_S$: thermal conductivities of Cu and steel

Equation (5-3) below can be derived from the combining equation (5-1) and (5-2).

$$\theta = \theta_P \frac{1 + \left(\frac{2}{\pi}\right)\left(\frac{k_E}{k_S}\right)\left(\frac{\Delta x}{\Delta x_E}\right)\cos\left(\frac{\pi}{2\Delta x}x\right)}{1 + \left(\frac{2}{\pi}\right)\left(\frac{k_E}{k_S}\right)\left(\frac{\Delta x}{\Delta x_E}\right)e^{\frac{\alpha\pi^2}{4\Delta x^2}t}}$$

<div align="right">(5-3)</div>

In the case of calculating the temperature at the contact surface area right after the weld was finished, it will be assumed that $\Delta x$ and $x$ are same, and t is zero. Thus, the equation (5-3) becomes simpler as shown in equation (5-4).

$$\theta = \frac{\theta_P}{1 + \left(\frac{2}{\pi}\right)\left(\frac{k_E}{k_S}\right)\left(\frac{\Delta x}{\Delta x_E}\right)}$$

<div align="right">(5-4)</div>

By using this equation, the temperature between electrode and steel sheet was estimated for normal electrode and inserted electrodes as seen in Table 5.2. The peak temperature in the spot weld was assumed to be equal, but it was revealed that the low thermal conductivities of inserted materials increase the temperature about 300°C more at the contact surface.

**Table 5.2** Estimated temperature on contact area

| Electrode | Estimated temp. [°C] | $k_E$ [W/m°C] | $k_S$ [W/m°C] | $\theta_P$ [°C] | $\Delta x$ [mm] | $\Delta x_E$ [mm] |
|---|---|---|---|---|---|---|
| Normal | 939.5 | 394 | 30 | | | |
| W inserted | 1262.8 | 172.5 | 30 | 1725 | 1.0 | 6.0 |
| Mo inserted | 1334.3 | 138 | 30 | | | |

These results were identified by the microstructure images of cross sectional specimens as shown in Figure 5.4. Fig 5.4 (a), which is welded with normal electrode and 9.5kA, was detected base metal microstructure on the top and bottom surface. Under the optimal weld current condition, Fig.5.4 (b), a fine grain structure was detected on both surfaces. On the other hand, W inserted electrode built a coarse grain structure near to the top surface of steel.



| | (a) Normal_9.5kA | (b) Normal_10.5kA | (c) WØ3mm inserted_9.5kA |
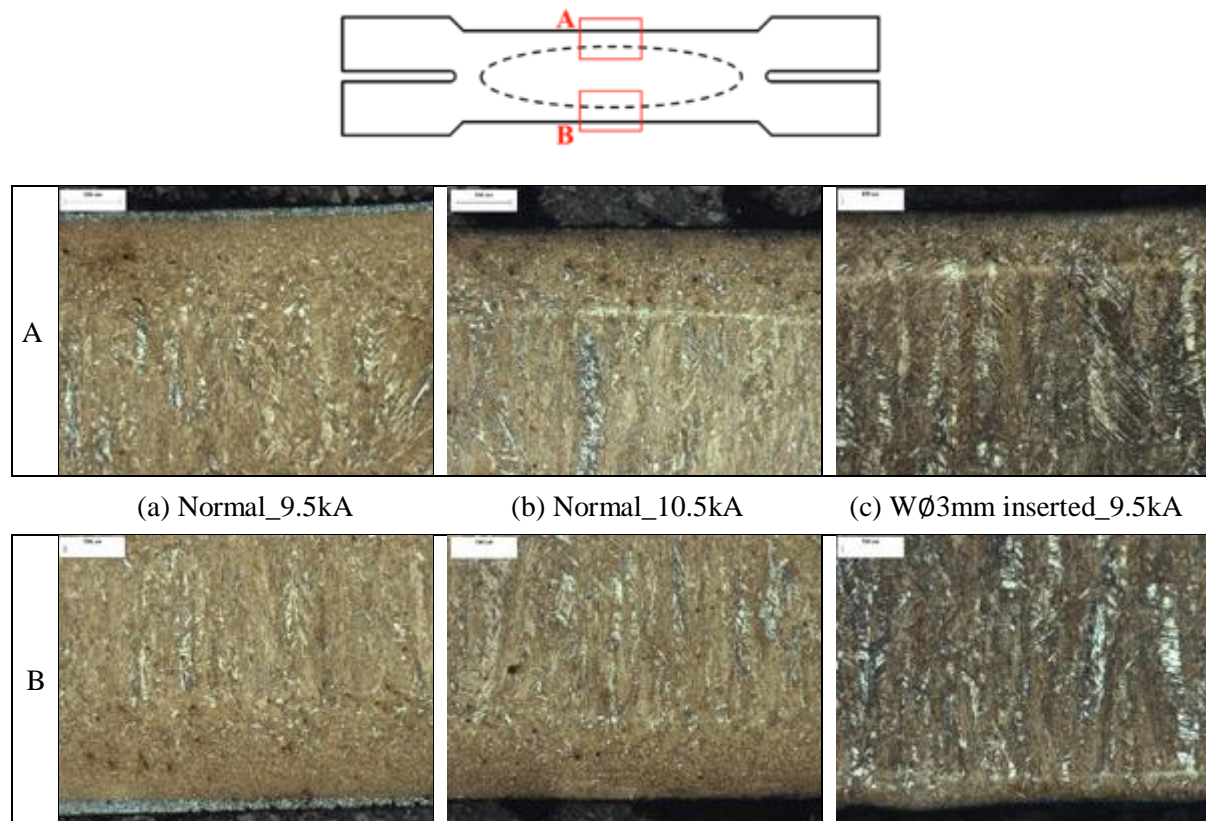
**Figure 5.4** Microstructure of weld on top and bottom surfaces

### 5.2.3 Weld nugget formation

Based on the above results, it was expected that the inserted electrode will be able to make a weld nugget with short weld time and low heat input. To evaluate the effect of inserted electrode, weld nugget formation was analyzed by using cross sectional specimens which are made every odd numbers of weld cycles as in Figures 5.5 and 5.6. From the steel surface and weld nugget images, the weld time which is started to form a weld nugget was detected, and also thermal transfer characteristic and the growth of weld nugget were analyzed from the specimens of each electrodes.

| Weld cycles | Normal electrode | | W Ø3mm inserted electrode | | W Ø4mm inserted electrode | |
|---|---|---|---|---|---|---|
| | Steel surface | Weld nugget | Steel surface | Weld nugget | Steel surface | Weld nugget |
| 3 | | | | | | |
| 5 | | | | | | |
| 7 | | | | | | |
| 9 | | | | | | |
| 11 | | | | | | |
| 13 | | | | | | |
| 15 | | | | | | |

**Figure 5.5** Weld nugget formation of W inserted electrode

Normal electrode started to melt from 5 cycles and nearly built a weld nugget at 9 cycles with 10kA of weld current. On the other hand, W and Mo inserted electrodes has started to generate the resistance heat from 3 cycles, and the weld nugget was created within 5 cycles at 9.5kA. Especially, the weld nugget of normal electrode continuously grew up until the weld finishes, but the inserted electrode produced almost same diameter of weld nugget within 11 cycles of weld time.

| Weld cycles | Normal electrode | | MoØ3mm inserted electrode | | MoØ5mm inserted electrode | |
|---|---|---|---|---|---|---|
| | Steel surface | Weld nugget | Steel surface | Weld nugget | Steel surface | Weld nugget |
| 3 | | | | | | |
| 5 | | | | | | |
| 7 | | | | | | |
| 9 | | | | | | |
| 11 | | | | | | |
| 13 | | | | | | |
| 15 | | | | | | |

**Figure 5.6** Weld nugget formation of Mo inserted electrode

70

The biggest difference between the normal electrode and the inserted electrode is a different resistance heat distribution direction in the early stage of weld time. The normal electrode generates a resistance heat from faying surface and transfer to electrode surface. However, the inserted electrodes start a melting on both of faying surface and the electrode-steel contact surfaces.

The main reason for this is that the insert materials have a lower thermal conductivity and higher electrical resistivity than a normal electrode. Another characteristic is that the normal electrode made an elliptical shape of heat distribution at 5 cycles of weld time, but the W and Mo inserted electrodes have shown a cylindrical form and fast heat distribution at 3 cycles of weld time. As mentioned in section 5.2, the temperature between electrode and steel was higher than normal electrode, and it was helpful for removing zinc layer. Finally, the fast removing of zinc layer was possible, and it made a welding condition such as a welding of uncoated steel. In the case of Mo inserted electrodes, the weld nugget formations were observed similar to the W inserted electrode. According to the electrode surface conditions and the diameter of insert materials, there was a slight difference on melting time, but the overall trend was almost same. The heat generation in both the faying surface and the contact surfaces, and the weld nugget was sufficient at 11 cycles based on the minimum weld nugget criterion. Through the analysis of weld nugget formation, it was verified that the inserted electrodes have a positive effect on making a weld nugget faster and easier than normal electrode.

The weld nugget formation of each electrode can also be identified by dynamic resistance curves in Figure 5.7 above. Overall, normal electrode has formed a low dynamic resistance because zinc coating makes a good contact condition, and it delays the time for increasing resistivity. For this reason, it was not until the 9 cycles of weld time that the normal electrode start to form a small weld nugget by the elevated temperature. Additionally, α and β-peaks were not detected in the curve because the zinc does not effectively remove in a short period of weld time. On the other hand, inserted electrodes have a clear β-peak because the melting temperature has increased fast and removed the zinc layer effectively. The appearance of β-peak was similar to the start time of weld nugget formation in Figure 5.6. Therefore, it was revealed that the high resistivity of insert materials can attribute to increase the temperature fast and remove zinc layer within a short weld time and is easy to form a good weld nugget (refer to the Appendix B).
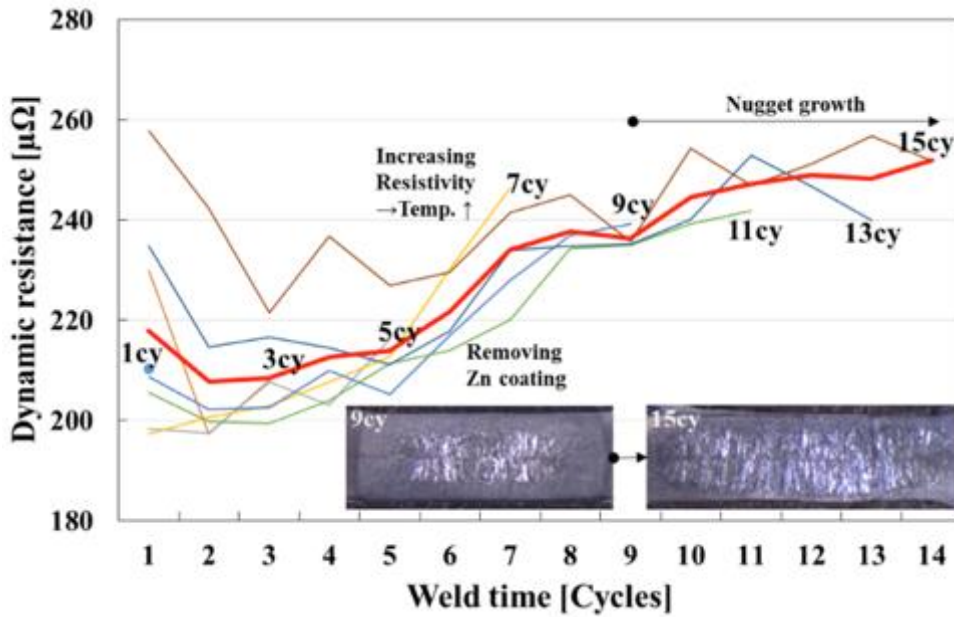
(a) Normal electrode
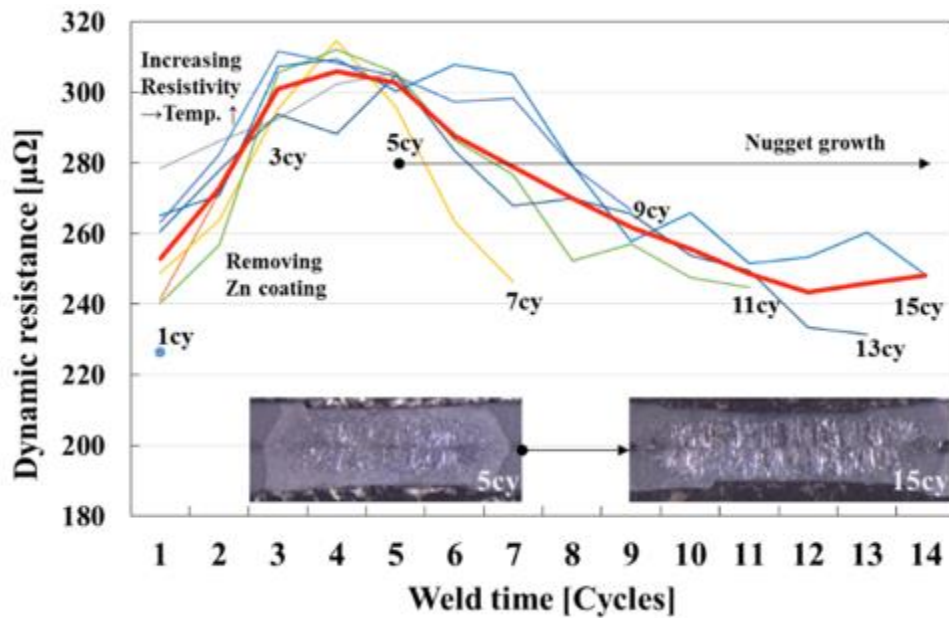


(b) W Ø3mm inserted electrode

**Figure 5.7** Cumulative dynamic resistance curves

Besides the dynamic resistance, monitoring of electrode movement and weld force is well known as an effective method to explain the weld nugget formation [72]. According to the welding stages in Figure 2.5, both of signals have a distinctive value at each stage. Thus, these welding signals can be overlapped

with dynamic resistance. There is a dominant mechanism that determines the electrode movement as shown in equation (5-5) below [13]. When the weld current flows after electrodes clamp steel sheets, the electrode has a movement (the same as the plastic deformation) from the surface breakdown and asperity softening of steel. After a few weld cycles, steel temperature increases by the continuous heat input, and thermal expansion of steel causes electrode separation. If the weld contains a suitable size of molten nugget, plastic deformation occurs in steel sheet, and the electrode displacement increases. If expulsion occurred, molten steel comes out, and it leads to a large amount of electrode movement. On the contrary, insufficient heat input makes a slow thermal expansion and eventually causes a decreasing the electrode movement.

$$Electrode\ movement = Plastic\ deformation - \ Thermal\ expansion$$

(5-5)

In terms of weld force, the shape of weld force curve is similar to the dynamic resistance curve. In the early weld cycles, the weld force is temporarily reduced by the surface breakdown and asperity softening of steel. This depends on the surface conditions of steel sheets and will come up a little later. As the weld nugget grows, weld force increases by the thermal expansion. Finally, if a good weld nugget is made, plastic deformation is made adequately, and it is expressed as indentation. On the other hand, a steep decrease and continuous increase of weld force are induced by an expulsion and not enough heat input, respectively.

Figure 5.8 and 5.9 are analysis results of welding signals measured from LVDT and weld force sensor at different level of weld current, a low weld current and an optimal weld current conditions. In Figure 5.8, normal and W inserted electrodes have shown a decrease of electrode movement after finish the surface breakdown. It means that the thermal expansion is still in progress. The normal electrode applying the weld current of 10 kA has shown a bigger movement at the beginning of welding, but the thermal expansion of weld nugget has progressed continuously. Another normal electrode which is applied lower weld current of 8 kA has a smaller movement and also was detected the thermal expansion until the end of weld time. W Ø3mm electrode has a bigger movement than the other electrodes, and W Ø4mm has shown a slight changing of electrode movement after 14 cycles. Finally, W Ø3mm inserted electrode has a bigger electrode movement than a normal electrode because the extruded length of insert material makes a bigger mechanical deformation. This phenomenon was also demonstrated from the weld force results in Figure 5.8 (b). Both of W inserted electrodes have a drop

73

of weld force at 3 cycles of weld time earlier than normal electrodes, and then, the curves of weld force have shown a peak at 9 cycles and 13 cycles. After finding a peak, the weld force was decreased because the weld nugget has become soft and decreased the thermal expansion. Normal electrode applied 10 kA of weld current has shown a peak at 9 cycles and had a lower weld force at 15 cycles. The reason why the normal electrode has a lower weld force than W inserted electrodes is that the total melting area of normal electrode is larger than W inserted electrodes. Therefore, the results of displacement and weld force are not same. However, in the case of the normal electrode welded with 8 kA, weld force was increased until 15 cycles because the thermal expansion is still progressing.
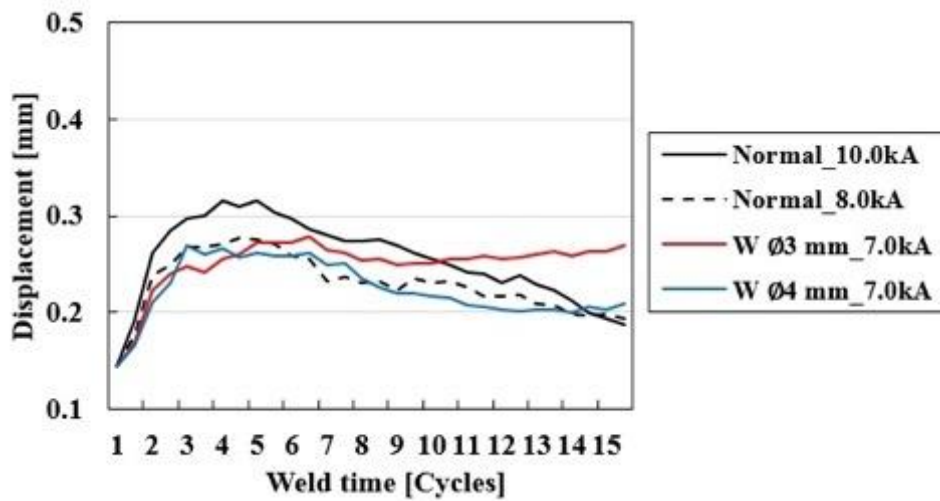


(a) Changing of electrode displacement
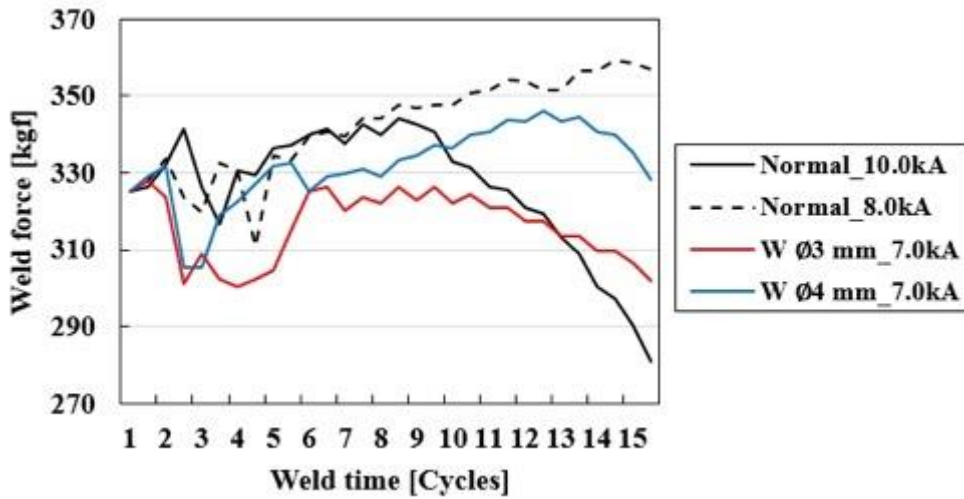


(b) Changing of weld force

**Figure 5.8** Comparison of displacement and force signals at a low weld current condition

Figure 5.9 describes electrode displacements and weld forces at high weld current and an optimal weld current. Unlike the result of low weld current, a normal electrode applying the weld current of 10.5 kA had a fast decrease of displacement similar to W inserted electrodes until 8 cycles. After that, it kept decreasing until 11 cycles, eventually, the expulsion was made from the excessive heat input. As a result of this, electrode movement has risen dramatically. At the same weld cycle, weld force has also shown a significant decrease because a large amount of molten metal moved out from the weld nugget. On the other hand, W inserted electrodes have started a mechanical deformation stably from 9 cycles.
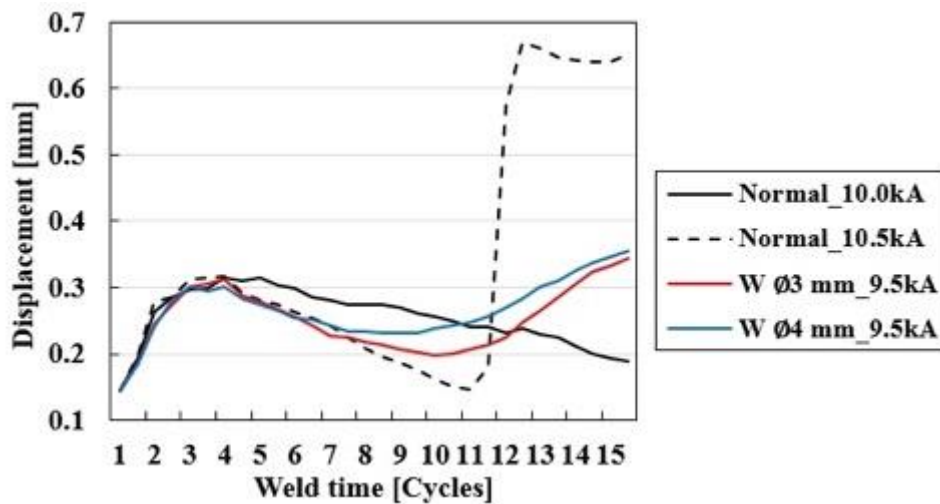


(a) Changing of electrode displacement
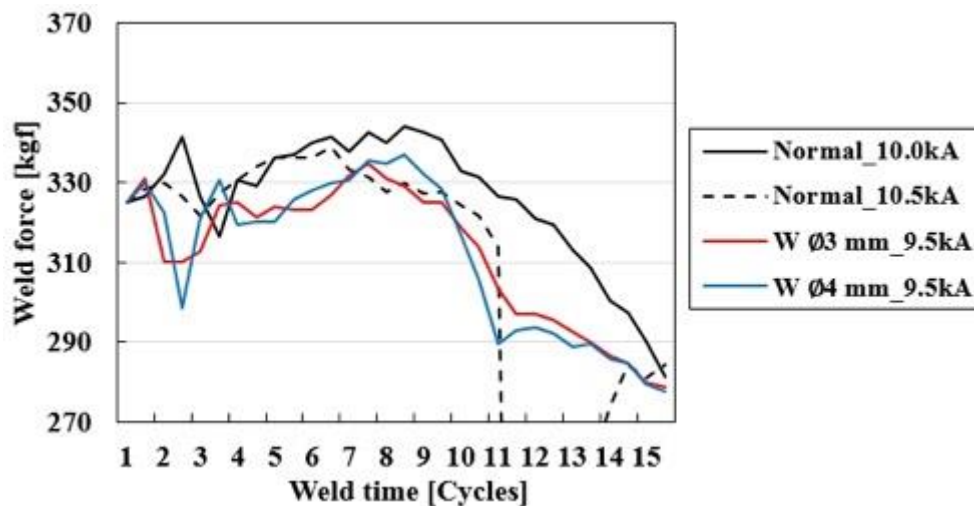


(b) Changing of weld force

**Figure 5.9** Comparison of displacement and force signals at an optimal weld current condition

Since the insert material was effective to melt the steel, the plastic deformation was made earlier, and the weld forces were reduced more than the normal electrode of 10 kA at 9 to 11 cycles. From the analysis of displacement and weld force, inserted electrodes have revealed that they have advantages for steel melting faster and easier.

### 5.2.4 Weld current flow analysis using FEA

From the result of the weld nugget formation, it was observed that there was a different type of weld current flow. To prove the weld current flow mechanism and the different assembled conditions, a spot welding simulation was performed by using a SORPAS® 2D commercial software [75]. The steel sheet and electrode were selected a zinc coated DP 600 and Class 2 (CuCrZr) electrode in the database, and the other welding parameters and boundary conditions were applied same as the real welding condition. Figure 5.10 shows the simulation results of the normal electrode and W inserted electrode for the weld nugget formation. The weld current density and the weld temperature plots were captured every 3 weld cycles. In the case of the normal electrode, current density (Avg. $0.8kA/mm^2$) was concentrated on the edge of the electrode and the melting was started at the faying surface that is formed a highest resistance. The current density in W inserted electrode also formed around the edge of electrode, but the intensity (Avg. $1.5 kA/mm^2$) was higher than normal electrode.

| Weld Cycles | Normal electrode | WØ3mm inserted electrode |
|---|---|---|
| 3 Cycles (50msec) | | |
| 6 Cycles (100msec) | | |
| 9 Cycles (150msec) | | |
| 12 Cycles (200msec) | | |
| 15 Cycles (250msec) | | |
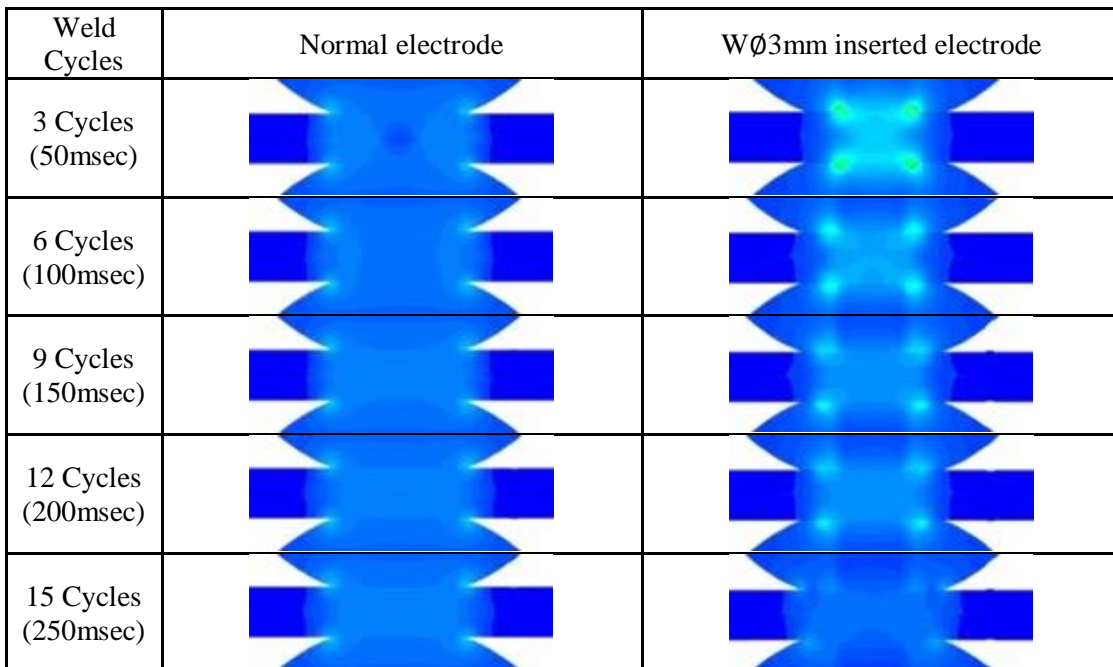
**Figure 5.10** Distribution of weld current density

As shown in Figure 5.10, W inserted electrode has shown a change in the flow of weld current. The weld current flew through the inserted material at the beginning of weld, but the weld current delivered through both the insert material and Cu electrode after 6 cycles. From the steel surface images of inserted electrodes in Figure 5.5, W inserted electrode was revealed that melted area was only made at the contact area of inserted material until 5 to 7 cycles. Therefore, the weld current density was formed high due to the small contact area of inserted material.
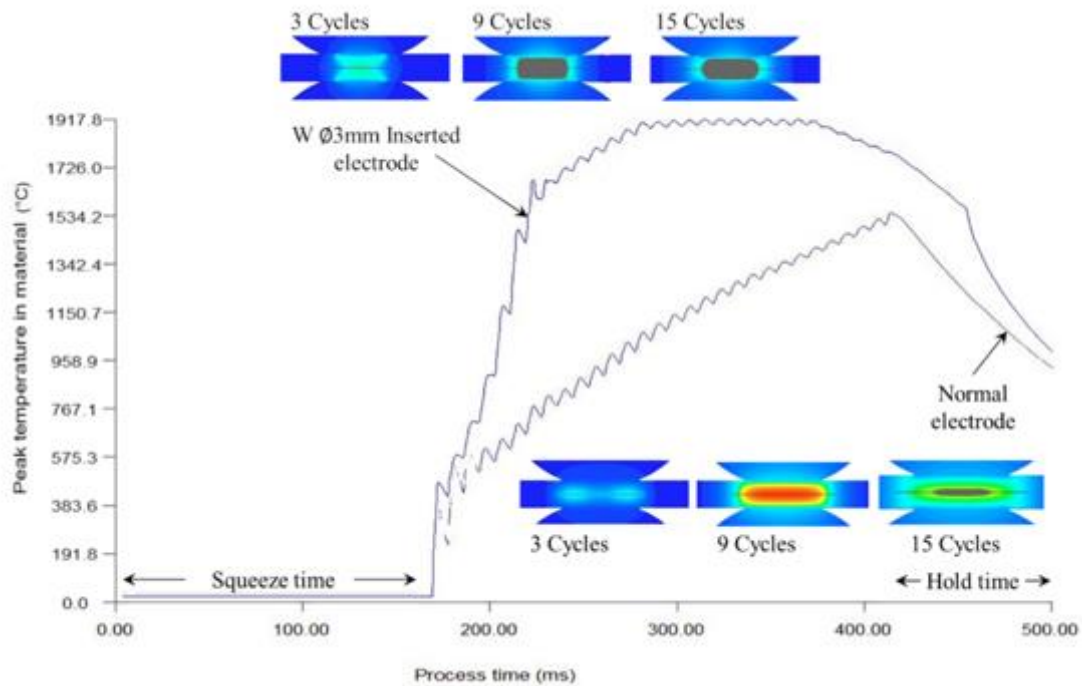


**Figure 5.11** Comparison of temperature profile

Figure 5.11 shows the welding temperature which is generating at each cycle. Normal electrode increased the weld temperature slowly, but W inserted electrode made a fast increase of temperature in weld nugget. Especially, W inserted electrode decreased the weld temperature after 12 cycles (200 msec.) because current flow changed from insert material to Cu electrode. Thus, the resistance heat which was generated from Cu electrode did not contribute to increase of weld temperature, but on the contrary it made the weld cool down. From the above results, the RSW process using inserted electrodes can be divided into two stages. The first stage, which accelerated melting speed, contributed to melt a zinc coating layer and steel effectively at the beginning of the weld. The second stage helps weld nugget grow stably.

In reality, according to the assembled electrode conditions, there was a disparity in weld performance. Representatively, three kinds of electrode conditions can be made during the fabrication. For example, the inserted material assembled with perfectly flat to the copper electrode, slightly extruded, and pushed up. Figure 5.12 shows the simulation results for these possible fabricating conditions having the length of -20, 0, and 20µm for extruded, flat, and pushed-up conditions. In the case of flat condition, the weld nugget formation was similar to the normal electrode, but the temperature did not increase enough to melt the steel. The pushed-up conditioned electrode had an unusual shape of temperature distribution. From the results of weld current density, flat and pushed-up conditioned electrodes did not flow the weld current through the insert material part. The flat electrode made an ideal contact, but weld current has dispersed and lower than pushed-up conditioned electrode. Eventually, the positive effect of inserted electrode is hard to implement in two assembled conditions.
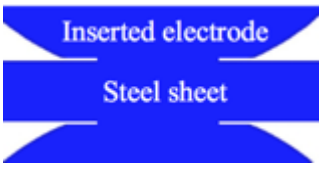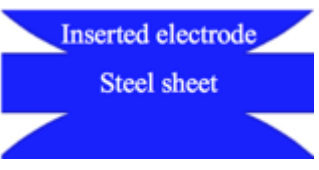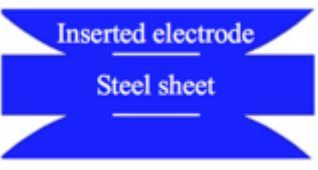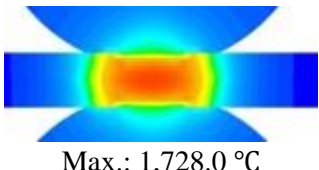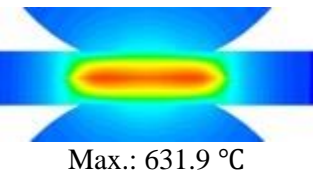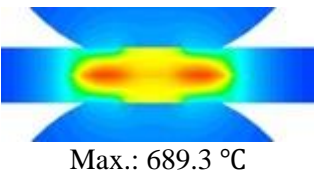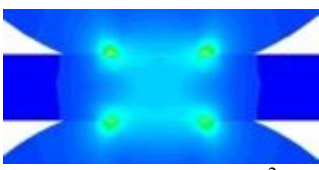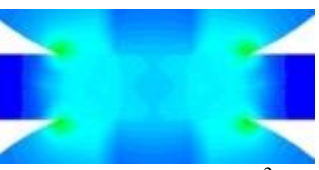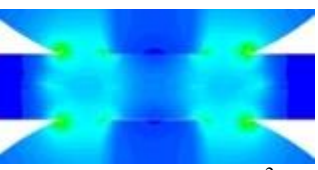
| Inserted condition | Extruded (-20µm) | Flat (0 µm) | Pushed-up (+20µm) |
|---|---|---|---|
| Electrode | Inserted electrode / Steel sheet | Inserted electrode / Steel sheet | Inserted electrode / Steel sheet |
| Temp. distribution (15cycles) | Max.: 1,728.0 ℃ | Max.: 631.9 ℃ | Max.: 689.3 ℃ |
| Current density | Max.: 1.82 kA/mm$^2$ | Max.: 0.40 kA/mm$^2$ | Max.: 0.44 kA/mm$^2$ |

**Figure 5.12** Simulation results for different fabricating conditions

Another important characteristic is that the heat affected area is generated larger than insert electrode having extruded condition. Since the weld current is concentrated on the edge of electrode [73], melting is started over a wide area, and finally the possibility of expansion of HAZ will be increased. Therefore, maintaining the clearance should be controlled very carefully when the insert material is assembled to Cu electrode.

78

## 5.3 Evaluation of Weldability for the Inserted Electrode

The weldability evaluation for the inserted electrodes was conducted with mechanical and metallurgical methods.

### 5.3.1 Weld lobe curve

As mentioned in Chapter 2, weldability can be described graphically in a 2-dimensional area by the weld lobe curve [1]. Table 5.3 shows the result of weld lobe curves for normal and WØ3mm inserted electrode base on the button diameter from the peel test. The other results are referred to in Appendix C. The green colored range, which is welded with low weld current or short weld time, is that the button diameter was not satisfied with the minimum criterion, and the orange colored area is the region which is made an expulsion repeatedly.

**Table 5.3** Weld lobe curves for Normal and W Ø3mm inserted electrode

| 24 | 0.00 | 5.20 | 5.79 | 6.72 | 6.49 | 5.64 | 7.31 | 5.75 |
| 21 | 0.00 | 4.47 | 5.49 | 6.43 | 5.42 | 6.63 | 5.19 | 6.01 |
| 18 | 0.00 | 3.92 | 4.88 | 6.65 | 5.42 | 5.46 | 5.70 | 5.81 |
| 15 | 0.00 | 3.32 | 4.53 | 6.51 | 5.24 | 6.29 | 5.86 | 5.44 |
| 12 | 0.00 | 0.00 | 3.14 | 4.84 | 5.33 | 7.65 | 5.65 | 5.67 |
| 9 | 0.00 | 0.00 | 0.00 | 3.95 | 4.15 | 4.74 | 5.20 | 5.15 |
| Cycles / Current[kA] | 7.5 | 8.0 | 8.5 | 9.0 | 9.5 | 10.0 | 10.5 | 11.0 |

(a) Normal electrode

| 24 | 2.77 | 4.84 | 5.43 | 5.88 | 7.53 | 7.38 | 5.73 | 5.68 |
| 21 | 2.71 | 4.69 | 5.25 | 7.83 | 7.90 | 8.25 | 6.38 | 6.37 |
| 18 | 1.12 | 4.96 | 5.1 | 7.59 | 7.45 | 8.27 | 7.26 | 6.26 |
| 15 | 0.00 | 4.83 | 5.43 | 6.98 | 7.82 | 8.10 | 7.98 | 7.90 |
| 12 | 0.00 | 4.66 | 5.04 | 5.40 | 6.92 | 7.22 | 5.88 | 6.16 |
| 9 | 0.00 | 3.09 | 4.28 | 5.14 | 6.67 | 7.19 | 5.18 | 7.46 |
| Cycles / Current[kA] | 6.5 | 7.0 | 7.5 | 8.0 | 8.5 | 9.0 | 9.5 | 10.0 |

(b) W Ø3mm inserted electrode

In the case of normal electrode, the largest width of weld current range was 2.0 kA at 15 cycles. On the other hand, the inserted electrodes, both of W and Mo, were expanded the lobe curves toward low weld current area, and made the weld button possible with short weld time. When a larger diameter of insert materials are used, the lobe curve range was reduced in low weld current range.

Figure 5.13 shows the expansion of weld lobe curves at the 15 cycles of weld time. Normal electrode had a welding possible range of 1.5kA, but inserted electrodes obtained an expanded welding range about 2.0 to 2.5 kA. At the maximum weld current for each electrode, expulsion was made, and it tended to reduce the button diameter due to the loss of liquid metal.
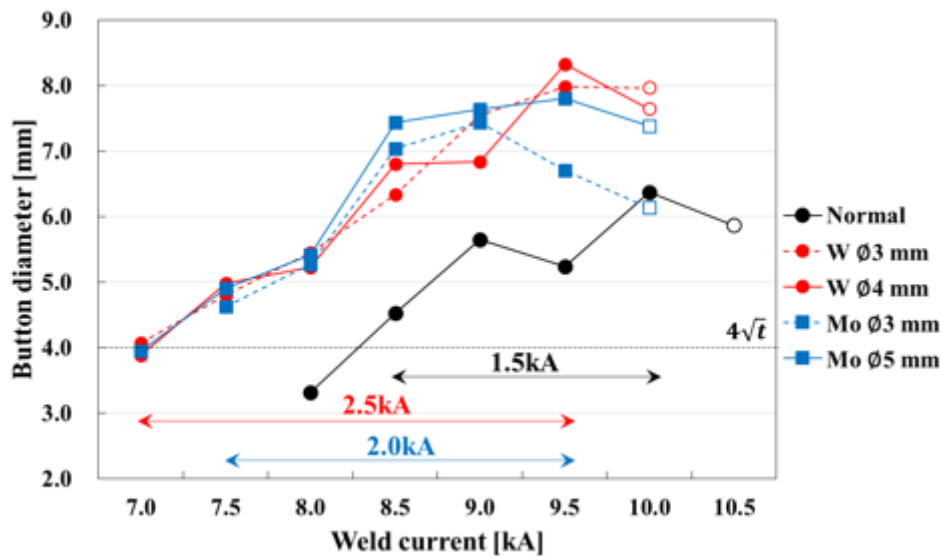


**Figure 5.13** Expansion of weld lobe curves for various electrode designs (open marks indicate expulsion)

## 5.3.2 Strength and microhardness results

Tensile shear (TS) and cross tension (CT) strength tests were conducted to evaluate more quantitatively as shown in Figure 5.14. As the weld current increases, the TS strengths for W and Mo inserted electrodes was increased linearly, and it slightly decreased at the maximum weld current. On the other hand, the CT strengths were not increased as much as TS strength. Similar to the trend of AHSS [6], the ductility ratio, which is used to represent the ductility of spot weld, decreased due to the high stiffness made from the high carbon equivalent. Interestingly, compared with the welding conditions

80

making a similar size in button diameter, normal electrode at 9.5kA has a lower CT strength than inserted electrodes at 7.5kA except Mo Ø3mm (refer to the Appendix D). The CT strengths of inserted electrode has improved about 28% more than normal electrode. And the CT strengths were improved in most of the weld current conditions except the maximum weld current making an expulsion.
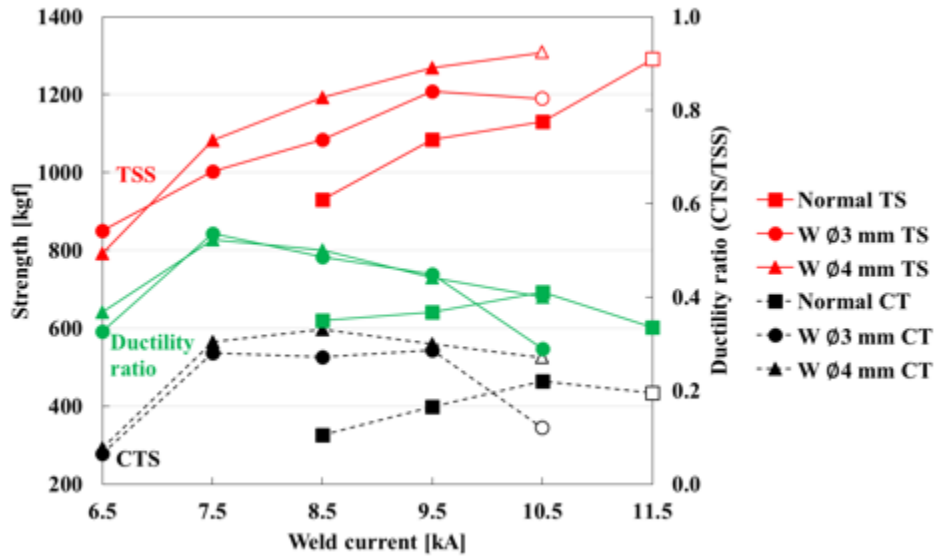


(a) Comparison of normal and W inserted electrodes
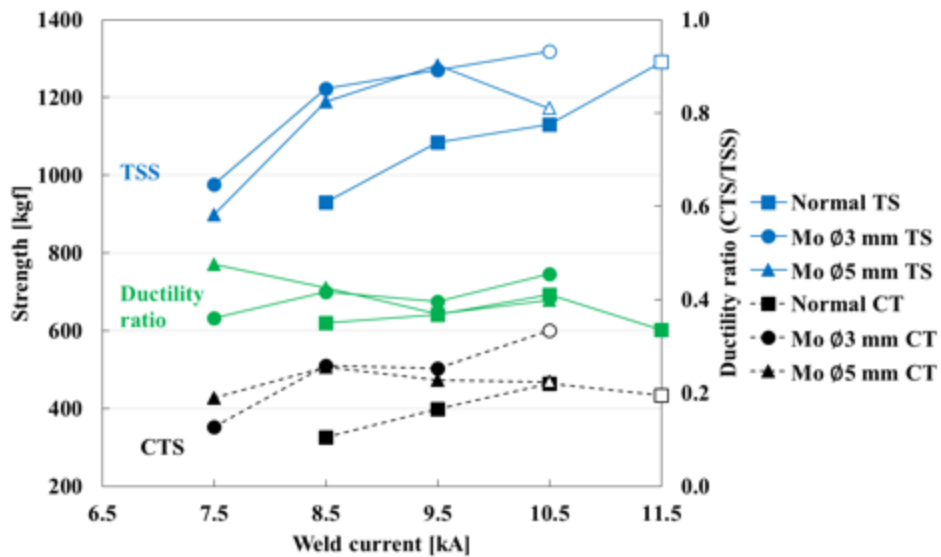


(a) Comparison of normal and Mo inserted electrodes

**Figure 5.14** Strength test results of DP600 spot welds produced using various electrodes

To evaluate the improved mechanical characteristic of inserted electrode, welding specimens, at 9.5kA and 7.5kA for normal and inserted electrodes, were selected because they have shown a similar CT strength. Figure 5.15 shows CT strengths, button diameters, and heat inputs. Based on the welding signal results in Figure 5.5 and 5.6, the heat input for nugget growth was calculated excluding early stage of weld. Heat input was calculated from the welding signals, weld current and voltage, during the weld time by equation (5.6).

$$Q = \int_{T1}^{T2} i(t)^2 R(t) \, dt \ = \int_{T1}^{T2} i(t) \, v(t) \, dt$$

(5.6)

Normal electrode has shown a bigger button diameter due to the large amount of heat input made from higher weld current, but CT strength was not improved as much as the inserted electrodes. To calculate the real heat input which was used for steel joining, the early heat input was removed and recalculated based on the result of weld nugget formation. Consequently, similar amounts of real heat input were used for joining. The red colored bars are the real heat input except the heat input spent for zinc removing and steel heating. The weld time was decided based on the weld nugget formation results in Figure 5.5 and 5.6. The heat input for normal electrode was calculated from 8 to 15 cycles, and inserted electrodes were calculated from 3 or 5 to 15 cycles.
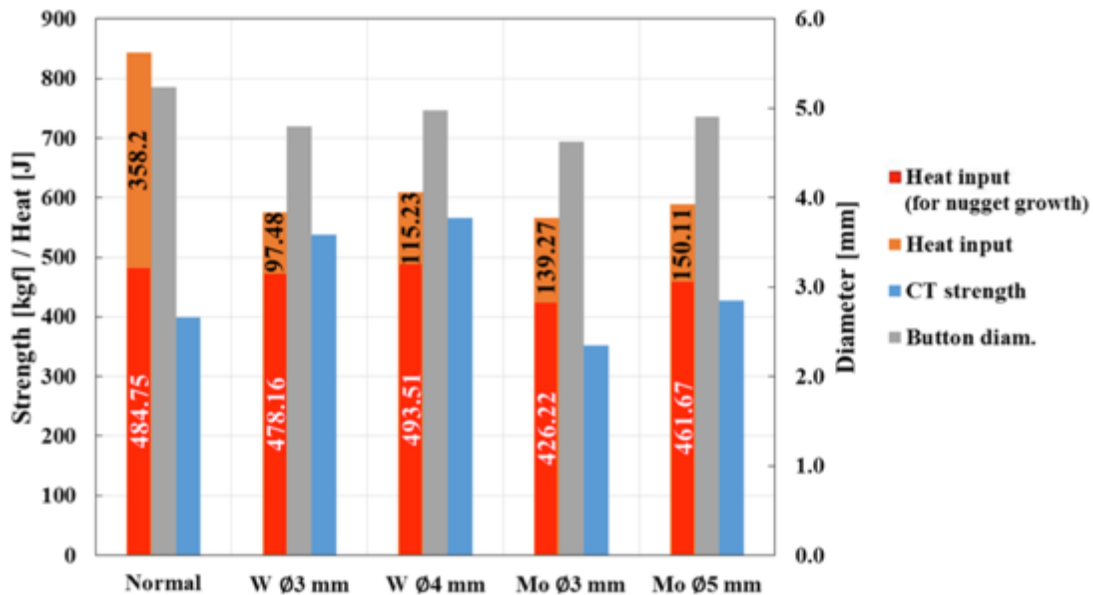


**Figure 5.15** Correlation between heat input and mechanical performance for each electrode

82

In general, inserted electrode has shown an improved weld qualities more than the normal electrode. However, in the case of Mo inserted electrodes, button diameter and CT strength were lower than W inserted electrode at 7.5kA because the weld current is so close to the lower limit of weld lobe curve that the weld qualities were not enough. However, considering the low weld current, the inserted electrodes, especially W inserted electrodes, have shown an improved CT strength with low weld current.

### 5.3.3 Micro-hardness results

To identify the reason for the improved CT strength above, the microhardness across each weld was measured. Figure 5.16 describes the overlapped results of hardness and microstructure images for normal and WØ3mm inserted electrode to achieve more accurate analysis. The regions affected by the heat were identified with FZ, CG-FG-ICHAZ, and SCHAZ/BM to be divided at the Ac1 line of critical transformation temperature, which is known as an austenizing temperature, based on optical microscopy [74]. The average hardness in FZ was formed about 400 to 430Hv, and BM had a hardness of about 210 to 230Hv. A sharp hardness drop was made between the boundary of SCHAZ/BM and CG-FG-ICHAZ (Ac1 line), and the hardness values decreased from 400Hv to below 250Hv. SCHAZ including softening zone has been detected and identified in AHSS [38], but for DP600 this region is hard to determine the region clearly. Thus, in this study, CG-FG-ICHAZ and FZ were used for the verification of the effect of inserted electrode.
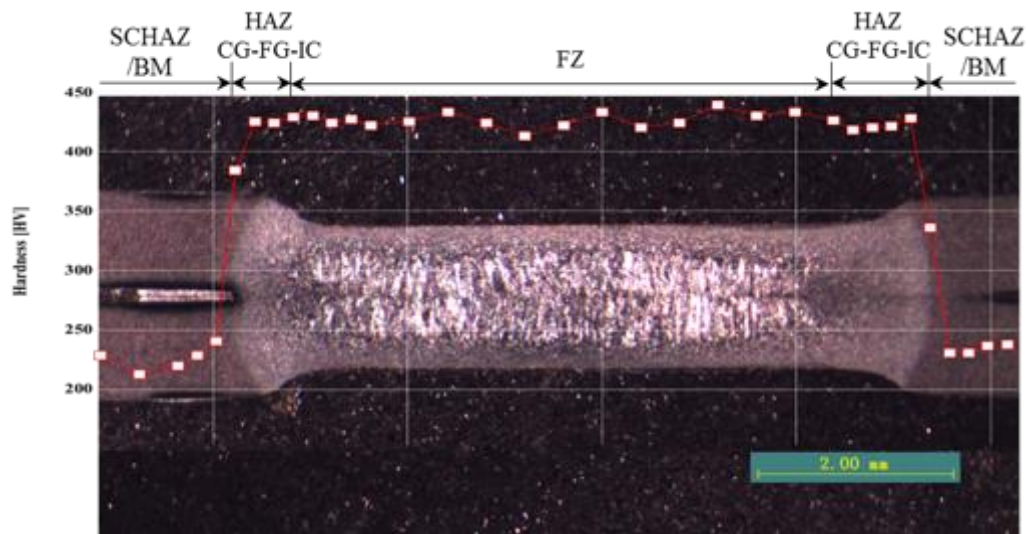


(a) Normal electrode with 10.5kA, 15 Cycles
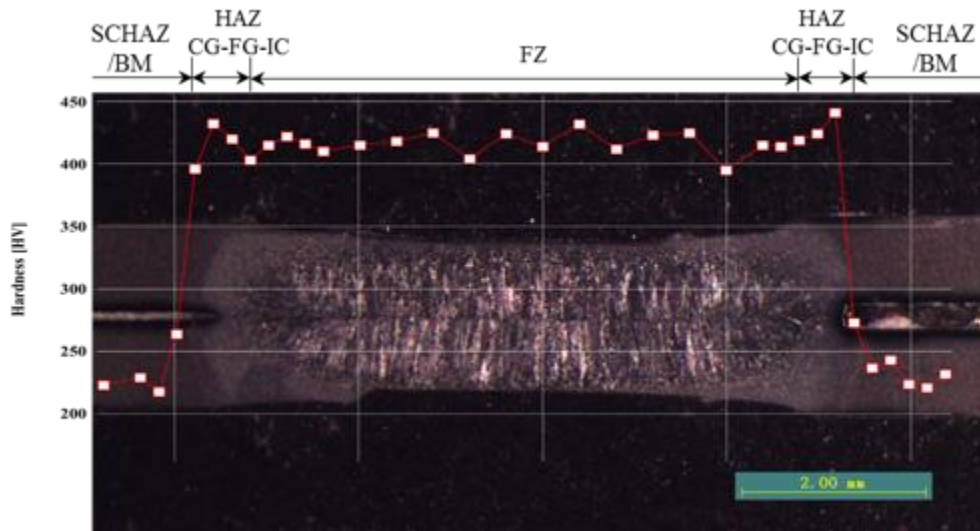
(b) WØ3mm inserted electrode with 7.5kA, 15Cycles
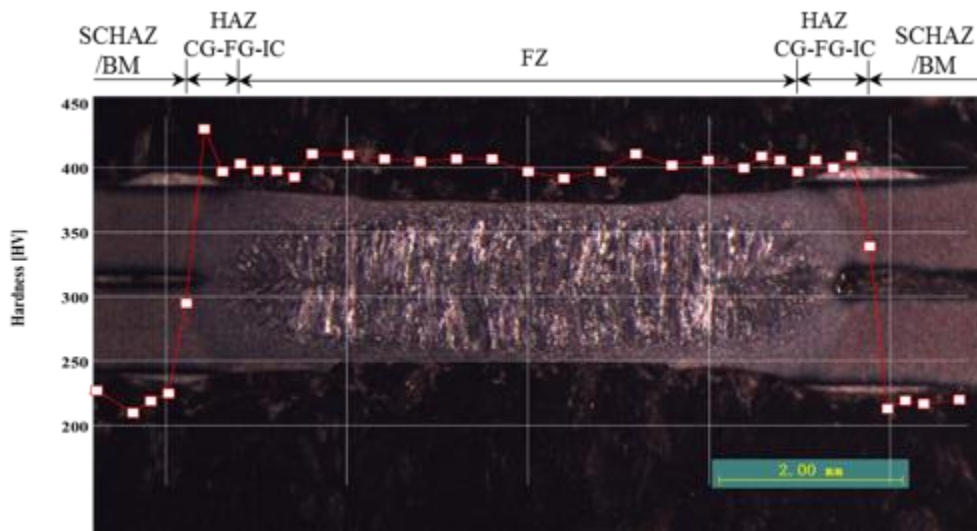


(c) WØ3mm inserted electrode with 9.5kA, 15 Cycles

**Figure 5.16** Micro-hardness test results

Normal electrode has been measured 5.54 mm and 7.14 mm for FZ and CG-FG-ICHAZ including FZ. To verify for the effect of low weld current and inserted material, cross-sectional specimens, which is welded with WØ3mm inserted electrode and 7.5 kA of weld current, were analyzed as seen in Figure 5.16 (b) and (c). The dimension of FZ and CG-FG-ICHAZ including FZ for Fig 5.16 (b) specimen has been measured 5.94 mm and 7.17 mm, and Fig 5.16 (c) has been determined 6.06 mm and 7.39 mm, respectively. As the previous result for the heat input, the weld specimen made by normal electrode

was expected that it will have a larger heat affect area than inserted electrodes. Approximately, the inserted electrode had a larger nugget diameter, but the CG-FG-ICHAZ was not expanded as much as normal electrode. As shown in equation (5-7) below, the HAZ ratio was defined for a quantitative comparison of HAZ expansion.

$$\text{HAZ ratio} = \frac{FZ\ width}{FZ\ width + HAZ_{CG-FG-IC}\ width}$$

(5-7)

Normal electrode has shown a ratio of 0.79, and W Ø3mm inserted electrodes represented a ratio of 0.83 and 0.82. For the other specimens, HAZ ratio was calculated as shown in Appendix E.
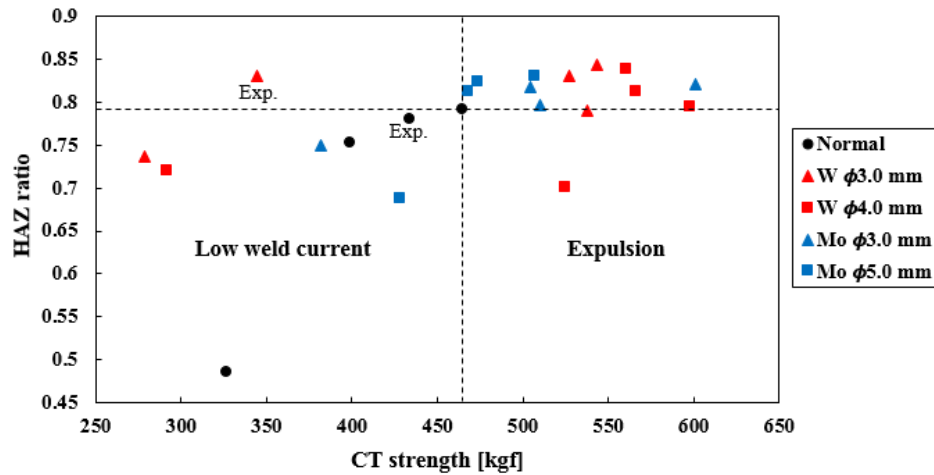


(a) CT strength vs HAZ ratio
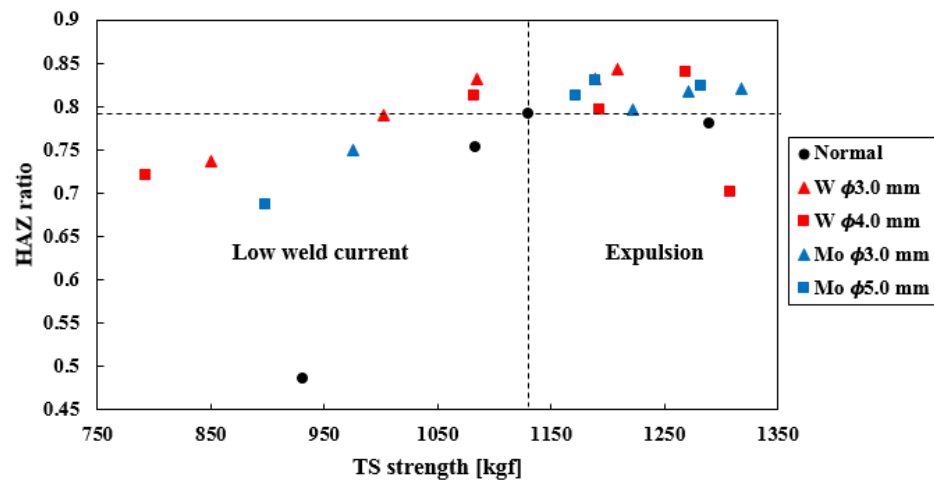


(b) TS strength vs HAZ ratio

**Figure 5.17** Correlation between strengths and HAZ ratio

85

Figure 5.17 describes the effect of HAZ ratio that affects the mechanical strengths. In each figure, the black colored dot lines are the strength and HAZ ratio of normal electrode which is welded with optimal weld current, and the result was used for criterion. From the result of CT strength in Figure 5.17 (a), low strengths were developed on the left side of the plot because the specimens were made a small weld nugget from the low weld current. On the right side, it was located the specimens which is made an expulsion. Since the severe expulsion made from high weld current can cause a drop in strength, few welds of W∅3mm and normal electrodes were made on the left side. Based on the HAZ ratio line of 0.79, most of specimens for inserted electrode were located at the top-right of the plot. Thus, it was revealed that inserted electrodes are able to make a better weld joining with low weld current. This trend similarly comes to the TS strength results of Figure 5.17 (b). The low strength specimens welded with low weld current were located underneath the left side of the plot, and the expulsion specimens are located on the right side with the low HAZ ratio generated from the excessive heat input.

As a result, the normal electrode has shown a lower TS and CT strength than W inserted electrodes. In comparison with W inserted electrodes, 7.5kA specimen has a slightly small FZ, and hence the TS and CT strengths were produced lower than the 9.5kA specimen. However, in terms of minimizing the CG-FG-ICHAZ, 7.5kA of welding condition has shown a bigger HAZ ratio. Therefore, it was proved that the more heat input will not guarantee the higher CT strength, and minimized HAZ lead to improved mechanical strength.

Even though the weld specimen of normal electrode was made in an optimal welding current, the CT strength was made lower than the inserted electrodes. To investigate the fracture characteristic, the weld specimens having a similar weld nugget diameter were selected. Figure 5.18 describes the fracture surface of each CT specimens. The normal electrode welded with 10.5 kA had a low HAZ ratio of 0.79 and was even observed cracks which are propagated from the steel surface to weld nugget and. In terms of fracture, crack initiation was not started at the base metal, but at the edge of the weld nugget. However, inserted electrodes promote fracture which starts from the boundary of CG-FG-ICHAZ and necking in BM area. Even though the weld nugget diameter was similar, the fracture shape was different. The measured fracture diameters from the fracture specimens were 7.12, 7.37, and 7.48mm in order of normal, W∅3mm, and Mo ∅5mm electrodes. As mentioned in Chapter 2, the value of CT strength mechanically depends on the diameter and thickness of weld nugget. Thus, the inserted electrodes, having a narrow CG-FG-ICHAZ, were more beneficial for improvement of CT strength than the normal electrode.

(a) Normal electrode at 10.5kA



(b) W Ø3.0mm electrode at 8.5kA



(c) Mo Ø5.0mm electrode at 8.5kA
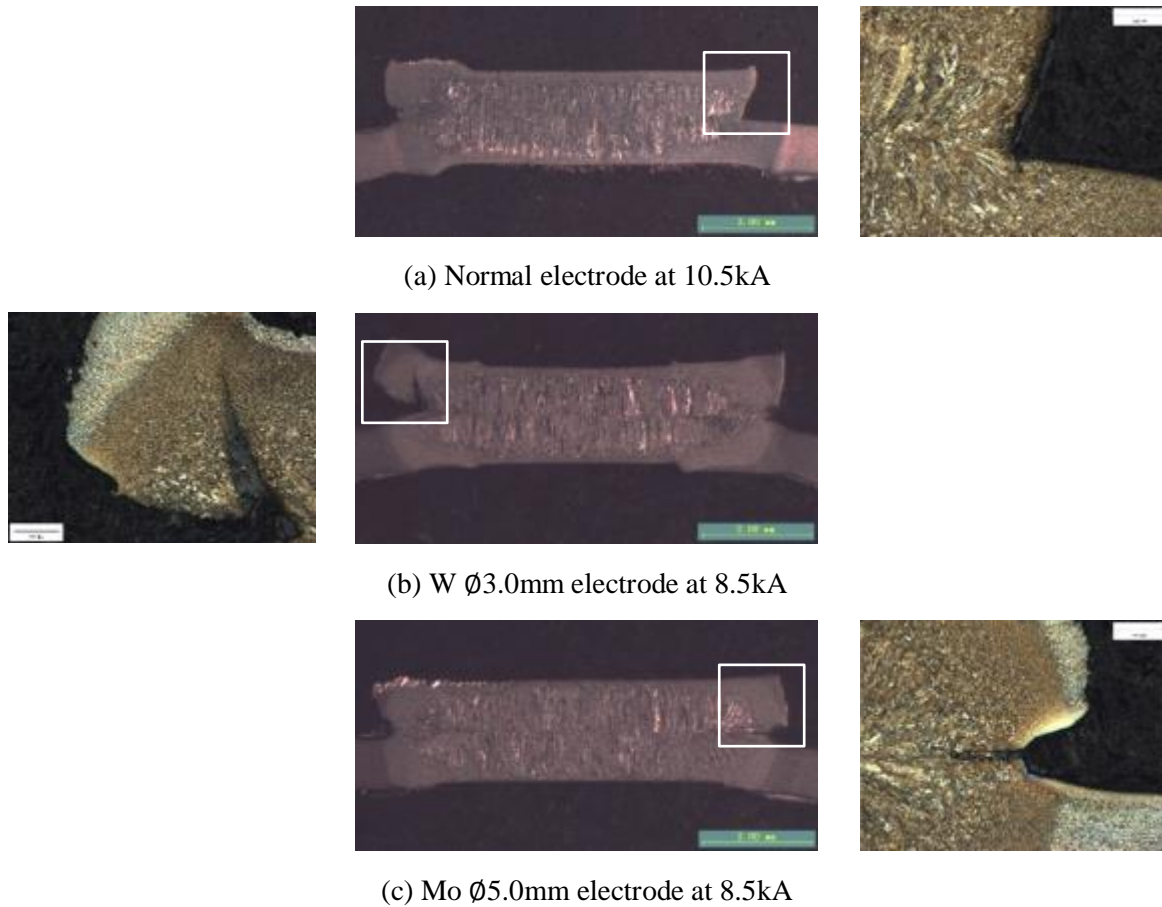
**Figure 5.18** Cross section of fracture specimens

## 5.4 Electrode life for the Inserted Electrode

Electrode life tests were conducted for the W and Mo inserted electrodes, and the results are the same as the Figure 5.19. According to the increasing of the diameter of insert material, the electrode life was increased. The electrode life of Mo Ø3mm was finished at the 1,800 welds. In comparison to W Ø3mm electrode, the electrode life was short. The main reason for the short electrode life of Mo Ø3mm electrodes was caused by the decreased current density. Since the Mo has a lower fracture toughness than Cu, buckling is easily made on the edge of electrode surface in the assembly process of inserted electrode. Additionally, from the imprinting images in Figure 5.20 (a), Mo has revealed that it was easily softened and made a good contact condition from the repeated weld force and the effect of resistance enhancement was reduced the same as the 'A' in the plot. As a result of the increase of contact area, the resistance, 'B', at the final cycles of weld was getting lower like 'C'. Thus, Mo Ø3mm

has a shorter electrode life compared to the other electrodes. However, W Ø3mm had an improved electrode life of 4,400 welds because the high current density was well maintained. This result detected from the imprinting images and dynamic resistance curves as shown in Figure 5.20 (b). As the welding progressed, β-peak was clearly made from the insert material earlier than the first weld same as the 'A' in the plot. Furthermore, the mechanical clearance led to form a high contact resistance at the initial weld cycle like 'C' in the figure. This shape of dynamic resistance was maintained until 4,000 welds. However, due to the increased Cu electrode area, the resistance to nugget growth sharply dropped, and finally the electrode life ended at 4,400 welds. W Ø4mm has shown a similar trend in dynamic resistance curve (refer to Appendix F). Instead, the bigger diameter of insert material generated the higher resistance after the β-peak. Thus, the button diameter has been made during 8,400 welds. In the case of Mo Ø5mm, the fracture toughness is low, but the contact area of insert material is relatively larger than the other electrodes. Therefore, the softening issue for insert material was relatively reacted low, and the high resistance was maintained until 10,500 welds, and it has a longest electrode life among all inserted electrodes.
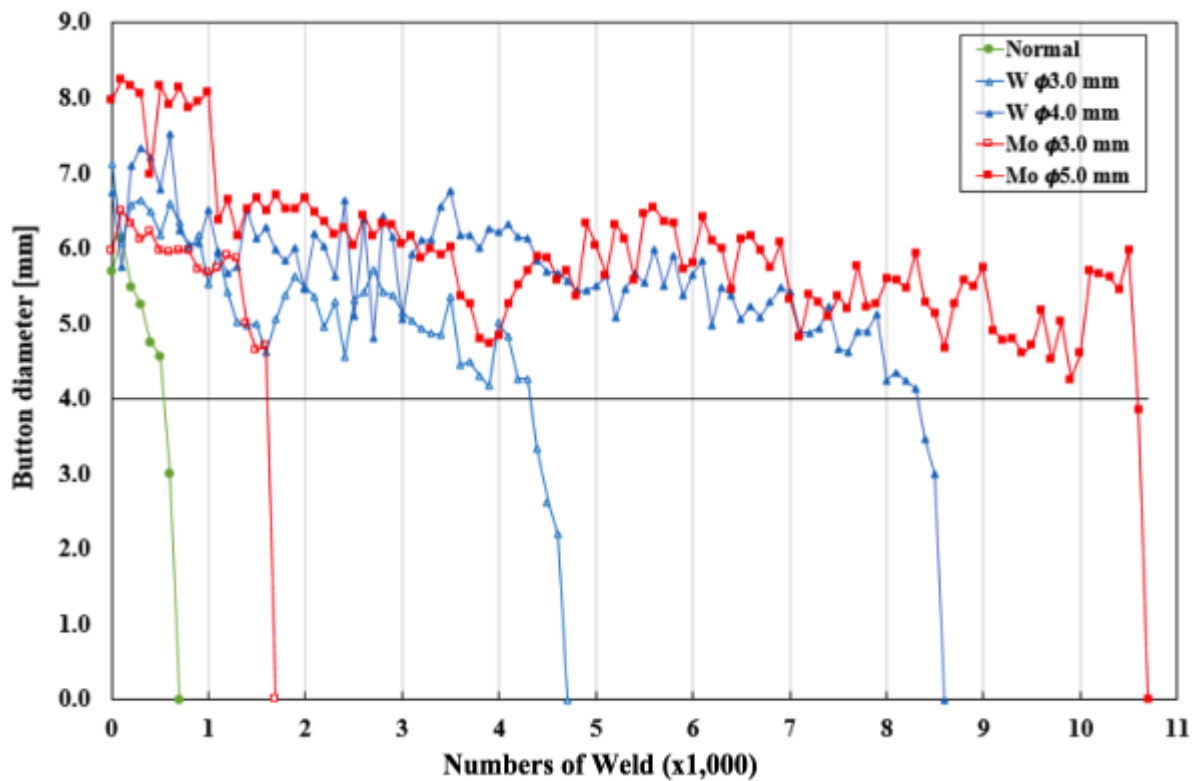


**Figure 5.19** Electrode life test results for the inserted electrodes
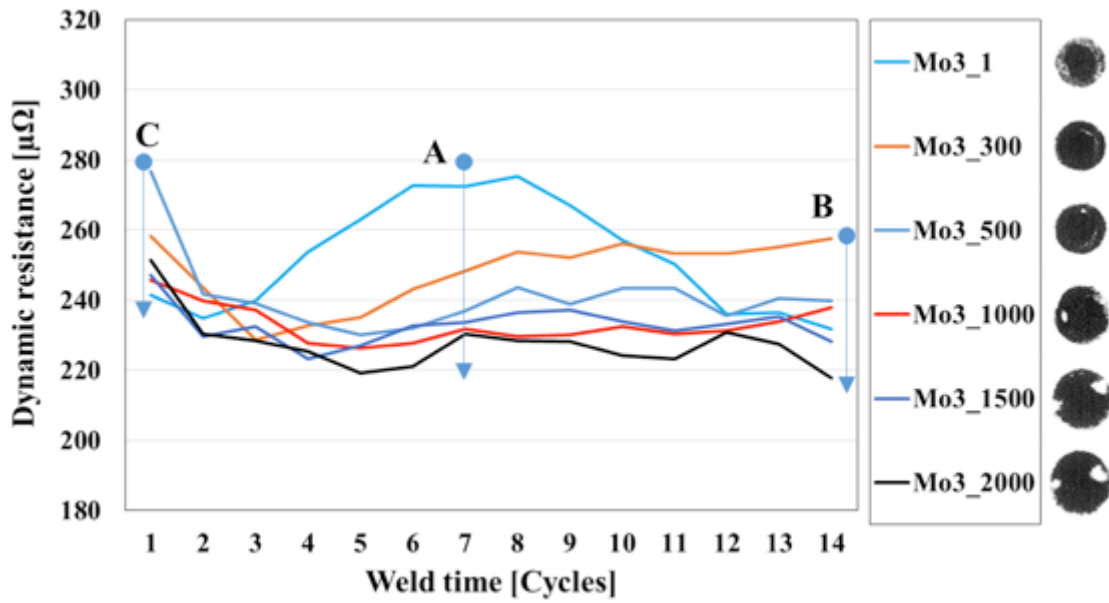
(a) Mo Ø3.0mm inserted electrode
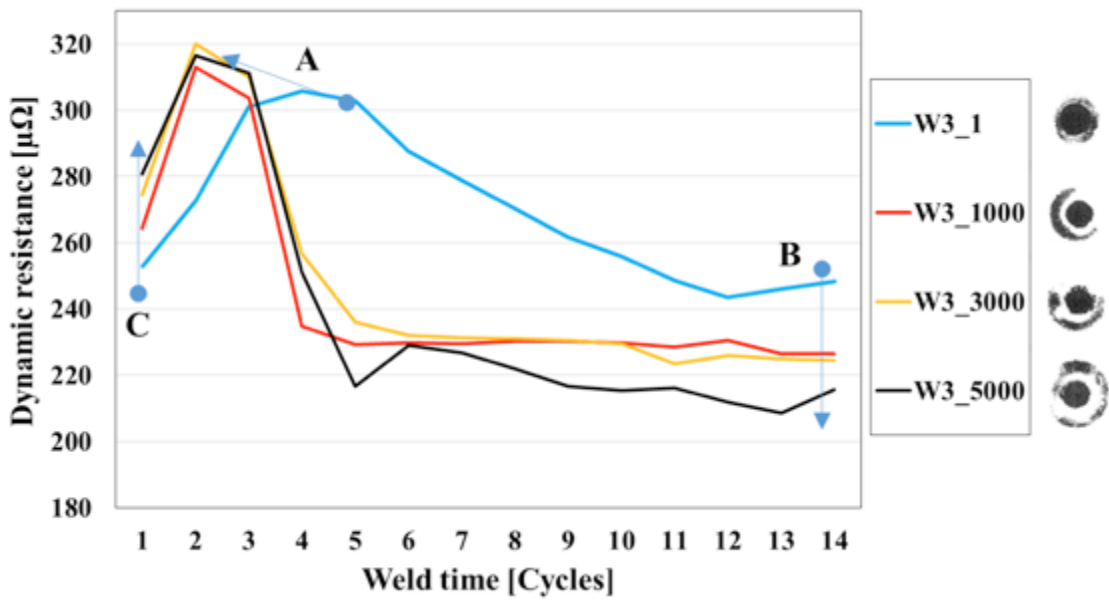


(b) W Ø3.0mm inserted electrode

**Figure 5.20** Changing of dynamic resistance at different number of welds

## 5.5 Summary

A new type of inserted electrode was investigated for improving weldability and increasing electrode life. The effect of inserted electrodes was demonstrated through the mechanical/metallurgical tests, welding signal analysis, and FEA.

Insert materials form a higher electrical resistance between electrodes and steel sheets, and it contributed to removing a zinc coated layer within a shorter weld time than normal electrode. By using a mechanical tolerance, the zinc removal has been made more effective. Additionally, the weld current flow changed from insert material to Cu electrode, and it helped to form a higher weld current density at the beginning of the weld. Therefore, the inserted electrode can reach the acceptable weld nugget with a short weld time or low weld current.

From the effect of the increased resistance, lobe curves of inserted electrodes were expanded. Especially, it was possible to achieve good weld qualities, such as strength and button diameter, with low weld current, about 7.0 kA to 8.5 kA. In the case of upper weld current limits, it has decreased 0.5 to 1.0 kA due to the high resistance of the insert materials.

At the welding conditions making a similar button diameter, inserted electrodes have shown bigger CT strengths than the normal electrode. This is because it was possible to melt a zinc and form a weld nugget with less heat input. As a result, the less heat input formed a narrow width of CG-FG-IC HAZ, and it was identified from the measurement of hardness and calculation of HAZ ratio.

Mo ∅5.0 mm inserted electrode has shown the most increased electrode life among the tested electrodes. Depending on the diameter of inserted electrode, there was a significant difference of electrode life. This is due to the fact that the larger contact area of inserted material has a higher possibility to make an acceptable weld nugget for the reduced weld current density.

# Chapter 6

# Conclusions and Recommendations

## 6.1 Evaluation of Electrode Life in RSW of Zinc Coated AHSS

Electrode life tests for the GI coated DP600 were conducted to evaluate electrode performance. Electrode material, geometry, and TiC/Ni coating were chosen and assessed for main electrode parameters. The following conclusions were reached:

1. Class 3 electrodes exhibited a larger recrystallized area (heat affected area) and thicker alloying on the electrode surface. These issues accelerated electrode softening and caused more heat loss during the weld. Therefore, Class 3 electrodes are not suitable for zinc coated AHSS RSW.

2. Parabolic shaped electrodes have a negative effect on the increase of electrode life. The small volume and sharp shape create poorer conditions for heat transfer. The contact surface area increased rapidly after 300 welds, and that induced a rapid decrease in weld current density. Therefore, parabolic shaped electrodes are not appropriate for reducing electrode deformation.

3. TiC/Ni coating was ineffective on Class 3 and parabolic shaped electrodes, but highly effective on dome shaped and Class 2 electrodes demonstrating electrode life as high as 1,900 welds. TiC/Ni coated electrodes showed less softening of the base electrode material and formed a thinner re-crystallized layer.

## 6.2 Improvement of Weld Performances with the Inserted Electrode

A new type of inserted electrode was proposed and investigated for improved weld quality and increased electrode life.

1. Insert materials form a higher electrical resistance between the electrode and the steel sheet, contributing to earlier removal of the zinc coating layer. The mechanical clearance of the insert material causes more effective zinc melting and improves weld current flow.

2. The analysis of dynamic resistance, electrode displacement, and weld force data shows that the inserted electrodes are able to form an acceptable weld nugget in a shorter time or with lower weld current.

3. The inserted electrodes shift the lobe curves toward lower weld currents and expand them.

4. Since the inserted electrodes require less energy for melting the zinc layer and forming the weld nugget, it was observed that a narrower HAZ width was formed. Consequently, higher CT strengths were observed.

5. W∅4.0 mm and Mo ∅5.0 mm inserted electrodes show the longest electrode life of those materials investigated.

## 6.3 Recommendations

1. Parabolic shaped electrodes have shown good weld current density within a lifetime of 300 welds. Therefore, investigation and optimization of geometry should be performed for minimizing electrode deformation.

2. The inserted electrode was proposed and investigated using only W and Mo refractory materials. Both materials have good mechanical and thermal properties, but investigation of other refractory materials or ceramic materials may result in further improvements.

3. Regarding reliability, the mechanical strength tests for inserted electrodes should be repeated sufficient to provide statistical confidence.

4. The inserted electrode has not made any cracks on the weld area of steel surface. Thus, the effect of reducing cracks needs to be investigated for other AHSSs.

# Bibliography

[1] N. T. Williams and J. D. Parker, "Review of resistance spot welding of steel sheets - Part 1," International Materials Reviews, vol. 49, no. 2, pp. 45-75, 2004.

[2] D.L. Olsen, 1993, "ASM Handbook: welding, brazing, and soldering", ASM International, Vol.6.

[3] P. K. Goldberg, 1998, "The effects of the corporate average fuel efficiency standards in the U.S. Journal of Industrial Economics", 46(1), pp.1-33.

[4] M. Ahman, 2001, "Primary energy efficiency of alternative powertrains in vehicles", Energy Vol.26, pp.973-989.

[5] G. S. Cole and A.M. Sherman, 1995, "Lightweight Materials for Automotive Applications", Material Characterization, Vol.35, pp.3-9.

[6] http://www.metalformingmagazine.com/magazine/article.asp?iid=64&aid=5942

[7] D. Y. Choi and Y. G. Kim, 2009, "Trend of Joining Technology for Automotive Sheet Steels", Journal of KWJS, Vol.27, No.2, pp.125-130.

[8] Auto Steel Partnership "Advance High Strength Steel Application Guidelines", IISI, March 2005.

[9] G. Williams, H.N. McMurray, M.J. Loveridge, 2010, "Inhibition of corrosion-driven organic coating disbondment on galvanized steel by smart release group II and Zn(II)-exchanged bentonite pigments", Electrochemical Acta, Vol. 55, pp.1740-1748.

[10] A. Amirudin, D. Thierry, 1996, "Corrosion mechanisms of phosphate zinc layers on steel as substrates for automotive coatings", Progress in Organic coatings, Vol.28, pp.59-76.

[11] Finlay, M. R., "Resistance Spot Welding of Metallic Coated Steels and PVD Coated Electrodes", CRC Australia and WTIA, CRC No. 18, 1996.

[12] N. T. Williams, "Resistance Spot Welding," in ASM Handbook, Volume 6, Welding, Brazing, and Soldering, D. LeRoy Olson, T. A. Siewert, S. Liu and G. R. Edwards, Eds., Materials Park, ASM International, 1993, pp. 226-229.

[13] H. Zhang and J. Senkara, Resistance Spot Welding - Fundamental and Application, Boca Raton, FL, Taylor & Francis Group, 2006, pp.50-59, pp.143-185.

[14] Shinkokiki Co.,Ltd, "Basis and Point of Resistance Welding (1)," Shinkokiki Co., Ltd, 2014.

[15] S. Aslanlar, A. Ogur, U. Ozsarac, E. Ilhan, and Z. Demir, 2007, "Effect of welding current on mechanical properties of galvanized chromized steel sheets in electrical resistance spot welding", Material and Design 28, pp.2-7.

[16] B. H. Chang, and Y. Zhou, 2003, "Numerical study on the effect of electrode force in small-scale resistance spot welding", Journal of Materials Processing Technology 139, pp. 635-641.

[17] M. Pouranvari, H. R. Asgari, S. M. Mosavizadch, P. H. Marashi, and M. Goodarzi, 2007, "Effect of weld nugget size on overload failure mode of resistance spot welds", Science and Technology of Welding and Joining Vol. 12 No. 3, pp.217-225.

[18] H. Tang, W. Hou, S. J. Hu, and H. Zhang, 2000, "Force Characteristics of Resistance Spot Welding of Steels", Welding Journal, pp.175-183s.

[19] M. P. Groover, 2007, "Fundamentals of Modern Manufacturing - Part VIII Joining and Assembly Processes, 30 Welding Process", John Wiley & Sons. Inc.

[20] J. G. Kaiser, G. L. Dunn, and T. W. Eagar, 1982, Welding research supplement, Journal of Electrical Materials, vol. 61, pp.167-174.

[21] Y. Cho, S. Rhee, Primary circuit dynamic resistance monitoring and its application to quality estimation during resistance spot welding, Weld. J. 81(2002) 104s–111s.

[22] Dickinson D W, Franklin J E and Stanya A, 1980, "Characterization of spot welding behavior by dynamic electrical parameter monitoring", Welding J., 59 pp.170s–176s.

[23] AWS D8.1M:2007, Specification for automotive weld quality-Resistance spot welding of steel

[24] J. Yu, J. Shim and S. Rhee, 2012, Characteristics of Resistance Spot Welding for 1 GPa Grade Twin Induced Plasticity Steel, Materials Transactions, Vol. 53, No. 11 (2012) pp. 2011-2018.

[25] Bain EC (1939) Functions of the alloying elements in steel (American Society for Metals, Cleveland, OH).

[26] H. Oikawa, T. Sakiyama, T. Ishikawa, G. Murayama, Y. Takahashi, Nippon Steel Technol. Rep. 2007, 95, 39.

[27] D. C. Saha, S. Han, K. Chin, I. Choi, and Y. D. Park, 2012, Weldability Evaluation and Microstructure Analysis of Resistance-Spot-Welded High-Mn Steel in Automotive Application, Steel Research International, Vol 83, No.4, PP. 352-357.

[28] A. R. Marder, 2000, "The metallurgy of zinc-coated steel" Progress in Materials Science 45, pp.191-271.

[29] Finlay, M. R., "Resistance Spot Welding of Metallic Coated Steels and PVD Coated electrodes", CRC Australia and WTIA, CRC No. 18, 1996.

[30] S.A. Gedeon, and T. W. Eagar, 1986, Resistance Spot Welding of Galvanized Steel-Part I. Material Variations and Process Modifications, Metallurgical transaction B, Vol. 17B, pp.879-885.

[31] S.A. Gedeon, C. D. Sorensen, K. T. Ulrich, and T. W. Eagar, 1987, "Measurement of Dynamic Electrical and Mechanical Properties of Resistance Spot Welds", Welding Journal, pp.378s-385s.

[32] E.W. Kim, and T. W. Eagar, 1988, "Transient Thermal Behavior in Resistance Spot Welding", AWS SMWC III, pp.1-28.

[33] Z.H. Rao, S.M. Liao, H.L. Tsai, P.C. Wang, and R. Stevenson, 2009, "Mathematical modeling of electrode cooling in resistance spot welding", Welding Journal. 88, pp.111s–119s.

[34] K. Chan, et al., 2006, "Effect of electrode geometry on resistance spot welding of AHSS", AWS Sheet Metal Welding Conference XII.

[35] Y.B. Lee, C.S. Chung, Y. K. Pack, and J. H. Choi, 1999, The effects of tail contact for spot welding peel-tension specimen, Journal of KWS, Vol. 17, No. 4, pp.69-75.

[36] C. Ma, D.L. Chen, S.D. Bhole, G. Boudreau, A. Lee, E. Biro, 2008, Microstructure and fracture characteristics of spot-welded DP600 steel, Materials Science and Engineering A, 485, pp.334–346.

[37] Chao, 2003, Journal of Engineering Materials and Technology, Ultimate Strength and failure Mechanism of Resistance Spot Weld Subjected to Tensile, Shear, or Combined Tensile/Shear Loads, Vol. 125, pp. 125-132.

[38] V. H. B. Hernandez, S. K. Panda, Y. Okita, and Y. Zhou, 2010, "A study on heat affected zone softening in resistance spot welded dual phase steel by nanoindentation", Journal of Material Science, pp.1638-1647.

[39] M. Tamiz, M. Pouranvari, and M. Movahedi, 2017, "Welding metallurgy of martensitic advanced high strength steels during resistance spot welding", Science and Technology of Welding and Joining, Vol.22, No.4, pp.327-335.

[40] P. K. Ghosh, P. C. Gupta, O. M. Pal, A. R, B. K. Jha and V. Sagar Dwivedi, Influence of Weld Thermal Cycle on Properties of Flash Butt Welded Mn-Cr-Mo Dual Phase Steel," ISIJ Int., vol. 33, no. 7, pp. 807-815, July 1993.

[41] V. H. Baltazar Hernandez, M. L. Kuntz, M. I. Khan, and Y. Zhou, 2008, Influence of microstructure and weld size on the mechanical behaviour of dissimilar AHSS resistance spot welds, Science and Technology of Welding and Joining, Vol. 13, No. 8, pp. 769-776.

[42] M. Xia, E. Biro, Z. Tian and Y. N. Zhou, "Effects of Heat Input and Martensite on HAZ Softening in Laser Welding of Dual Phase Steels," ISIJ Int., vol. 48, no. 6, pp. 809-814, June 2008.

[43] E. Biro and A. Lee, "Welded Properties of Various DP600 Chemistries", Sheet Metal Welding Conference XI, Sterling Heights, MI, 2004.

[44] Parker, Williams, and Holliday, 1998, "Mechanisms of electrode degradation when spot welding coated steel", Sci. and Tech. of Welding and Joining, pp.65-74.

[45] Metal Handbook, Desk edition, 1985, Part III. Processing-28 heat treating-Cu-Zn phase diagram, pp.28-76.

[46] S. Maroie, G. Haemers, and J. Verbist 1984, "Surface oxidation of Polycristallization of a and b Brass as studied by XPS: Influence of Oxygen Pressure", Applications of Surface Sci., pp. 463-476.

[47] Dong, Li, and Kimchi, 1998, "Finite element analysis of electrode wear mechanisms: face extrusion and pitting effects", Sci. and Tech. of Welding and Joining, pp.59-64.

[48] Zhang, Chen, Zhang, 2008, "Characteristics of electrode wear in resistance spot welding dual-phase steels", Material & Design, pp.279-283.

[49] CES Edupack software, Granta Design Limited, Cambridge, UK, 2014.

[50] RWMA-Resistance Welding Manual, 2003, RWMA, pp.18-3.

[51] C. E. Carlton, P. J. Ferreira, 2007, "What is behind the inverse Hall–Petch effect in nanocrystalline materials", Acta Materialia, pp.3749-3756.

[52] M. A. Meyers, A. Mishra, D. J. Benson, 2006, "Mechanical properties of nanocrystalline materials", Progress in Materials Science, pp.427-556.

[53] Adamczyk, J. (2004). Engineering of metallic materials, Publishers of Silesian University of Technology, ISBN 83-7335-223-6, Gliwice, Poland.

[54] K.R. Chan, 2005, "Weldability and Degradation Study of Coated Electrodes for Resistance Spot Welding", Master's thesis, Univ. of Waterloo.

[55] J. Zou, Q. Zhao, and Z. Chen, 2009, "Surface modified long-life electrode for resistance spot welding of Zn-coated steel", Journal of Materials Processing Tech., pp.4141-4146.

[56] Z. Chen, Y. Zhou, and N. Scotchmer, 2006, "Coatings on Resistance Welding Electrodes to Extend Life", SAE Technical report, pp1-5.

[57] J. F. Key, and T. H. Courtney, 1974, "Refractory Metal Composite Tips for Resistance-Spot Welding of Galvanized Steel", Welding Journal, pp.261-266s.

[58] W. M. Shafer, A. V. Nadkarni, "Resistance Spot Welding of Columbium Alloy", US Patent: 4,045,644. Aug, 1977.

[59] S. Mukae, K. Okamura, S. Teramoto, J. Kurobe, H. Asada, S. Inoue, and S. Matsubara, "Electrode for Spot Welding", US Patent: 8,471,169 B2. Jun, 2013.

[60] Y. Zhao, Y. S. Zhang, X. M. Lai, and P. C. Wang, 2014, "Effect of Inserted Strips on Electrode Degradation in Resistance Spot Welding", Welding Journal, pp.411s-420s.

[61] AWS D8.9M:2012 Test Methods for Evaluating the Resistance Spot Welding Behaviour of Automotive Sheet Steel Materials, Miami, Fl.: American Welding Society, 2012.

[62] Freytag, N. A., 1965, "A Comprehensive Study of Spot Welding Galvanized Steel," Weld. J., 44(4), pp. 145s-156s.

[63] Y. Zhao, Y. Zhang, X. Lai, and P. C. Wang, 2013, "Resistance Spot Welding of Ultra-Thin Automotive Steel", ASME, Vol. 135, pp.021012 1-10.

[64] K. Zhou and L. Caia, 2014, Study on effect of electrode force on resistance spot welding process, JOURNAL OF APPLIED PHYSICS, 116, 084902, pp.1-6.

[65] R. Abbaschian, L. Abbaschian, and R. E. Reed-Hill, 1994, "Physical Metallurgy Principles Chapter8. Annealing", Cengage Learning, pp.237-240.

[66] J. P. Holman, 2010, "Heat Transfer-10th edition", McGraw-Hill.

[67] Y. Li, Z Wei, Y. Li, Q. Shen, and Z. Lin, 2013, "Effects of cone angle of truncated electrode on heat and mass transfer in resistance spot welding", International Journal of Heat and Mass Transfer, 65, pp.400-408.

[68] S.J. Dong and Y. ZHOU, 2003, "Effects of TiC Composite Coating on Electrode Degradation in Microresistance Welding of Nickel-Plated Steel", Metallurgical and Material Transaction A, pp.1501-1511.

[69] US Patent, No. 3,363,086, "Resistance spot welding of columbium alloy", 1968.

[70] US Patent, No. 8,471,169 B2, "Electrode for spot welding", 2013.

[71] R. J. Bowers, C.D. Sorensen, T. W. Eagar, 1990, "Electrode Geometry in Resistance Spot Welding", Welding Journal, pp.45s-51s.

[72] W. Chuko and J. Gould, 2002, "Development of Appropriate Resistance Spot Welding Practice for Transformation-Hardened Steels", AISI/DOE technical report, pp.16-19.

[73] C.T. Ji, and Y. Zhou, 2004, "Dynamic Electrode Force and Displacement in Resistance Spot Welding of Aluminum", Journal of Manufacturing Science and Engineering, Vol. 126, pp.605-610.

[74] H. Bhadeshia, and R. Honeycombe, 2006, "Steels: Microstructure and Properties, Chapter.3 Iron-carbon equilibrium and plain carbon steels", Elsevier. Online version.

[75] http://www.swantec.com

# Appendix A

## Weld nugget shape of inserted electrodes
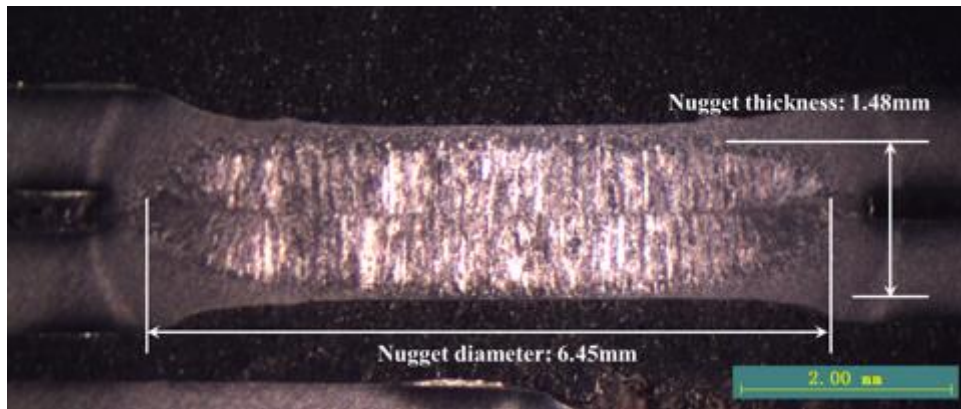


(a) WØ4mm inserted electrode
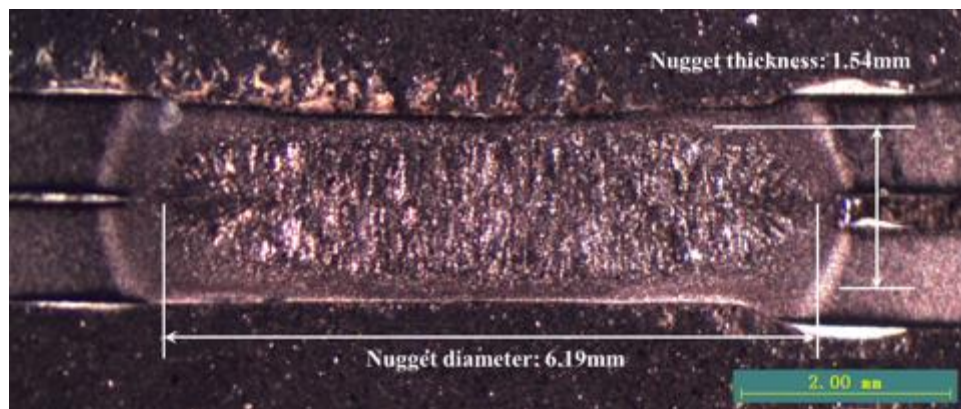


(b) MoØ3mm inserted electrode

# Appendix B

## Dynamic resistance curves



(a) W Ø4mm inserted electrode



(b) Mo Ø3mm inserted electrode

100
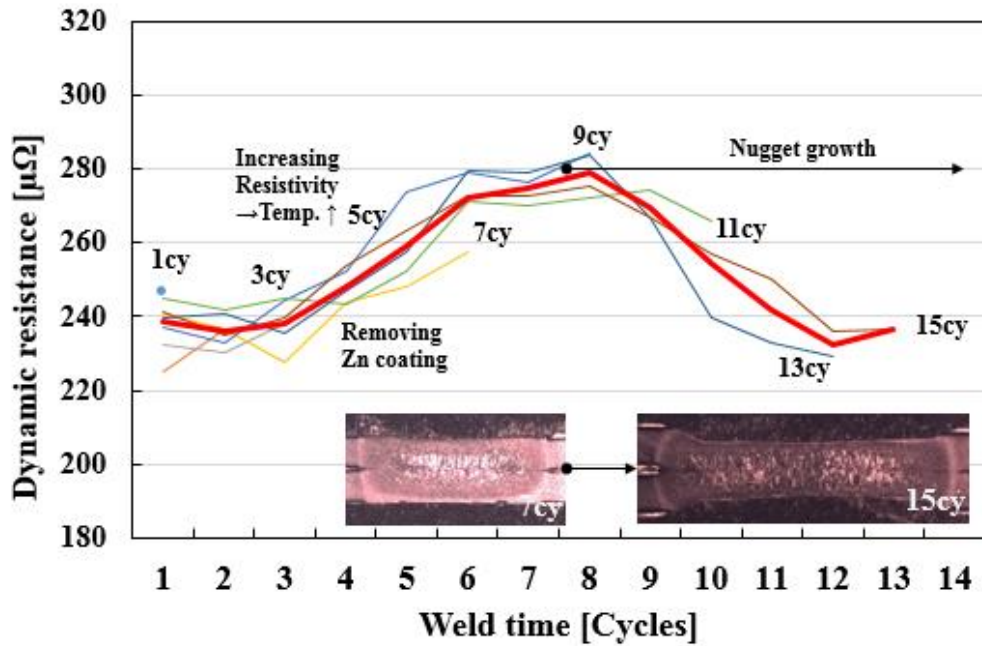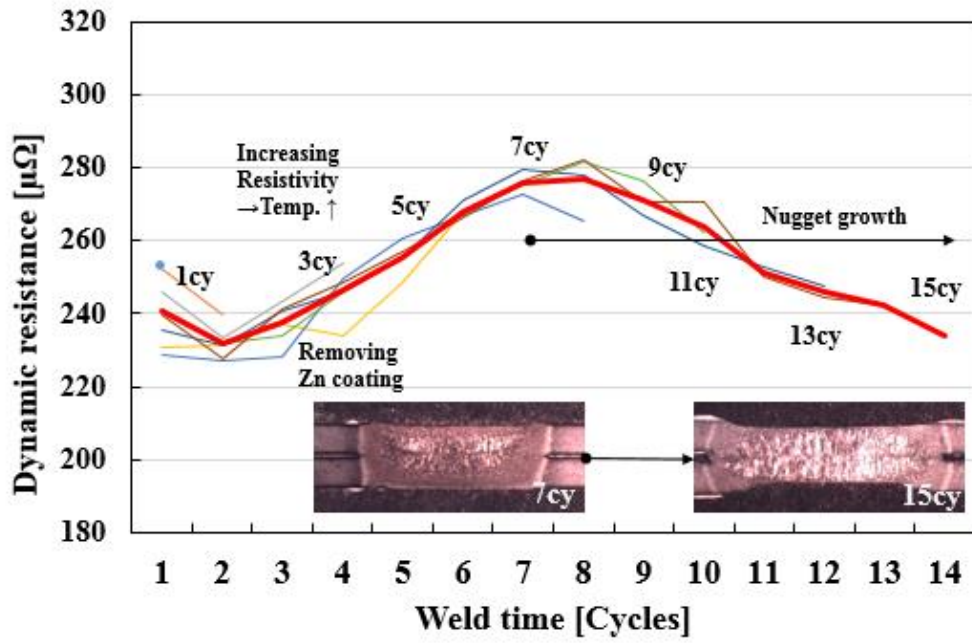
(c) Mo Ø5mm inserted electrode

# Appendix C

# Weld lobe curves for each electrode (button diameter)

| 24 | 3.14 | 4.12 | 6.23 | 6.70 | 7.10 | 8.45 | 8.34 | 6.18 |
|---|---|---|---|---|---|---|---|---|
| 21 | 3.07 | 4.70 | 5.25 | 5.54 | 6.77 | 8.13 | 7.22 | 6.15 |
| 18 | 2.51 | 4.57 | 5.09 | 5.38 | 7.15 | 7.32 | 8.89 | 7.92 |
| 15 | 2.57 | 3.88 | 4.98 | 5.23 | 6.80 | 6.84 | 8.33 | 7.64 |
| 12 | 0.00 | 3.37 | 4.72 | 4.83 | 5.36 | 7.18 | 7.92 | 5.92 |
| 9 | 0.00 | 0.00 | 3.15 | 4.28 | 4.77 | 5.67 | 6.90 | 7.44 |
| Cycles / Current[kA] | 6.5 | 7.0 | 7.5 | 8.0 | 8.5 | 9.0 | 9.5 | 10.0 |

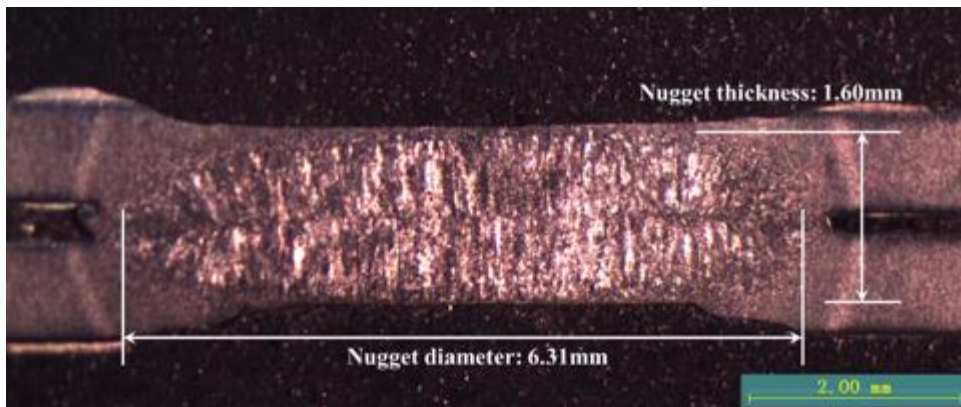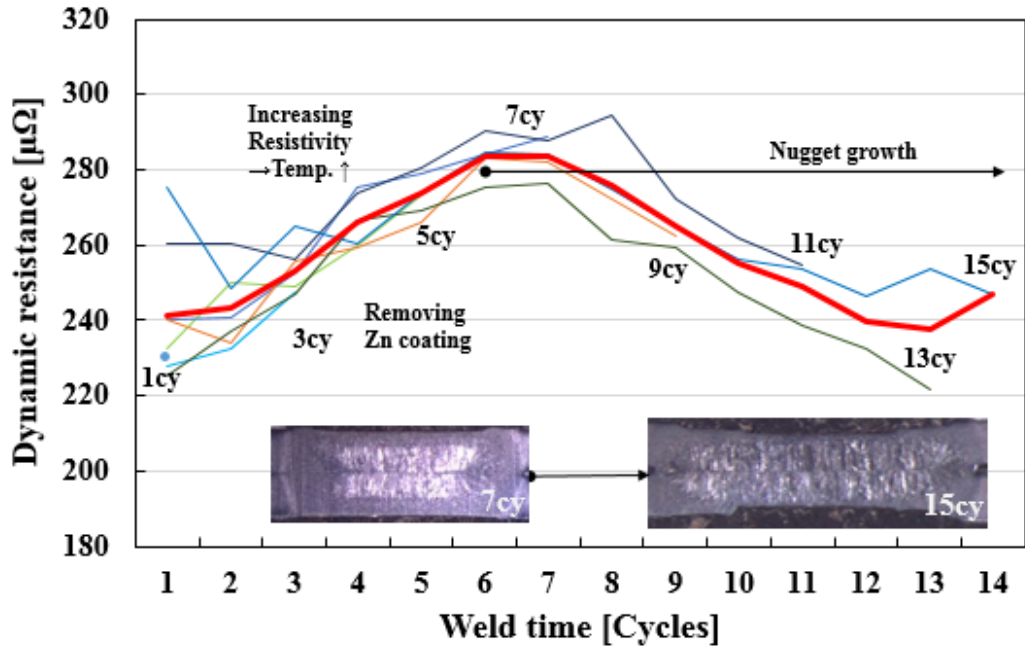(a) W Ø4mm inserted electrode

| 24 | 2.48 | 4.30 | 5.32 | 6.71 | 6.81 | 7.42 | 6.50 | 6.14 |
|---|---|---|---|---|---|---|---|---|
| 21 | 0.00 | 4.42 | 5.21 | 5.53 | 6.01 | 6.86 | 5.33 | 5.98 |
| 18 | 0.00 | 2.68 | 4.91 | 5.51 | 5.95 | 6.35 | 7.42 | 6.38 |
| 15 | 0.00 | 0.00 | 4.63 | 5.27 | 7.04 | 7.44 | 6.70 | 6.13 |
| 12 | 0.00 | 0.00 | 1.76 | 4.60 | 5.06 | 5.94 | 6.83 | 6.14 |
| 9 | 0.00 | 0.00 | 0.00 | 0.00 | 4.39 | 4.84 | 4.89 | 5.51 |
| Cycles / Current[kA] | 6.5 | 7.0 | 7.5 | 8.0 | 8.5 | 9.0 | 9.5 | 10.0 |

(b) Mo Ø3mm inserted electrode

| 24 | 4.15 | 4.93 | 5.50 | 6.77 | 7.95 | 8.87 | 8.17 | 6.63 |
|---|---|---|---|---|---|---|---|---|
| 21 | 4.33 | 4.90 | 5.45 | 5.80 | 7.80 | 8.51 | 8.63 | 7.02 |
| 18 | 3.30 | 4.68 | 5.34 | 5.71 | 7.78 | 8.12 | 8.51 | 6.82 |
| 15 | 0.00 | 3.95 | 4.90 | 5.42 | 7.44 | 7.64 | 7.80 | 7.38 |
| 12 | 0.00 | 0.00 | 3.93 | 4.91 | 7.07 | 7.10 | 7.25 | 5.92 |
| 9 | 0.00 | 0.00 | 0.00 | 0.00 | 3.56 | 4.42 | 4.89 | 6.57 |
| Cycles / Current[kA] | 6.5 | 7.0 | 7.5 | 8.0 | 8.5 | 9.0 | 9.5 | 10.0 |

(c) Mo Ø5mm inserted electrode

\* Green colored: Unacceptable, White colored: Acceptable, Orange colored: Expulsion

\* Weld criterion: 4.0mm ($4\sqrt{t}, t = Thickness\ of\ steel\ sheet$)

102

# Appendix D

# Mechanical test results

1) Normal electrode

|  | 6.5 kA | 7.5 kA | 8.5 kA | 9.5 kA | 10.5 kA | 11.5 kA |
|---|---|---|---|---|---|---|
| Max. TS Strength [kgf] | No weld | No weld | 930.89 | 1083.94 | 1130.58 | 1290.37 |
| Max. CT Strength [kgf] | No weld | No weld | 326.45 | 398.93 | 464.82 | 433.57 |
| Button diameter [mm] | No weld | No weld | 4.53 | 5.09 | 5.86 | 6.10 |

2) W Ø3mm inserted electrode

|  | 6.5 kA | 7.5 kA | 8.5 kA | 9.5 kA | 10.5 kA | 11.5 kA |
|---|---|---|---|---|---|---|
| Max. TS Strength [kgf] | 850.48 | 1002.68 | 1084.94 | 1209.11 | 1189.40 |  |
| Max. CT Strength [kgf] | 278.40 | 537.68 | 527.06 | 543.27 | 244.27 | - |
| Button diameter [mm] | 0.00 | 5.43 | 7.82 | 7.98 | 7.90 | - |

3) W Ø4mm inserted electrode

|  | 6.5 kA | 7.5 kA | 8.5 kA | 9.5 kA | 10.5 kA | 11.5 kA |
|---|---|---|---|---|---|---|
| Max. TS Strength [kgf] | 792.08 | 1082.98 | 1192.66 | 1269.40 | 1308.28 | - |
| Max. CT Strength [kgf] | 292.03 | 565.91 | 598.13 | 560.77 | 524.69 | - |
| Button diameter [mm] | 2.57 | 4.98 | 6.80 | 8.33 | 7.64 | - |

4) Mo Ø3mm inserted electrode

|  | 6.5 kA | 7.5 kA | 8.5 kA | 9.5 kA | 10.5 kA | 11.5 kA |
|---|---|---|---|---|---|---|
| Max. TS Strength [kgf] | No weld | 975.83 | 1222.34 | 1270.90 | 1317.94 | - |
| Max. CT Strength [kgf] | No weld | 351.91 | 509.94 | 504.05 | 600.71 | - |
| Button diameter [mm] | No weld | 4.63 | 7.04 | 6.70 | 6.13 | - |

5) Mo Ø5mm inserted electrode

|  | 6.5 kA | 7.5 kA | 8.5 kA | 9.5 kA | 10.5 kA | 11.5 kA |
|---|---|---|---|---|---|---|
| Max. TS Strength [kgf] | No weld | 898.20 | 1188.87 | 1282.50 | 1171.87 | - |
| Max. CT Strength [kgf] | No weld | 427.89 | 506.87 | 473.92 | 468.08 | - |
| Button diameter [mm] | No weld | 4.90 | 7.44 | 7.80 | 7.38 | - |

# Appendix E

# Analysis of FZ / HAZ area

1) Normal electrode

|  | 6.5 kA | 7.5 kA | 8.5 kA | 9.5 kA | 10.5 kA | 11.5 kA |
|---|---|---|---|---|---|---|
| FZ width [mm] | No weld | No weld | 2.76 | 4.86 | 5.51 | 5.54 |
| HAZ$_{CGFGIC}$ width [mm] | No weld | No weld | 5.68 | 6.46 | 6.96 | 7.10 |
| HAZ Ratio | No weld | No weld | 0.49 | 0.75 | 0.79 | 0.78 |

2) W Ø3mm inserted electrode

|  | 6.5 kA | 7.5 kA | 8.5 kA | 9.5 kA | 10.5 kA | 11.5 kA |
|---|---|---|---|---|---|---|
| FZ width [mm] | 4.43 | 4.64 | 5.82 | 6.23 | 5.81 | - |
| HAZ$_{CGFGIC}$ width [mm] | 6.01 | 5.89 | 7.00 | 7.39 | 6.99 | - |
| HAZ Ratio | 0.74 | 0.79 | 0.83 | 0.84 | 0.83 | - |

3) W Ø4mm inserted electrode

|  | 6.5 kA | 7.5 kA | 8.5 kA | 9.5 kA | 10.5 kA | 11.5 kA |
|---|---|---|---|---|---|---|
| FZ width [mm] | 4.79 | 5.48 | 5.53 | 6.21 | 4.73 | - |
| HAZ$_{CGFGIC}$ width [mm] | 6.64 | 6.74 | 6.95 | 7.40 | 6.75 | - |
| HAZ Ratio | 0.72 | 0.81 | 0.80 | 0.84 | 0.70 | - |

4) Mo Ø3mm inserted electrode

|  | 6.5 kA | 7.5 kA | 8.5 kA | 9.5 kA | 10.5 kA | 11.5 kA |
|---|---|---|---|---|---|---|
| FZ width [mm] | No weld | 4.78 | 5.46 | 6.03 | 6.25 | - |
| HAZ$_{CGFGIC}$ width [mm] | No weld | 6.37 | 6.85 | 7.38 | 7.61 | - |
| HAZ Ratio | No weld | 0.75 | 0.80 | 0.82 | 0.82 | - |

5) Mo Ø5mm inserted electrode

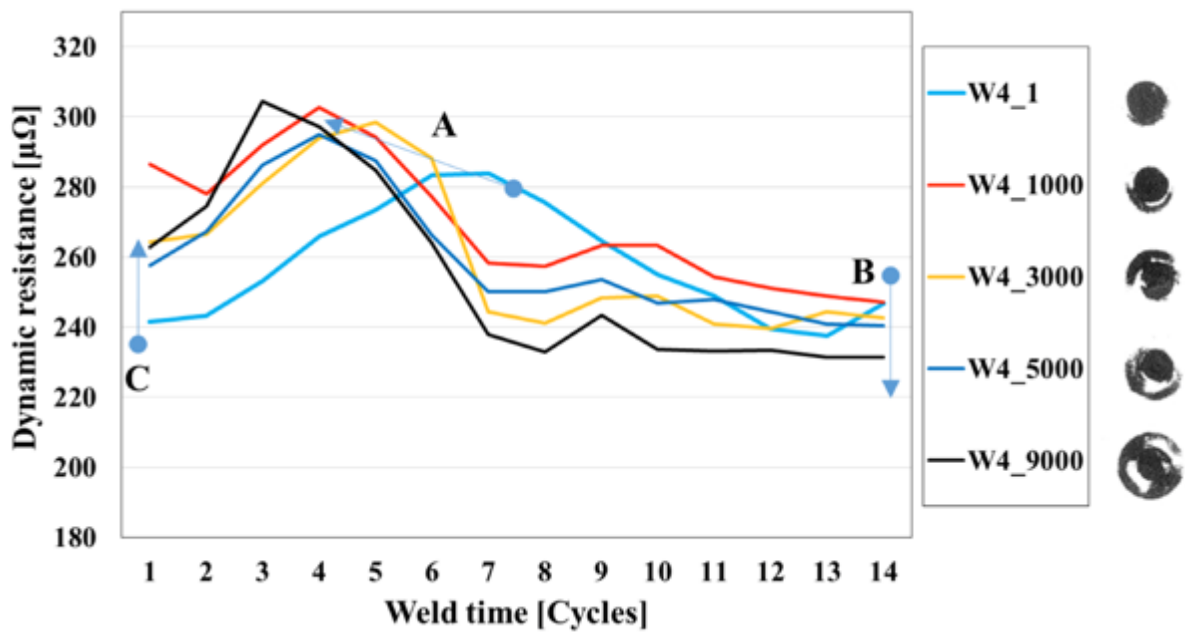|  | 6.5 kA | 7.5 kA | 8.5 kA | 9.5 kA | 10.5 kA | 11.5 kA |
|---|---|---|---|---|---|---|
| FZ width [mm] | No weld | 4.27 | 5.68 | 5.93 | 6.10 | - |
| HAZ$_{CGFGIC}$ width [mm] | No weld | 6.21 | 6.84 | 7.20 | 7.50 | - |
| HAZ Ratio | No weld | 0.69 | 0.83 | 0.82 | 0.81 | - |

# Appendix F

# Changing of dynamic resistance during electrode life test

1) Normal electrode
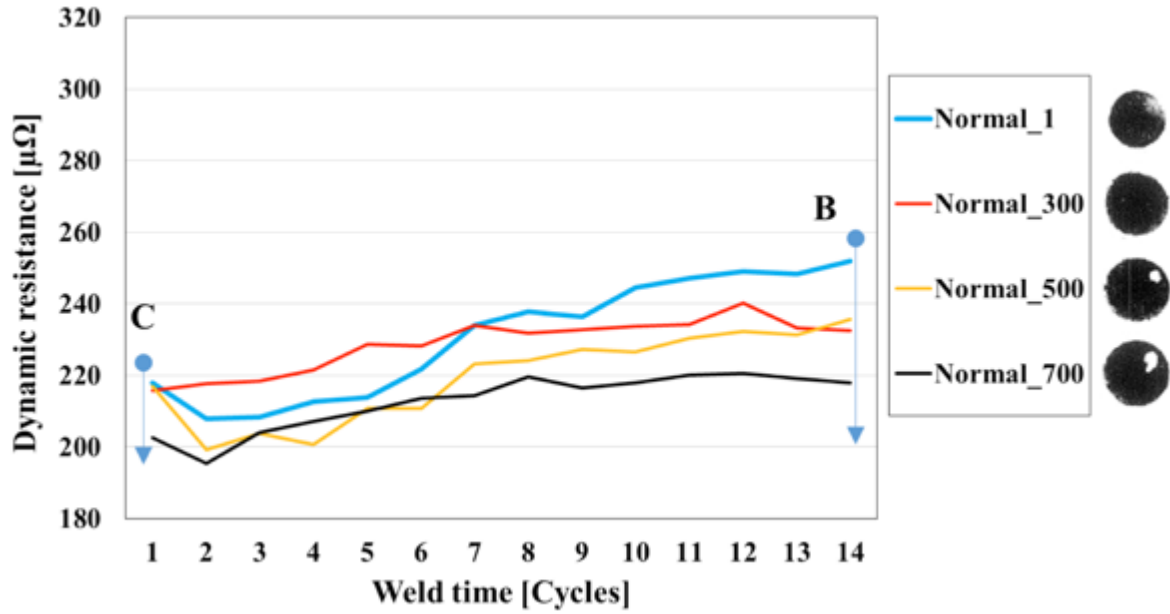


2) W Ø4mm inserted electrode

3) Mo Ø5mm inserted electrode